UNIVERSITY OF
LIVERPOOL

Investigation into multifunctional catalysis for organic synthesis

Thesis submitted in accordance with the requirements of the University of Liverpool for the degree of Doctor of Philosophy

by

Fahd Thabit Salman Al-Wadaani

July 2009

Abstract

The aim of this work is to develop new heterogeneous multifunctional catalysts based on Zn^{II}-Cr^{III} and Zn^{II}-Cr^{III}-Cu^{II} mixed oxides for one-step synthesis of methyl isobutyl ketone (MIBK) from acetone and hydrogen and one-step dehydroisomerisation of α-pinene to p-cymene. Our goal is to understand the operation of these catalysts and to explain and exploit their multifunctional properties in the above reactions.

Pd metal supported on Zn^{II}-Cr^{III} mixed oxide and Pd-free Zn^{II}-Cr^{III}-Cu^{II} mixed oxide were found to be efficient bifunctional catalysts for the one-step synthesis of MIBK from acetone and H_2 both in gas-phase and liquid-phase processes. The reaction involves acid-catalysed condensation of acetone to mesityl oxide followed by its hydrogenation to MIBK. Diisobutyl ketone (DIBK) is a useful by-product in this process. Zn-Cr (Zn/Cr = 20:1–1:30) and Zn-Cr-Cu oxides (Zn/Cr/Cu = 1:1:0.1–1:1:2) were prepared by co-precipitation of Zn^{II}, Cr^{III} and Cu^{II} hydroxides. The catalysts were characterised using N_2 adsorption (surface area and porosity), TGA (water content), XRD (crystallinity) and ICP (catalyst composition). The acidity of Zn-Cr oxides was characterised using NH_3 and pyridine adsorption in combination with infrared spectroscopy and calorimetry. Pd dispersion in the Pd/Zn-Cr catalysts was measured by H_2 adsorption. For both the continuous gas-phase process and the batch liquid-phase process of MIBK synthesis, the preferred catalyst formulation comprises 0.3 wt% Pd on the amorphous Zn-Cr (1:1) oxide (S_{BET} = 132 m^2/g) possessing Lewis acid sites (1.2 mmol/g density) with an enthalpy of NH_3 adsorption of -155 kJ/mol. Both processes produce MIBK with a selectivity of 70-78% and 90% MIBK + DIBK total selectivity at 38-40% acetone conversion, on a par with the best results reported to date. Evidence was obtained that the hydrogenation of mesityl oxide to MIBK is the rate-limiting step in the gas-phase process.

The hydroisomerisation of α-pinene to p-cymene was carried out over Zn^{II}-Cr^{III} mixed oxides in the gas-phase. These oxides, which possess both acid and dehydrogenation functions, were found to be efficient, noble-metal-free catalyst for the one-step dehydroisomerisation of α-pinene to p-cymene. This reaction is a good example of the use of heterogeneous multifunctional catalysis for the conversion of renewable feedstock (α-pinene) into value-added chemicals. It involves acid-catalysed

α-pinene isomerisation, followed by the dehydrogenation of p-cymene precursor(s). The reaction was carried out over a fixed catalyst bed in the gas phase at 350°C. Amongst Zn-Cr oxides studied (Zn/Cr = 20:1–1:30), the preferred catalyst is Zn-Cr (1:1) oxide which produces p-cymene with a 78% yield at 100% α-pinene conversion. This catalyst shows stable performance for over 30 h without co-feeding hydrogen to the reactor. The new catalyst is superior to the Pd/SiO_2 catalyst, previously developed by Holdrich et al., in both p-cymene yield (78% compared to 67%) and its stability.

The main results presented in this thesis have been published in refereed journals [1, 2] and presented at several scientific meetings [3-9]:

1. F. Al-Wadaani, E.F. Kozhevnikova, I.V. Kozhevnikov, Pd supported on Zn^{II}–Cr^{III} mixed oxide as a catalyst for one-step synthesis of methyl isobutyl ketone, J. Catal. 257 (2008) 199.
2. F. Al-Wadaani, E.F. Kozhevnikova, I.V. Kozhevnikov, Zn(II)–Cr(III) mixed oxide as efficient bifunctional catalyst for dehydroisomerisation of a-pinene to p-cymene, Appl. Catal. A 363 (2009) 153.
3. F. Al-Wadaani, E.F. Kozhevnikova, I.V. Kozhevnikov, Poster presentation, Postgraduate research week, the University of Liverpool, Liverpool, UK, March, 2007.
4. F. Al-Wadaani, E.F. Kozhevnikova, I.V. Kozhevnikov, Poster presentation, Saudi Innovation Conference (SIC), the University of Newcastle, UK, May, 2007.
5. F. Al-Wadaani, E.F. Kozhevnikova, I.V. Kozhevnikov, Poster presentation, Catalysis: Fundamentals and Practice , Summer School at University of Liverpool, Liverpool, UK, September, 2007.
6. F. Al-Wadaani, E.F. Kozhevnikova, I.V. Kozhevnikov, Poster presentation, Saudi International Innovation Conference (SIIC), the University of Leeds, UK, June, 2008.
7. F. Al-Wadaani, E.F. Kozhevnikova, I.V. Kozhevnikov, Poster presentation, Taibah International Chemistry Conference – 2009 (TIIC-2009), Taibah University, Al-Madinah Al-Munawwarah, Saudia Arabia, March, 2009.
8. F. Al-Wadaani, E.F. Kozhevnikova, I.V. Kozhevnikov, Poster presentation, 6th World Congress on Catalysis by Acids and Bases, Genova, Italy, May, 2009.
9. F. Al-Wadaani, E.F. Kozhevnikova, I.V. Kozhevnikov, Oral presentation, 21st North American Catalysis Society Meeting (21st NAM), San Francisco, USA, June, 2009.

Acknowledgements

First, I would like to thank my supervisor Professor Ivan Kozhevnikov for his supervision and guidance during the years of my PhD studies.

I would also like to thank Dr Elena Kozhevnikova for her assistance with the lab work and equipment as well as her kindness.

I am also grateful to the people related to the experimental results presented in this thesis: Gary Evans for his help with the XRD analysis, Steve Apter for ICP and elemental analysis, Moya McCarron and Alan Mills for GC-MS analysis.

I would also like to express my gratitude to my colleagues in our catalysis group: Abdullah Alhanash, Ali Alsalme and Robert Hetterley. I wish them every success in the future.

Thanks are due to my parents, my wife, my children and all my family members and friends for their love and support.

Finally, I am grateful to Taibah University Saudi Arabia and EPSRC for their financial support.

CONTENTS

Abstract I

Acknowledgements III

Contents IV

Chapter 1. Introduction 1

1.1. Cascade processes using multifunctional catalysis 1

1.2. Heterogeneous catalysis 2

1.2.1. Classification of heterogeneous catalysis 4

1.2.2. Kinetics of catalysed heterogeneous reactions 5

1.2.2.1. Rate of reaction 5

1.2.2.2. Temperature dependence of reaction rate 7

1.2.2.3. Steps of heterogeneous catalysed reaction 7

1.2.2.4. Adsorption on the catalyst surface 9

1.3. Multifunctional catalysis 11

1.4. Multifunctional catalysis for one-step conversion of acetone to methyl isobutyl ketone (MIBK) 12

1.5. α-Pinene as renewable feedstock for organic synthesis 22

1.5.1. Isomerisation of α-pinene 22

1.5.2. Dehydroisomerisation of α-pinene 26

1.6. Zn-Cr and Zn-Cr-Cu mixed oxide catalysts 27

1.6.1. Preparation of Zn-Cr mixed oxide 28

1.6.2. Properties of Zn-Cr and Zn-Cr-Cu oxides 29

1.6.2.1. The composition of Zn-Cr and Zn-Cr-Cu oxides 29

1.6.2.2. Thermal behaviour 30

1.6.2.3. Surface area and porosity 31

1.6.2.4. Acidity of Zn-Cr oxides 33

1.6.2.5. Enhancement of activity of Zn-Cr-Cu catalyst 33

1.7. Objectives and thesis outline 34

References 37

Chapter 2. Experimental 45

2.1. Introduction 45

2.2. Chemicals and solvents 45

2.3. Catalyst preparation 46

2.3.1. Preparation of Zn-Cr mixed oxide catalysts 46

2.3.2. Preparation of palladium doped Zn-Cr mixed oxide catalysts 46

2.3.3. Preparation of Zn-Cr-Cu mixed oxide catalysts 47

2.4. Techniques 47

2.4.1. Thermogravimetric analysis (TGA) 47

2.4.2. Surface area and porosity analysis 48

2.4.3. Fourier transform infrared spectroscopy (FTIR) 49

2.4.4. Powder X-ray diffraction 49

2.4.5. Inductive coupled plasma atomic emission spectroscopy (ICP-AES) 50

2.4.6. Elemental analysis 51

2.4.7. Ultraviolet (UV) spectroscopy 51

2.4.8. Differential scanning calorimetry (DSC) 52

2.4.9. Microcalorimetry 54

2.4.10. Metal dispersion from hydrogen adsorption 55

2.4.11. Gas chromatography-mass spectrometry (GC-MS) 58

2.4.12. Gas chromatography 59

2.4.13. GC calibration 60

2.5. Reaction studies 65

2.5.1. Gas phase reactions 65

2.5.2. Liquid phase reactions 68

2.6. Calculation of reaction results 70

2.6.1. Calculation of reaction results in gas phase processes 70

2.6.2. Calculation of reaction results in liquid phase processes 72

References 73

Chapter 3. Catalyst characterisation 74

3.1. Introduction 74

3.2. Inductively coupled plasma atomic emission spectroscopy (ICP-AES) 74

3.3. Powder X-ray diffraction 77
3.3.1. XRD for Zn-Cr oxides 77
3.3.2. XRD for Zn-Cr-Cu oxides 79
3.4. Thermogravimetric analysis (TGA) 81
3.4.1. TGA of Zn-Cr oxides 82
3.4.2. TGA of Zn-Cr-Cu oxides 85
3.5. Surface area and porosity 88
3.5.1. Surface area and porosity of Zn-Cr oxides 92
3.5.2. Surface area and porosity of Zn-Cr-Cu oxides 98
3.6. H_2 adsorption experiments 106
3.7. Acidity of Zn-Cr oxide catalysts 107
3.7.1. TG-DSC study of ammonia adsorption (continuous flow and pulse methods) 108
3.7.2. Microcalorimetry of pyridine adsorption 111
3.7.3. FTIR study of pyridine adsorption 112
3.8. Summary of catalyst characterisation 113
References 117

Chapter 4. One-step synthesis of MIBK from acetone and hydrogen 120
4.1. Introduction 120
4.2. Catalyst testing 121
4.2.1. Gas phase reactions over Pd/Zn-Cr oxide catalysts 121
4.2.1.1. Effect of Zn/Cr ratio 121
4.2.1.2. Effect of Pd loading 124
4.2.1.3. Effect of contact time 125
4.2.1.4. Effect of flow rate at constant contact time 126
4.2.1.5. Activation energy 127
4.2.2. Liquid-phase reactions over Pd/Zn-Cr oxide catalysts 128
4.2.2.1. Effect of stirring speed 128
4.2.2.2. Effect of Zn/Cr ratio 129
4.2.2.3. Effect of Pd loading 130

4.2.2.4. Reaction time course 132
4.2.3. Gas phase reactions over Zn-Cr-Cu oxide catalysts 134
4.2.3.1. Effect of Cu content in Zn-Cr-Cu oxide 136
4.2.3.2. Effect of reaction temperature 137
4.2.3.3. Effect of acetone/hydrogen ratio in the gas flow 138
4.2.3.4. Effect of Pd loading 139
4.3. Catalyst reproducibility and re-use 140
4.3.1. Catalyst reproducibility in the gas-phase process 141
4.3.2. Catalyst reproducibility and re-use in the liquid-phase process 141
4.4. Discussion of catalyst performance on one-step synthesis of MIBK 143
4.5. Conclusion 144
References 145

Chapter 5. One-step synthesis of p-cymene from α-pinene over Zn-Cr oxide in gas phase 146
5.1. Introduction 146
5.2. α-Pinene conversion to p-cymene: Results and Discussion 146
5.2.1. Effect of catalyst acidity 148
5.2.2. Catalyst stability 148
5.2.3. Effect of Zn/Cr atomic ratio 150
5.2.4. Effect of reaction temperature 151
5.2.5. Effect of contact time 152
5.2.6. Effect of Pd loading 153
5.3. Reaction mechanism 154
5.4. Conclusion 155
References 156

Chapter 6. Conclusions 157
References 162

Appendix 163

Appendix (I) 163

Appendix (II) 164

Appendix (III) 166

Appendix (IV) 167

Appendix (V) 168

Appendix (VI) 169

Chapter 1. Introduction

1.1. Cascade processes using multifunctional catalysis

Synthetic organic chemistry frequently employs multi-step syntheses in which the desired products are obtained in a sequence of reaction steps. Traditionally, each step involves the separation of intermediate product, which is then used in the following step. The large amount of waste produced, the long operation times and the high cost of intermediate steps in multi-step organic reactions have led scientists in the field of organic synthesis to consider a new strategy for developing cascade reactions (also known as tandem, one-pot, or one-step reactions) without the intermediate separation steps. The inspiration for a new pathway was to be found in Nature and, in particular, living organisms, which produce a high degree of selectivity with regard to final products (D) from converted starting materials (A) through multi-step reactions without the recovery of intermediates (Figures 1.1 and 1.2) [1-3]. The great selectivity of biosynthetic reactions that developed over thousands of millions of years is the result of their exceedingly complicated nature compared to the simplistic nature of organic synthesis. The key to the great selectivity and productivity of biochemical processes is multifunctional catalysis.

Organic synthesis, which is chemistry developed by Man, is hugely inferior to biosynthesis, i.e. natural chemistry. In organic synthesis we carry out simple step-by-step reactions, often using a catalyst with a single chemical function (acid, base, metal, etc.), which result in the production of intermediates requires isolation and purification for each conversion step. Along with the long time needed to undertake these steps,

there are many other drawbacks of which the most important are the low space-time yield and the huge amount of unwanted by-products [1].

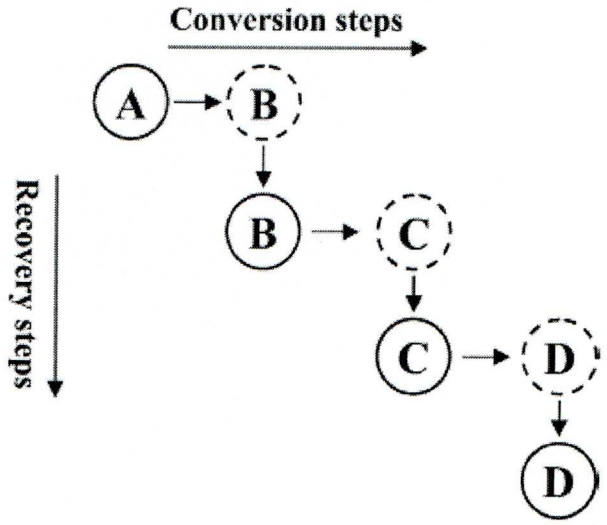

Figure 1.1 Multistage organic synthesis in a traditional chemical process which needs a recovery step after each conversion step [1].

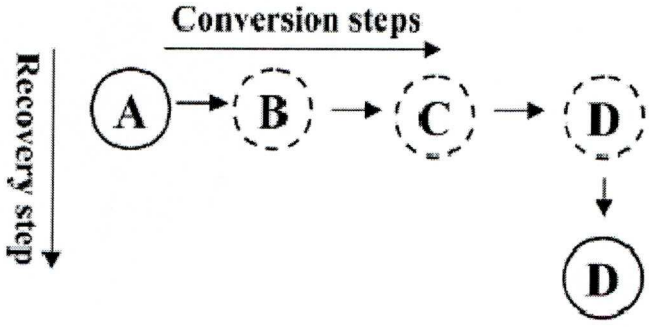

Figure 1.2 Cascade organic synthesis using multifunctional catalysis involves a combination of reaction steps without need for the recovery of intermediate products after each conversion step [1].

1.2. Heterogeneous catalysis

A catalyst is defined as a material which can accelerate the rate of a chemical reaction without being consumed or affected in the reaction process [4]. More than 90%

of chemicals and materials in the modern industrial economy are produced with the use of catalysis [4]. Heterogeneous catalysed processes, where the catalyst and the reactants are in different phases, are widely used for main production processes in industry due to the advantages of easy product separation and catalyst recycle, which contrast with the phase separation problems encountered with homogeneous catalysed reactions [5]. An example of industrial heterogeneous catalysis is the use of zeolite catalyst, ZSM-5, for the cracking of naphtha to produce ethene and propene which are used as the basis of many modern materials [6, 7].

Several factors have to be taken into account when designing and/or developing a catalyst to be used for a particular reaction process. These are presented in Table 1.1.

Table 1.1 Properties considered in catalyst development [4].

1) Correct active phase
2) Appropriately high surface area
3) Strength of active sites
4) Longevity
5) Correct shape
6) Environmental compatibility
7) Cost

The main factor that has to be considered for the developed catalyst to be efficient and active for a particular chemical reaction, in order for an effective balance of reactant conversion and desired product selectivity to be achieved, is to have a correct active phase with a high surface area exposed to the reactant and appropriate

strength of active sites. For example, a high reactant conversion with a low selectivity to the desired product may be obtained using catalysts containing very strong active sites. Another important factor which has to be taken into account when designing and/or developing a catalyst which can affect the cost effectiveness of the process is the longevity of the catalyst. For commercial use, high catalyst stability is important for the catalyst to be considered for further development. The loss of catalyst activity over time in major catalysed processes is mainly caused by sintering, which is the loss of the active phase surface area, or poisoning where loss of activity per unit area occurs.

1.2.1. Classification of heterogeneous catalysis

As is well known, for a heterogeneous catalysed reaction to occur, a chemical interaction between reactants and products with the catalyst must exist, without any change to the chemical nature of the catalyst, with the exception of the surface. This interaction between the substrates and the catalyst depends on the catalytic activity of the surface which will reflect the chemistry of the catalyst bulk [8]. Depending on this result, a qualitative classification of heterogeneous catalysts is given as follows:

- **Redox catalysts**
- **Acid-base catalysts**
- **Multifunctional catalysts**

Redox catalysts usually include transition metals such as Pd, Pt, Ni and Ag which have an active phase containing metal ions or metal atoms. These metals are able to adsorb hydrogen and hydrocarbons on the surface, and therefore can be used as a catalyst for hydrogenation, dehydrogenation, halogenation and hydrogenolysis. Noble metals such as Pd and Pt can also be used for oxidation reactions and this is due to their resistance to oxidation at the relevant temperature.

Acid-base catalysts usually include solid acids and bases such as zeolites, ZnO, SiO_2-Al_2O_3, H_3PO_4/SiO_2, MgO and CaO in which active sites can be described as Bronsted and Lewis acidic and basic sites. These can be used as catalysts in alkylation, hydration and cracking because of their ability to interact with reactants by acid-base mechanism [8, 9].

Multifunctional catalysts consist of two or more catalytic functions such as acid-base and redox functions. As an example, Pd supported on heteropoly acid has been used as an effective bifunctional catalyst for the one-step conversion of acetone to MIBK [10]. This reaction involves acid-catalysed dehydration and metal-catalysed hydrogenation steps. Another bifunctional catalyst Pt/ZSM-5 has been used for the dehydroisomerisation of n-butane [11].

1.2.2. Kinetics of catalysed heterogeneous reactions

1.2.2.1. Rate of reaction

For any catalysed reaction, the catalyst plays an important role for converting reactants into products. This is determined by the activity of the catalyst which is defined as the rate of the reactant's consumption or the rate of the product's production [4, 8, 12]. In general, the stoichiometric equation that characterises a single chemical reaction can be given by equation (1.1):

$$aA + bB \rightarrow cC + dD \qquad (1.1)$$

where A, B, C, and D are the components of the reaction system and a, b, c, and d are the stoichiometric coefficients. From equation (1.1) the rate of the reaction is defined as the change in moles of the reactant or product per unit time, as shown in equation (1.2):

$$r = -\frac{dA}{adt} = -\frac{dB}{bdt} = \frac{dC}{cdt} = \frac{dD}{ddt} \qquad (1.2)$$

At a fixed temperature the reaction rate depends on the concentration of all regents and therefore the reaction rate is expressed as:

$$r = k\,A^{p}\,B^{n} \qquad (1.3)$$

where k is the rate constant, and p and n are the order of reaction with respect to the corresponding components. In general p and n are not equal to the stoichiometric coefficients a and b. The overall reaction order is the sum of $(p+n)$.

For a heterogeneous catalysed reaction, the reaction rate can be defined per catalyst weight, W, or per catalyst surface area, S (equation (1.4)):

$$\mathrm{r} = -\frac{dA}{Wdt} \quad or \quad r = -\frac{dA}{Sdt} \qquad (1.4)$$

From equation (1.4) another expression for the rate can be given in terms of molecules reacted per single active site and per unit time. This is known as the turnover frequency, TOF, which can be expressed as shown in equation (1.5):

$$TOF = -\frac{dA}{n.Sdt}\,.N \qquad (1.5)$$

where N is the Avogadro's number and n is the number of active sites per unit catalyst surface area.

1.2.2.2. Temperature dependence of reaction rate

In most chemical reactions the rate increases with temperature. This can be expressed by the Arrhenious equation [12]:

$$k = A\ exp\ (-E/RT) \tag{1.6}$$

where k is the rate constant, A is the pre-exponential factor, E is the activation energy of the reaction, R is the gas constant (R = 8.31 $JK^{-1}mol^{-1}$), and T is the absolute temperature. Values of A and E can be measured by plotting lnk against $1/T$ from equation (1.7).

$$lnk = lnA - E/RT \tag{1.7}$$

1.2.2.3. Steps of heterogeneous catalysed reaction

For any heterogeneous catalysed reaction to occur, an interaction between the reactant molecules or atoms with the catalyst surface should happen. For this to occur, five steps are involved, as shown in Figure 1.3 [8].

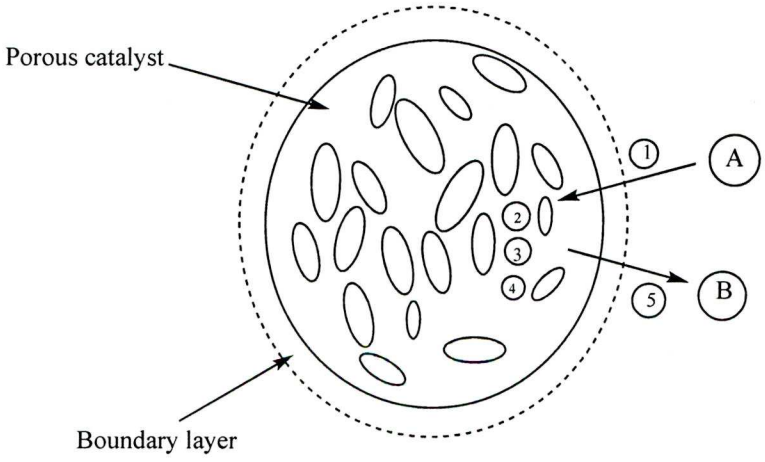

Figure 1.3 Reaction steps on a solid porous catalyst.

The first step is the transport of the reactant to the catalyst. The second step is the adsorption of the reactant on the catalyst in order to allow a chemical reaction to occur in the third step. In the fourth step, the desorption of the products from the catalyst occurs. Finally, there is the transport of the products away from the catalyst. In both the first and the last steps, there is a mass transfer due to three types of diffusion - molecular diffusion, Knudsen diffusion and configurational diffusion. The classification of these diffusions is based on the pore size of the catalyst (d) and the mean free path of molecules (λ), as shown in Figure 1.4 [13].

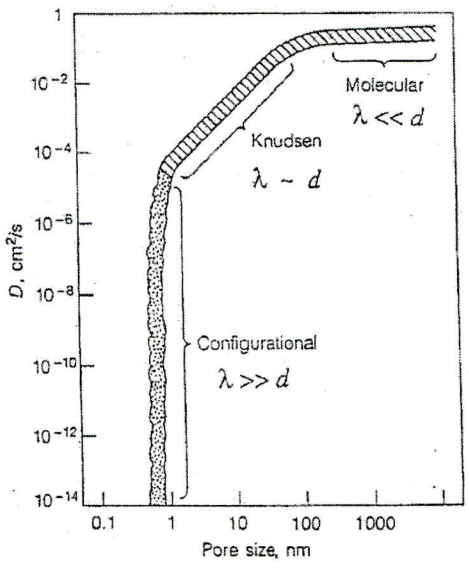

Figure 1.4 Effective diffusion coefficient of molecules in a porous solid [13].

Mass transfer can affect many aspects of catalytic process. If there are no mass transfer limitations, the reaction is referred to as occurring in chemical regime. In addition, there are two diffusion controlled regimes which are distinguished for chemical reactions occurring on solid porous catalysts [8, 9]:

- External diffusion regime. This regime sets up when the reaction is limited by the mass transport to the external surface. In this case the rate will increase with increasing the flow rate, until the concentrations of reactants on the outer surface of the catalyst

particle and in the gas flow become equal. For this regime, the apparent activation energy of the reaction will be low (<10 kJ/mol).

- Internal diffusion regime. If the reaction is limited by the mass transport to the internal catalyst surface, the reaction rate will increase upon decreasing catalyst particle size. In this case, the value of apparent activation energy will be half the value of the true activation energy ($E_a = E/2$), where E is the activation energy for the chemical regime.
- Chemical regime. If there are no diffusion limitations and the adsorption and desorption steps are at fast equilibrium, the chemical reaction will be the rate-limiting step. This means that the reaction rate will be independent on the flow rate and the catalyst particle size. In this type of kinetic regime, the value of the apparent activation energy will be higher than that in diffusion controlled regimes (20 - 200 kJ/mol).

1.2.2.4. Adsorption on the catalyst surface

Two different forms of adsorption on the catalyst surface are distinguished [8, 9]. The first one is called physical adsorption, or physisorption. This involves a weak interaction between the adsorbate (reactant) and the adsorbent, and is termed Van der Waals adsorption. The second adsorption is known as chemical adsorption, or chemisorption, and involves the rearrangement of electrons within the interacting molecule and then new chemical bonds will be formed. Other differences between physisorption and chemisorption are presented in Table 1.2.

Table 1.2 Chemisorption and physisorption [8, 9].

Criterion	Physisorption	Chemisorption
• The interaction between adsorbate and adsorbent	Weak (Van der Waals forces)	Strong (chemical bonds)
• Enthalpy of adsorption $(-\Delta H_{ads})$	8-40 kJ/mol	40-800 kJ/mol
• Number of layers adsorbed	Multilayers	Monolayer
• Material specificity	No	Yes
• Activation energy, E	Zero, non-activated process	Small, activated process
• Restriction to temperature	Yes, depends on boiling point of adsorbate	No, does not depend on boiling point adsorbate

Figure 1.5 shows the oxidation of CO to CO_2 over a metal supported catalyst as an example of reaction that occurs on a heterogeneous catalyst. In this reaction, the oxidation of CO to CO_2 over a metal supported catalyst occurs via the following steps:

Firstly, the reactant molecules of CO are diffused to the metal surface through the gas phase and then bonded to the metal surface *via* adsorption.

Secondly, dissociation of O_2 molecules into atoms occurs at the surface due to the relatively low internal bond strength of O_2 (500 kJ/mol). In contrast, CO does not dissociate because its internal bond is much stronger (1076 kJ/mol).

Thirdly, the adsorbed product CO_2 forms through the surface reaction of CO and an oxygen atom.

Finally, the adsorbed product CO_2 desorbs from the surface by breaking the metal-product bond, then diffuses into the gas phase. It should be taken into account that the presence of bonding sites on the catalyst can provide a lower energy pathway in order for molecular bonds to be rearranged and for the energy of the reaction intermediates, which remain bonded to the catalyst surface, to be stabilised [8, 14].

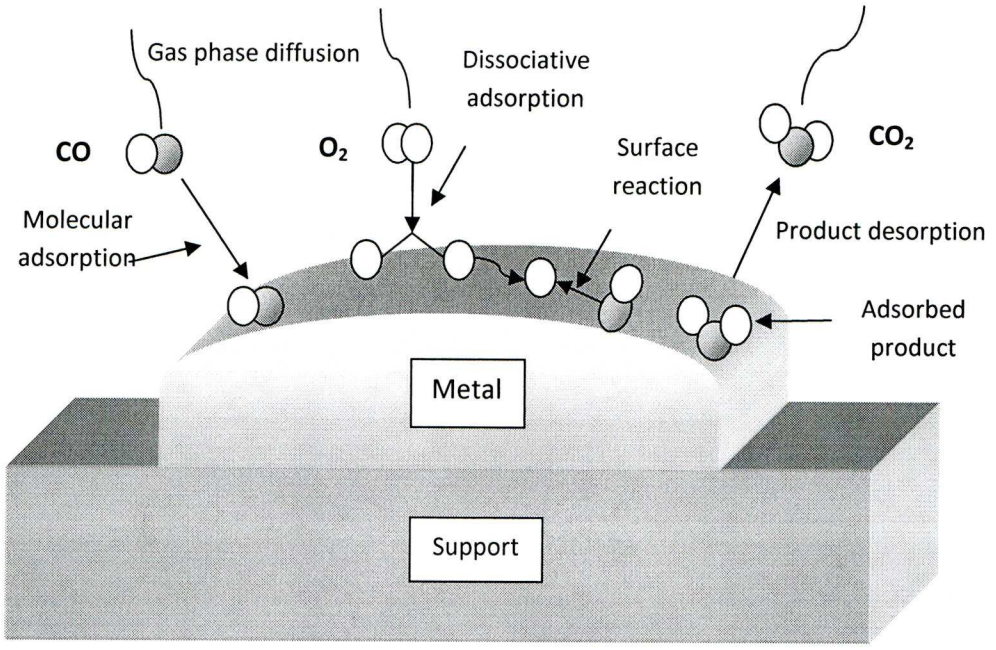

Figure 1.5 Molecular and atomic events occurring in oxidation of CO on a heterogeneous catalyst [4].

1.3. Multifunctional catalysis

Multifunctional catalysts can be defined as catalysts containing two or more catalytic functions (acid, base, metal, etc.) acting synergistically to effect a cascade reaction in a one-pot system, without the separation of intermediate products [15].

For a multifunctional catalyst to be effective in a cascade process, it should meet certain requirements regarding simultaneous action of active sites, rate constants of single reaction steps, as well as the distance between the active sites [15]. Each active site must maintain its activity, even in the presence of a large number of compounds. The selectivity of each of the active sites must be high in order to avoid a decrease in the concentration of the intermediate by dilution processes. Otherwise, the rates of the single reaction steps will decrease and the separation of the target product from the reaction medium will become difficult [15].

Numerous multifunctional catalysts containing metal doped acid/base bifunctional catalysts have been successfully developed and used for cascade reactions in organic syntheses, where the solid acid/base support is active for condensation reactions, while the metal (e.g. Pd, Pt, Ni, Ru, Cu, Rh) function is active in the hydrogenation/dehydrogenation of an adsorbed organic substrate. An example of this is the use of Pd supported on zeolite KX for the one-pot synthesis of 2-ethylhexanol from n-butanal [16]. Other examples include Ni supported on γ-alumina (Ni/γ-Al_2O_3 for the propagation of propylamine to dipropylamine [17], Cu supported on Mg(Al)O mixed oxide for the coupling of MeOH and 2-propanol to form isobutanol (Guerbet reaction) [18], Pd/Mg(Al)O for the synthesis of 2-methyl-3-phenyl-propanal from propanal and benzaldehyde [19], Pt/ZSM-5 for the dehydroisomerisation of n-butane [11], Pt supported on a high surface area carbon with a mixture of silica and alumina for the hydrocracking of n-dodecane to form a mixture of C_3-C_8 hydrocarbons [20].

1.4. Multifunctional catalysis for one-step conversion of acetone to methyl isobutyl ketone (MIBK)

Industrially, after methyl methacrylate and bisphenol, methyl isobutyl ketone (MIBK) is the third most important product obtained from acetone [21]. It is produced from acetone and hydrogen through an aldol condensation reaction and is used in a wide variety of chemical processes. For instance, it is used as a solvent in the manufacture of inks, paints, lacquers, and protective coating systems [22-25]. It is also used in the extraction of inorganic salts, in the separation of zirconium from hafnium, plutonium from uranium, niobium from tantalum [26], cellulose treatment, initiation of polymerisation, and as a reagent in dewaxing mineral oils [27].

MIBK is manufactured from acetone and hydrogen via a three step process as shown in Figure 1.6. The first step is the base catalysed liquid phase aldol condensation of acetone to form diacetone alcohol (DAA). The second step is the liquid phase acid catalyzed dehydration of DAA to form mesityl oxide (MO) and water, The final step is selective hydrogenation of the unsaturated MO to form MIBK in the liquid phase [28, 29].

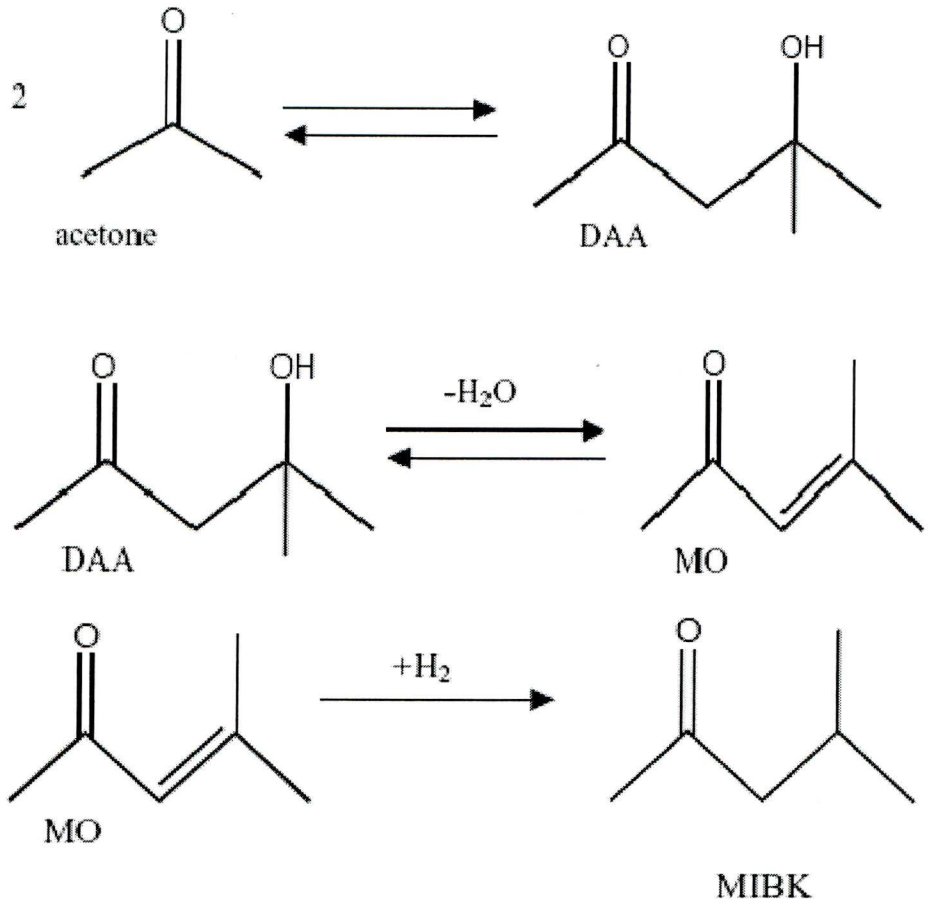

Figure 1.6 Reaction scheme of the self-condensation of acetone to diacetone alcohol (DAA), dehydration of DAA to mesityl oxide (MO), followed by hydrogenation to MIBK [30].

Traditionally, acetone conversion to MIBK involves three reaction steps carried out separately. In these processes, the first reaction of aldol condensation of acetone to DAA is typically catalysed by dilute sodium hydroxide, followed by the DAA

separation from the reaction mixture by distillation. It is then catalytically dehydrated to mesityl oxide using phosphoric or sulphuric acid at a temperature of 100°C. In the final reaction step, MO is hydrogenated to MIBK in either the gas or liquid phase at 150-200°C and a 3-10 bar H_2 pressure using a Cu, Pd or Ni catalyst [31]. The first two reaction steps of this process are carried out over strong alkali and acid catalysts in homogeneous phase, and this leads to a complicated and expensive separation of the final products. Moreover, in the first two steps, mesityl oxide is produced with a low yield due to an equilibrium limitation [32, 33]. In addition, the variance between the change in the Gibbs free energy values (Table 1.3) reported at a temperature of 127°C for the first reaction (acetone conversion to mesityl oxide) and for the overall conversion of acetone to MIBK, indicate that the first equilibrium reaction is thermodynamically unfavourable. The overall one-step process is a significantly more favoured reaction as the negative change of Gibbs free energy suggests, and hence less restricted by equilibrium effects.

Table 1.3 Thermodynamic equilibrium data for the conversion of acetone to MIBK at 127°C [34].

Reaction	$\Delta H_{127°C}$ (kJ mol^{-1})	$\Delta G_{127°C}$ (kJ mol^{-1})
$2CH_3COCH_3$ (acetone) $\rightleftharpoons$ $(CH_3)_2=CHCOCH_3 + H_2O$ (mesityl oxide)	-21.8	13.8
$(CH_3)_2=CHCOCH_3$ (mesityl oxide) $\rightarrow$ $(CH_3)_2CHCH_2COCH_3$ (MIBK)	-60.7	-50.6
$2CH_3COCH_3$ (acetone) $\rightarrow$ $(CH_3)_2CHCH_2COCH_3$ (MIBK)	-82.4	-36.8

Therefore, the one-step synthesis of MIBK from acetone and hydrogen is a more favoured reaction pathway. This reaction involves both dehydration and hydrogenation

steps occuring over a heterogeneous bifunctional catalyst which contains acid and metal active sites [30].

Because the one-step process for MIBK synthesis is simpler and more economical than the step-by-step process, there is an incentive for researchers to find and develop a new and more efficient catalyst for this process. Heterogeneous multifunctional catalysts that contain acid-base and metal functionalities and are therefore capable of carrying out all three reactions in one step in the liquid or gas phase without separating the intermediate DAA and MO have attracted considerable interest [35].

The Tokuyama Soda process is an example of using multifunctional catalysts for MIBK synthesis via a one step reaction mechanism in the liquid phase. In this process, about 95% MIBK selectivity is achieved with an acetone conversion of 30-40%. This is obtained at a H_2 pressure of 20-50 bar and a reaction temperature ranging from 120-160°C using Pd doped zirconium phosphate [31]. A Pd doped acidic ion exchange resin is another example of using a multifunctional catalyst for MIBK synthesis. This particular catalyst was employed by RWE-DEA, formerly Deutsche Texaco. In this process, an acetone conversion of 40% and MIBK selectivity of up to 83% were achieved at 30 bar and between 130 and 140°C reaction temperature [31]. In both examples, the reaction of aldol condensation of acetone to DAA and its dehydration to mesityl oxide are carried out over acidic sites on the catalyst support. The hydrogenation step of mesityl oxide to methyl isobutyl ketone is then catalysed over palladium particles supported on the catalyst surface. However, both examples represent a process involving high pressures and energy inputs. This contributes significantly to the operating costs and puts an extra burden on the environment.

Therefore, a desirable target for researchers in terms of developing multifunctional catalysts for the one-pot synthesis is to operate this reaction process at ambient pressure.

Many of the previous experiments that were carried out with regard to the one-step process in the liquid phase were operated at 120-200°C and 20-50 bar H_2 pressure, employing bifunctional acid-base/redox catalysts comprising acidic cation-exchangers, zeolites, or zirconium phosphate with the addition of platinum group metals, typically palladium [35]. The one-step synthesis of MIBK in the gas phase has also attracted interest. However, the MIBK selectivity is generally lower than in the liquid-phase process, and catalyst deactivation may be a problem.

Numerous bifunctional catalysts have been studied with regard to the one-step synthesis of MIBK, both in gas and liquid-phase reactions. These include Pd or Pt supported on the zeolite, ZSM-5 [36-43], Pt supported on a gallosilicate and alminosilicate [44], NaX and CsX zeolites [27]; Pd supported on a MCM-22 [45], MCM-56 [28], SAPO-11 and AlPO-11 [46], ion exchange resins [29, 47], zirconium phosphate [48], niobic acid [49, 50] and heteropoly acid [10]; Pd, Ni, Cu or Pd-Cu supported on MgO, Mg/Al hydrotalcite and alumina [24, 26, 51-56]. Della Pina *et al.* have recently reported the one step conversion of acetone and carbon monoxide to MIBK in the absence of H_2, using copper supported on alumina as a catalyst [57]. The hydrogen gas obtained from the water gas shift reaction was used for the hydrogenation of mesityl oxide to MIBK. Recently, palladium supported on a ZnO-Cr_2O_3 mixed oxide (Zn/Cr = 1:10 mol/mol) has been reported to be a new, efficient bifunctional catalyst for the one-step synthesis of MIBK in the gas and liquid phases [58].

The aldollisation of acetone and the dehydration of DAA can be seen operating through the mechanism of bifunctional catalysis as proposed by Chen *et al.* [50]. This

mechanism was based on a comparative study carried out between Pd/Nb_2O_5-SiO_2 and Pd/SiO_2-Al_2O_3 catalysts which have been shown to possess a mixture of Brønsted acid and Lewis acid sites, with the Brønsted acidity being greater in the latter catalyst. It involves the rearrangment of one acetone molecule to form the enol tautomer over Lewis acid sites. It then reacts with an acetone molecule chemisorbed on a Brønsted acid site to form diacetone alcohol. After that, the DAA molecule is dehydrated to form MO (Figure 1.7). In spite of having a similar surface area, porosity and Pd dispersion in both systems, the catalyst activity for the Pd/SiO_2-Al_2O_3 was lower than that for the Pd/Nb_2O_5-SiO_2 catalyst system. However, other studies have shown high activity towards the one-step conversion of acetone to MIBK over Pd supported on a zeolite which was found to possess predominantly Brønsted acid sites. This would indicate that the presence of Lewis acid sites to form enol molecules at the reaction surface is not critical [36, 38].

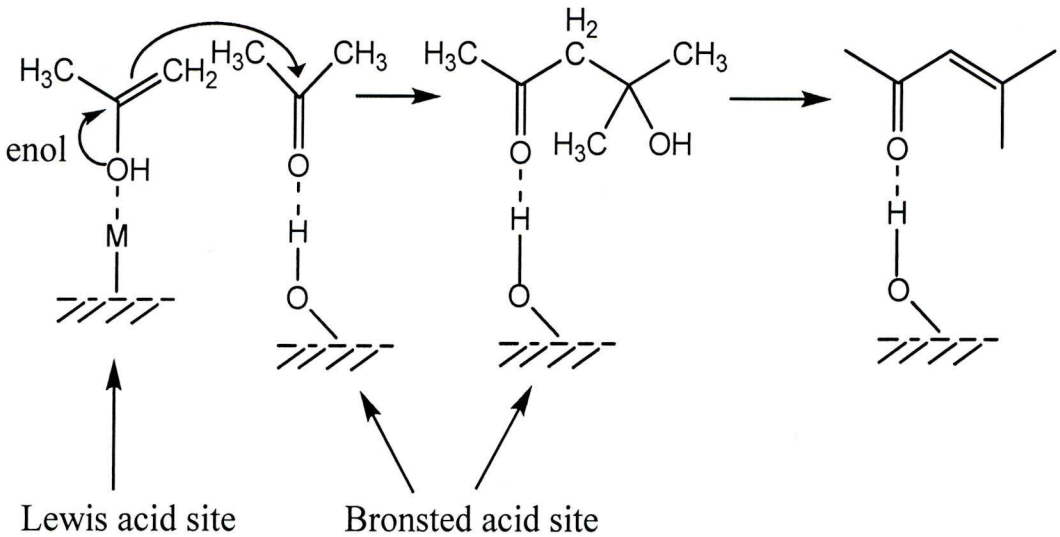

Figure 1.7 The suggested reaction mechanism for acetone condensation to mesityl oxide [50].

Higashio *et al.* described the reaction of one step conversion of acetone to MIBK over $Pd/Nb_2O_5 \cdot nH_2O$ catalyst as occuring via a consecutive mechanism [49]. In

this mechanism, mesityl oxide is formed directly by acetone condensation without the desorption of the intermediate diacetone alcohol and is then hydrogenated to MIBK over Pd particles that exist on the support surface. This was supported by the absence of diacetone alcohol among reaction products. Moreover, they carried out reaction between diacetone alcohol and mesityl oxide under the same reaction conditions and found that the conversion of diacetone alcohol was much higher than that of acetone to MIBK and that mesityl oxide was almost completely converted to MIBK at a fast rate. These findings suggest that the the aldol reaction of acetone to diacetone alcohol on the acid sites is the rate-determining step in this process.

It has been shown that for α, β unsaturated aldehydes and ketones, palladium and platinum are selective for the hydrogenation of the C=C bond instead of the carbonyl group. Metal-substrate adsorption studies were carried out by Delbecq and Sautet who concluded that platinum and palladium were selective for hydrogenating the C=C double bond for several reasons [59]. One reason is that the C=O π electron system is not utilized in the molecular adsorption, as only the C=C bond is involved in the chemisorption (e.g. in a di-σ_{CC} coordination), with the only carbonyl-metal interaction being an electrostatic interaction between the oxygen lone pair and the surface. Secondly, both double bonds are involved in a quasi-planar η_4 adsorption. This results in the hydrogenation of the C=C bond being kinetically more favourable because of the repulsion of the surface by the four electrons involved in the adsorption [59].

Even though Pd and Pt are both selective for C=C hydrogenation, they have different efficiencies in this reaction. In previous studies on hydrogenation of alkenes, Pd metal sites were shown to be more efficient than Pt metal sites, and therefore Pd is more commonly employed for hydrogenation of α-β unsaturated ketones [60-62]. This can be due to the fact that bulk palladium metal has a slightly higher Fermi level than

Pt, and the width of d-band significantly lower compared to that of Pt. As a consequence, the radial expansion of Pd d-orbitals is smaller than that of the Pt orbitals. Therefore the overlap of the metal's d-orbitals with the orbitals of the adsorbate molecule is reduced with Pd, and a weaker interaction results between the adsorbate molecules and the surface. This weaker interaction leads to less repulsion between the Pd metal surface and the adsorbate, and stabilizes the C=C adsorption geometry [59]. Therefore, hydrogenation of mesityl oxide occurs *via* chemisorption of C=C bond to Pd atoms doped on the catalyst support (Figure 1.7).

The opportunity for a higher C=C hydrogenation selectivity is increased by producing a catalyst with a small average metal particle size. When palladium particle size decreases, the average distance between the metal particles and the acid/base sites also decreases [46]. For MIBK synthesis, the co-operation between the hydrogenation and the acid/base functions is required to drive the reaction forward towards the desired product MIBK when the distance between these functions are smaller. In contrast, increasing the distance between hydrogenation and acid/base functions might influence the equilibrium by shifting it back towards the starting reagent, acetone. Chen *et al.* explained how Pd particles may aggregate when the Pd loading is at higher levels, leading to covering of basic sites on their Pd/hydrotalcite derived catalyst [53].

In the one-step synthesis of MIBK, isopropanol (IP) forms as a by-product by direct hydrogenation of the C=O group in acetone on metal sites. C_3 by-products are also formed by the acid-catalysed dehydration of IP to propene on the acidic sites, followed by hydrogenation of propene to propane on metal sites. C_9 by-products such as diisobutyl ketone (DIBK), mesitylene, and isophorone, also form as a result of further condensation reactions of MIBK or DAA and MO on the active sites (Figure 1.8).

DIBK is a useful chemical material used as a solvent for a variety of natural and synthetic resins.

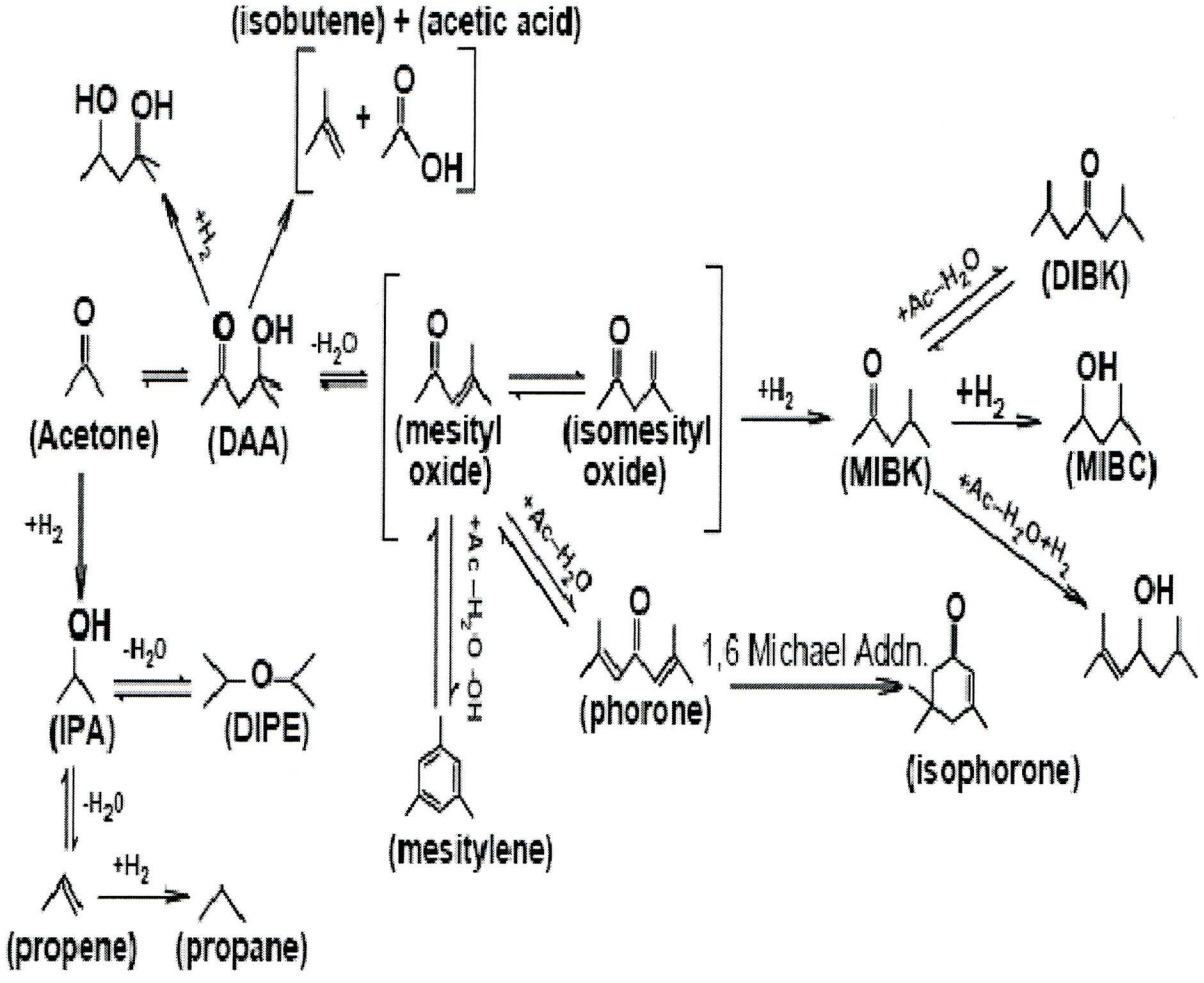

Figure 1.8 Major reaction pathways in the synthesis of MIBK from acetone (Ac) [63].

The strength of acid/base sites and the activity of metal sites in the MIBK bifunctional catalytic system play an important role in the reaction network. For example, acetone is directly hydrogenated to IP in the presence of extremely active hydrogenating metals. Similar to this, the selectivity to C_{9+} by-products increases in the presence of strong acid/base sites coupled with a metal that possesses low hydrogenating activity. Therefore, it is essential that a proper balance of acid/base sites

for acetone condensation and metal site concentration for mesityl oxide hydrogenation to MIBK is obtained.

The optimal reaction conditions require extensive catalyst testing for each individual bifunctional catalyst. The nature of the metal and acidity/basicity of the catalyst has an influence on optimal reaction conditions such as the H_2/acetone feed ratio and reaction temperatures. Therefore, extensive catalyst testing for each individual bifunctional catalyst is necessary. Increasing reaction temperatures leads to a rise in the selectivity towards over condensation products [33, 51]. Two possible explanations for this trend are: (i) the metal sites activity decreases at higher temperatures, and/or (ii) the activity of the acid/base sites towards C_{9+} by-products increases with increasing reaction temperatures.

Catalyst stability, which is defined as the ability of a catalyst to maintain constant activity over a prolonged period of time, depends on the relative activity and strength of both the acid/base and the metal functions. It is most likely that the catalyst deactivation occurs when the acid/base sites are too strong relative to the hydrogenating sites, which leads to the formation of high boiling products. This process is known as coking, where the high boiling products formed block the acid/base sites, causing a decrease in reaction conversion [64]. However, coke formation can be reduced by designing an optimal balance of both acid/base and metal functions.

1.5. α-Pinene as renewable feedstock for organic synthesis

Bicyclic terpene α-pinene is an inexpensive major component of turpentine oils obtained from coniferous trees by steam distillation [65]. α-Pinene, like many other terpenes, is a highly reactive compound. It undergoes thermal rearrangement in the gas phase between 300°C and 400°C without any catalyst, to give a complex mixture of cyclic and acyclic monoterpene isomers $C_{10}H_{16}$ such as *β*-pinene, tricyclene, camphene, limonene, *p*-cymene, terpinenes, terpinolenes, phelandrenes, etc. [66]. It can be used as a starting material for the synthesis of many valuable products in various chemical processes such as isomerisation, epoxidation, hydration and dehydroisomerisation [65]. In this section, isomerisation and dehydroisomerisation of α-pinene are the processes that will be discussed in more detail because of their relevance to our work.

1.5.1. Isomerisation of α-pinene

Catalysts have a great effect on the products of α-pinene isomerisation [65, 67]. Figure 1.9 shows the products that form in the isomerisation of α-pinene. This isomerisation can be performed via a two-step process as suggested by Rudakov *et al.* ([68, 69] and references therein). The first step is protonation of the α-pinene double bond to form a pinylcarbenium ion intermediate. In the second step, this carbenium ion rearranges to form monocyclic terpenes such as limonene and limonene-derived products, as well as tricyclic terpenes such as camphene and tricyclene. Because limonene has greater reactivity than camphene, further transformations of limonene into various monocyclic terpenes may occur, followed by disproportionations into

menthenes and cymenes. It has been suggested that disproportionation of terpenes into menthenes and cymenes can only take place on mesoporous and macroporous catalysts [65]. Severino *et al.* studied the effect of extra-lattice aluminium species on the activity, selectivity and stability of acid zeolites in α-pinene isomerisation in the liquid phase. They found that formation of p-menthadienic compounds is favourable in the presence of strong acid sites at high temperatures. In contrast, formation of camphenic compounds is feasible at low temperatures and with weak acid sites [70].

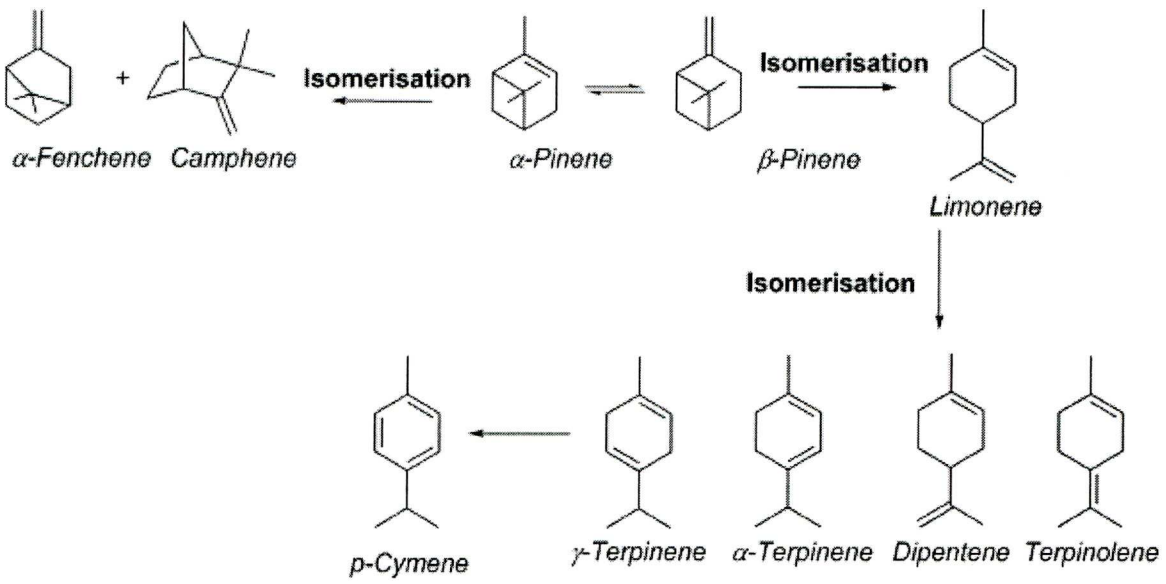

Figure 1.9 Some of the possible products resulting from isomerisation of pinene [65].

In industry, TiO_2 is used as the catalyst for isomerisation of α-pinene under atmospheric pressure at temperatures >100°C in closed systems. The rate of isomerisation is low to yield around 75-80% camphene, limonene, tricyclene, and small amounts of flenchenes and bornylene [71]. The disadvantage of the low rate of isomerisation has led researchers to develop new catalysts which have the ability to carry out the reaction with a higher degree of activity and greater selectivity to camphene and/or limonene.

Many solid acids such as zeolites have been used as effective catalysts for α-pinene isomerisation because they possess an appropriate acidity as well as shape selectivity. As an example, Lopez *et al.* [72] reported dealuminated mordenites and Y-zeolites as catalysts for the isomerisation of α-pinene. These reactions were carried out in the liquid phase using a batch reactor at 393 K. They found that camphene and limonene were produced as main products over both zeolites with similar selectivity of 54% to camphene/(camphene+limonene). The total yield was 68% over mordenite, while over Y zeolite the formation of undesired compounds was favoured. This was explained by the wider pore diameter and larger pore volume of the zeolite Y, which are favourable for the formation of undesired products.

Allahverdiev *et al.* [68, 73, 74] reported isomerisation of α-pinene over clinoptilolite, a natural zeolite, in the liquid phase using a batch reactor under various reaction conditions (pressures of 1-25 bar and temperatures of 373-453 K). They found that camphene and limonene were the main products. Small amounts of other products, such as monocyclic and tricyclic terpenes, were also formed when conversion was at a higher level (80-85%). Increasing reaction temperature led to an increase in the catalyst activity. Also the rate of reaction was found to depend on pressure below 10 bar while at a >10 bar pressure there was no influence.

Akpolat *et al.* [75] also studied clinoptilolite as a catalyst for this reaction. The reaction was carried out under atmospheric pressure in nitrogen at a temperature of 428 K in the liquid phase using a batch slurry reactor. They found that camphene and limonene were the main products with total selectivity for both compounds between 61-77% and conversion of more than 50%. Catalyst activity was found to depend on the catalyst calcination temperature. When the temperature decreased, the activity increased. This was explained by the disappearance of Bronsted acidic sites at higher

calcination temperatures. Moreover, limonene selectivity increased from 37% to 51% when conversion decreased from 42% to 25%, while selectivity to camphene was independent on the change in conversion.

Another study using zeolites Beta, ZSM-5, mordenite and MCM-41 for isomerisation of α-pinene in the liquid phase under ambient pressure at 100°C was carried out by Gunduz et al. [76-78]. They found that over Beta zeolite with a Si/Al ratio of 55 conversion of α-pinene was the highest (>99%), with yields between 25-28% and 13-21% for camphene and terpinenes, respectively. Other products, such as terpinolenes and heavy byproducts, were also observed. The highest limonene selectivity of around 38% was obtained for the MCM-41 zeolite, whereas the α-pinene conversion was lower than that for Beta zeolite. The high level of activity of Beta zeolite is probably due to an appropriate combination of acidity and pore size [76, 77].

Modified clays have also been used as effective solid acid catalysts for isomerisation of α-pinene. These include acid-activated, polycation exchanged clays [79], acid pretreated montmorillonite [80], Indian montmorillonite modified by sulphuric acid or exchanged with Ce^{3+}, Fe^{3+}, La^{3+}, or Ag^{+} [81] and kaolinitic acid-treated clays [82]. As an example, Volzone *et al.* [82] used a kaolinitic H_2SO_4-treated clay for α-pinene isomerisation in the liquid phase, under atmospheric pressure at a temperature of 100°C. They found that camphene and limonene were the major products with selectivities around 65% and 25%, respectively, at α-pinene conversion between 67 and 94%.

Many other catalysts have been reported for α-pinene isomerisation such as metal (IV) phosphate polymer [83], silica-supported rare earth oxide [84], ytterbium oxide supported on silica [85], Amberlyst-35 resin [86] and mesoporous

SO_4/ZrO_2/HMS [87, 88]. High conversions of up to 98% were obtained with the production of camphene and limonene as the major products.

1.5.2. Dehydroisomerisation of α-pinene

p-Cymene is an important chemical produced on an industrial scale and is used as a solvent for dyes and varnishes, as an additive in musk perfume and fragrances and as a masking odour for industrial products. It is also used as a heat transfer medium, but mainly it is used for the synthesis of p-cresol, which is further transformed to the widely used antioxidant 2,6-di-tert-butyl-p-cresol [31].

Numerous bifunctional catalysts have been studied in p-cymene synthesis, both in gas- and liquid-phase reactions. These include activated Al_2O_3 [89], activated nickel [90], Na supported chromia-alumina [91], supported alkali metal hydroxide [92], alumina and chromia-alumina [93], Ce promoted Pd/ZSM5 [94].

Currently, p-cymene is produced in a mixture with o- and m-isomers by the alkylation of toluene with propene, followed by isomer separation. Given the projected shortage of petroleum-based feedstocks, a more attractive route to p-cymene might be the transformation of cyclic monoterpenes – naturally occurring renewable feedstock. It has been demonstrated that limonene, carene, α-pinene and monoterpene mixtures can be converted to p-cymene with good yields, co-producing H_2 ([65, 67] and references therein). Hölderich *et al.* [67] have reported an advanced catalytic synthesis of p-cymene by dehydrogenating α-pinene. Reaction was carried out in a fixed bed reactor over a 0.5% Pd/SiO_2 catalyst in the gas phase at 300°C to yield 67% p-cymene at 100% α-pinene conversion. The catalyst suffers from deactivation due to coke formation. Co-feeding hydrogen allows improvement in the stability of the catalyst performance.

Furthermore, Jaramillo *et al.* [95] have reported heteropoly acid supported on a mesoporous silica as a bifunctional catalyst for p-cymene synthesis from α-pinene in the liquid phase using a batch reactor. Reaction was performed at a temperature between 40-160°C to yield 70% p-cymene at 100% α-pinene conversion.

The transformation of α-pinene to p-cymene can be viewed as proceeding via the mechanism of bifunctional catalysis as proposed by Hölderich *et al.* [67]. It involves fast α-pinene isomerisation to p-menthadienic (limonene and its isomers) and camphenic compounds on acid sites of the catalyst, followed by the rate-limiting dehydrogenation of p-menthadienic precursor(s) to form p-cymene (equation 1.8).

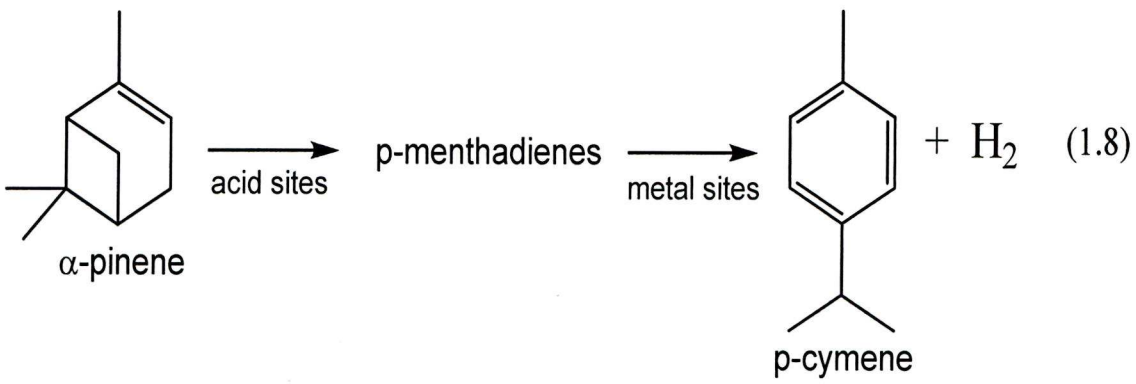

(1.8)

1.6. Zn-Cr and Zn-Cr-Cu mixed oxide catalysts

Zn^{II}-Cr^{II} and Zn^{II}-Cr^{III}-Cu^{II} mixed oxide catalysts which contain Lewis and Bronsted acid sites have been used as effective catalysts and supports for various reactions in organic synthesis, such as hydrocarbon fluorination with HF [96, 97], carboxylic acid hydrogenation [98], alcohol dehydrogenation [99], quinoline production from aniline and glycerol [100], dehydrogenation of 2-butanol to 2-butanone [101], dehydrogenation of cyclohexanol to cyclohexanone [102] and selective catalytic reduction of NO with NH_3 [103]. Zn-Cr oxide has also been used in methanol synthesis

[104, 105], hydrocarbons synthesis [106], methanol dehydrogenation [107] and higher alcohol synthesis [108, 109]. Moreover, Pt/Zn–Cr has been used as an effective catalyst for the low-temperature dehydrogenation of isobutane [110, 111].

In this study we investigate the one-step synthesis of MIBK in the gas and liquid phase over Pd supported on Zn-Cr oxide, as well as over Pd-free Zn-Cr-Cu oxides in the gas phase. In addition, we report on Zn-Cr and Pd/Zn-Cr catalysts for the one-step synthesis of p-cymene in the gas phase. Although Zn-Cr and Zn-Cr-Cu oxides have long been used as catalysts for various reactions, neither Zn-Cr and Zn-Cr-Cu oxides, nor Pd/Zn-Cr, have been used for the synthesis of MIBK or p-cymene prior to our work.

1.6.1. Preparation of Zn-Cr mixed oxide

Several methods have been documented for the preparation of Zn-Cr and Zn-Cr-Cu oxide catalysts. For example, Ohta *et al.* [110] described three different methods for the preparation of Zn-Cr oxide in their study of the preparation and characterisation of a Pt/ZnO-Cr_2O_3 catalyst for low-temperature dehydrogenation of isobutene. First, ZnO-Cr_2O_3 mixed oxide was obtained by kneading ZnO together with an aqueous suspension of Cr_2O_3 for 2 h. The resultant paste was dried at room temperature for 24 h, followed by calcination at 500°C for 1 h under air flow. Secondly, ZnO-Cr_2O_3 was prepared by coprecipitation method by dropwise addition of an aqueous solution of NH_4OH or Na_2CO_3 to an aqueous solution of Zn^{II} and Cr^{III} nitrates at a controlled pH. The precipitates were filtered off, washed with deionised water until ammonia or carbonate free, dried in air at 100°C for 12 h and finally calcined under air flow at 500°C for 1 h. The third preparation method involved heating a mixed aqueous solution

of Zn^{II} and Cr^{III} nitrates and urea at 95–98°C. The precipitate obtained was washed, dried and calcined under the same conditions as in the second preparation method. Coprecipitation was found to be the most convenient method for the preparation of Zn-Cr and Zn-Cr-Cu oxides [58, 102, 105-107, 112].

The Pd-doped Zn-Cr mixed oxide catalysts have been prepared by impregnating Zn-Cr oxides with a 0.02 M solution of $Pd(OAc)_2$ in benzene for 1 h at room temperature, followed by evaporation of the solvent in a rotary evaporator and subsequent reduction of Pd^{II} to Pd^0 by a hydrogen flow (30 mL/min) at 250°C for 2 h [58].

Wu *et al.* prepared a range of Cu-Zn-Cr layered double hydroxides (LDHs) with different Cu/Zn/Cr atomic ratios and studied their stability towards leaching in aqueous media [113]. They have found that all LDHs have similar chemical stability with a decreased Cr^{3+} leaching at pH > 5. The leaching of Cu^{2+} and Zn^{2+} is decreased at pH > 6.

1.6.2. Properties of Zn-Cr and Zn-Cr-Cu oxides

1.6.2.1. The composition of Zn-Cr and Zn-Cr-Cu oxides

Zn-Cr oxides can be amorphous or crystalline, depending on the calcination temperature [58]. Kozhevnikova *et al.* have characterised Zn-Cr (1:10) oxide calcined at 300°C and 350°C by XRD and found that the oxide is amorphous after calcination at 300°C and crystalline after calcination at 350°C [58]. The crystalline oxide contained the Cr_2O_3 and $ZnCr_2O_4$ phases.

Simard *et al.* [106] and Bradford *et al.* [105] observed that when the Cr/Zn ratio is increased from 0.5 to 15 (calcined at 350°C) and from 0 to 1.9 (calcined at 700°C) respectively, the content of ZnO phase decreases and $ZnCr_2O_4$ increases. Further increase in the chromium content resulted in the appearance of Cr_2O_3 crystalline phase and a concomitant decrease in $ZnCr_2O_4$ content.

XRD measurement of a Zn-Cr-Cu oxide catalyst which has been carried out by Wang *et al.* [112] shows how variation of copper content affects the structure of Zn-Cr-Cu oxide. They noticed that at a copper content $\leq 40\%$ in the catalysts, copper is present as Cu_2O and Cu(0), and no signal of chromium species appears in XRD patterns. This indicates that chromium species are completely dispersed and present in amorphous phase. The same results were subsequently reported by Kumar *et al.* [102]. They prepared and characterised a Zn-Cr-Cu oxide for dehydrogenation of cyclohexanol to cyclohexanone and found that characteristic peaks attributable to CuO and ZnO are clearly observed in the XRD patterns of calcined catalysts, and characteristic peaks attributable to Cu metal are observed in the XRD patterns of the reduced catalysts. Peaks of chromium oxide have not been observed in either the calcined or reduced catalysts, and this is an indication of the presence of chromium oxide in the amorphous phase.

1.6.2.2. Thermal behaviour

Thermal behaviour of Zn-Cr and Zn-Cr-Cu oxides is of great importance for their use in heterogeneous catalysis. It is usually characterised by thermal analytical methods (thermal gravimetric analysis (TGA), differential thermal analysis (DTA), and differential scanning calorimetry (DSC)), frequently in combination with other techniques such as X-ray diffraction, infrared spectroscopy, solid state NMR, etc.

Thermal behaviour of Zn-Cr and Zn-Cr-Cu oxides has already been the subject of many investigations under different atmospheric environments such as air, H_2 and N_2 [58, 106, 113-116]. The thermal measurements that have been carried out under nitrogen atmosphere show two main stages of loss of water from the catalysts in the temperature range from 0 - 1000°C. These can be explained as follows:

- The first stage takes place in the range from room temperature to 250 - 300°C. It shows an endothermic peak centred between 120 - 160°C, which corresponds to the removal of physisorbed water from the catalyst surface, as well as the removal of water resulting from hydroxyl group condensation to form solid products such as ZnO, $ZnCr_2O_4$ and CrOOH [113-116].

- In the second stage, in the temperature range from 300 to 1000°C, a second endothermic weight loss centred between 500 - 560°C appears. This weight loss can be attributed to the removal of water resulting from further condensation of hydroxyl groups in CrOOH to form a lower chromium oxide Cr_2O_3 as well as $ZnCr_2O_4$ [106, 116].

The amorphous and crystalline Zn-Cr oxides can have different water content, as reported by Kozevnikova *et al.* [58]. Thus, amorphous Zn-Cr (1:10) oxide calcined at 300°C, contains 8.3 wt% water, whereas crystalline oxide calcined at 350°C only 2.0 wt% [58].

1.6.2.3. Surface area and porosity

Texture properties of Zn-Cr and Zn-Cr-Cu oxide catalysts has been the subject of many investigations [58, 100, 105, 106, 117, 118] and, whenever possible, the results

obtained from these studies are used for comparison with our data for both amorphous and crystalline oxides. Zn-Cr and Zn-Cr-Cu oxides possess various surface areas depending on catalyst composition (amorphous or crystalline), as well as on preparation method and calcination temperature [58, 101, 105, 106, 110, 119-121]. Ohta *et al.* prepared and characterised $Pt/ZnO\text{-}Cr_2O_3$ catalysts for the low-temperature dehydrogenation of isobutene using different preparation methods [110]. They found that the catalyst surface area varies, depending on the method by which the catalyst was prepared. They have also found that the larger the surface area, the smaller the ZnO crystallite size. It has also been reported in the literature [105, 106] that surface area increases with an increase in the chromium content at the same calcination temperature. At a constant Zn/Cr ratio, surface area increases with a decrease in the calcination temperature [58, 105, 106]. Catalyst pore volume also increases with decreasing the calcination temperature, in contrast to pore diameter, which increases with an increase in the calcination temperature [58, 106].

Sintering of microcrystalline metallic copper may also reduce the surface area, as observed by Wang *et al.* [101]. They have prepared and characterised $Cu\text{-}ZnO\text{-}Cr_2O_3/SiO_2$ catalysts for dehydrogenation of 2-butanol to 2-butanone and found that surface area decreases with the increase in reduction temperature. They have suggested that sintering of microcrystalline metallic copper may be the main reason for this. Moreover, they have found that the average pore volume increases with the increase in the reduction temperature, without change in the average pore diameter.

1.6.2.4. Acidity of Zn-Cr oxides

Catalyst acidity plays an important role in heterogeneous catalytic reactions. It is determined using a range of techniques [122]. The nature (Brønsted or Lewis) of acid sites in solid catalysts can be determined by FTIR of an adsorbed probe molecule, e.g. pyridine [122]. The fingerprint region of IR spectrum (1560-1420 cm^{-1}) is of the most interest, revealing information about the nature of acid sites.

Recently, acidity of Zn-Cr oxide catalysts was studied by differential scanning calorimetry (DSC) of adsorbed NH_3 [58]. This study showed that both amorphous (calcined at ≤300°C) and crystalline (calcined at >350°C) oxides possess acid sites of moderate strength. The number of acid sites in amorphous Zn-Cr (1:10) oxide measures 1.95 $mmol/g_{cat}$, and the initial enthalpy of ammonia adsorption −117 kJ/mol. The corresponding values for the crystalline oxide are 1.21 $mmol/g_{cat}$ and −127 kJ/mol.

1.6.2.5. Enhancement of activity of Zn-Cr-Cu catalyst

Sintering of Cu particles resulting from prolonged hydrogen treatment at higher temperatures, as well as the formation of coke on the Cu active sites, can be the reasons for the drop in activity of Cu catalysts [26]. Therefore, many studies have been carried out to enhance catalyst activity of these catalysts in organic reactions. The literature has discussed the improvement of catalyst activity with Zn added to Cu for methanol synthesis [119, 123, 124] and for the dehydrogenation of isoamyl alcohol [121]. Melian-Cabrera *et al.* [123] have reported such enhancement of catalyst activity for the hydrogenation of CO_2 to methanol. They suggested that this improvement is caused by the addition of Zn to the catalyst which has led to the appearance of the CuO reduction peak at a lower temperature (183°C) in comparison with that for pure CuO oxide

(271°C), as found by temperature-programmed reduction of CuO-ZnO. Moreover, addition of palladium as palladium oxide to CuO-ZnO also enhances reduction of CuO by shifting the CuO reduction peak towards a lower temperature (168°C) compared with that in pure CuO and CuO-ZnO. Furthermore, the appearance of a reduction peak at 72°C is an indication of partial reduction of PdO as well as CuO in the PdO-CuO-ZnO catalyst. This is supported by the greater amount of hydrogen consumed for the reduction of both PdO and CuO than that needed for the PdO reduction only. All these results are evidence that H_2 spillover from Pd(0) to Cu(0) takes place, which has led to improved activity and performance stability of the PdO-CuO-ZnO catalyst [123].

1.7. Objectives and thesis outline

The aim of this work is to develop new heterogeneous multifunctional catalysts based on Zn^{II}-Cr^{III} and Zn^{II}-Cr^{III}-Cu^{II} mixed oxides for the one-step synthesis of methyl isobutyl ketone (MIBK) from acetone and hydrogen and one-step dehydroisomerisation of α-pinene to p-cymene. Our goal is to understand the operation of these catalysts and to explain and exploit their multifunctional properties in the above reactions.

This work involves:

a) Preparation of a series of Zn-Cr and Zn-Cr-Cu oxides and Pd doped Zn-Cr oxides.

b) Thorough characterisation of the prepared catalysts by BET (surface area and porosity), TGA (water content and thermal stability), XRD (crystallinity), ICP (chemical composition), NH_3 and pyridine adsorption combined with calorimetry and infrared spectroscopy (acidity) and H_2 adsorption (Pd dispersion).

c) Catalyst testing in one-step MIBK synthesis in liquid phase (batch reactor) and gas phase (fixed-bed reactor).

d) Catalyst testing in one-step dehydroisomerisation of α-pinene to p-cymene in gas phase (fixed-bed reactor).

Chapter 2, the experimental section, focuses on preparation of Pd doped Zn-Cr oxide and bulk Zn-Cr-Cu oxide, which are used in this study as redox/acid multifunctional catalysts for the synthesis of MIBK from acetone and hydrogen and p-cymene from α-pinene. Following the discussion of catalyst preparation, the characterisation techniques that have been used in the determination of water content, surface area and porosity and the acidity of the catalysts will be described in detail. Finally, a description of the reaction procedure and the experimental set up will be provided.

Chapter 3 will concentrate on the results and discussion of the catalyst characterisations of the prepared Zn-Cr and Zn-Cr-Cu oxides and palladium doped Zn-Cr oxide catalysts involved in this study. The catalyst characteristics discussed are the thermal stability, elemental composition, surface area, pore structure and pore volume, acidity, crystallinity of the catalyst materials and the palladium dispersion on the catalyst surfaces.

Chapter 4 presents the catalytic performance of the Pd/Zn-Cr and Zn-Cr-Cu catalysts in the one-step synthesis of MIBK from acetone and hydrogen. The catalyst performance has been monitored under varied operating conditions and at different Pd and Cu content in the catalysts.

Chapter 5 details the results for the one-step conversion of α-pinene to p-cymene in the gas phase using the Zn-Cr and Pd doped Zn-Cr oxide catalysts.

Finally, **Chapter 6** provides a summary of the findings from the previous sections and offers some concluding comments.

References

[1] A. Bruggink, R. Schoevaart, T. Kieboom, Org. Process. Res. Dev. 7 (2003) 622.

[2] J.C. Wasilke, S.J. Obrey, R.T. Baker, G.C. Bazan, Chem. Rev. 105 (2005) 1001.

[3] D.E. Fogg, E.N. dos Santos, Coord. Chem. Rev. 248 (2004) 2365.

[4] M. Bowker, The Basis and Application of Heterogeneous Catalysis, Oxford Science Publications, 53, 1998.

[5] W. Keim, Green. Chem. 5 (2003) 105.

[6] C.D. Chang, Catal. Rev. -Sci. Eng. 26 (1984) 323.

[7] C.D. Chang, W.H. Lang, A.J. Silvestri, US Patent 4062905, 1977.

[8] G.C. Bond, Heterogeneous Catalysis: Principles and Applications, 2 ed., Clarendon Press, Oxford, p 23-30.

[9] J.M. Thomas, W.J. Thomas, Principles and Practice of Heterogenious Catalysis, - Weinheim; New York; Basel; Cambridge; Tokyo: VCH, 1996.

[10] R.D. Hetterley, E.F. Kozhevnikova, I.V. Kozhevnikov, Chem. Commun. (2006) 782.

[11] G.D. Pringruber, K. Seshar, J.A. Lercher., J. Catal. 186 (1999) 188.

[12] B.G. Cox, The Basis and Application of Heterogeneous Catalysis, Oxford Science Publications, 1994.

[13] B.C. Gates, Catalytic Chemistry, Wiley, 1991.

[14] G.C.A. Schuit, B.C. Gates, CHEMTECH, 1983, Sept, 556.

[15] B. Cornils, W. A. Herrmann, R. Schlogl, C.-H. Wang, (Eds.), Catalysis from A to Z: A Concise Encyclopedia, Wiley-VCH, New York, 2000, p. 395.

[16] W. Fliege, G. Heiien, A. Nissen, E. Sapper, A. Wittver, US Patent 4239657, 1980.

[17] M.J.F.M. Verhaak, A.J. Vandillen, J.W. Geus, Appl. Catal. A 109 (1994) 263.

[18] C. Carlini, M. Marchionna, M. Noviello, A.M.R. Galletti, G. Sbrana, F. Basile, A. Vaccari, J. Mol. Catal. A. 232 (2005) 13.

[19] D. Tichit, B. Coq, S. Cerneaux, R. Durand, Catal. Today. 75 (2002) 197.

[20] P.B. Weisz, E.W. Swegler, J. Phys. Chem. 59 (1955) 823.

[21] J.I. Kroschwitz, M. Howe-Grant, Kirk-Othmer Encyclopedia of Chemical Technology, 4th ed., 1995.

[22] J.I. Di Cosimo, G.Torres, C.R. Apesteguı´a, J. Catal. 208 (2002) 114.

[23] F. Winter, M. Wolters, A.J.V Dillen, K.P. de Jong, Appl. Catal. A 307 (2006) 231.

[24] K. Lin, A. Ko, Appl. Catal. A 147 (1996) L259.

[25] N. Cheikhi, M. Kacimi, M. Rouimi, M. Ziyad, L.F. Liotta, G. Pantaleo, G. Deganello, J. Catal. 232 (2005) 257.

[26] V. Chikan, A. Molnar, K. Balazsik, J. Catal. 184 (1999)134.

[27] L.V. Mattos, F.B. Noronha, J.L.F. Monteiro, J. Catal. 209 (2002) 166.

[28] P.P. Yang, J.F. Yu, Z.L. Wang, M.P. Xu, Q.S. Liu, X.W. Yang, T.H. Wu, Catal. Commun. 6 (2005) 107.

[29] W. Nicol, E.L.d. Toit, Chem. Eng. Process. 43 (2004) 1539.

[30] F. Winter, A.J. Dillen, K.P. Jong, J. Mol. Catal. A 219 (2004) 273.

[31] K. Weissermel, H.-J. Arpe, Industrial Organic Chemistry, 3rd ed., VCH Publishers, Weinheim, 1997.

[32] Y. Onoue, Y. Mizutani, S. Akiyami, Y. Izumi, Y. Watanabi, J. Mackawa, Bull. Jpn. Petr. Inst. 16 (1974) 55.

[33] G.G. Podrebarac, F.T.T. Ng, G.L. Rempel, Chem. Eng. Sci. 52 (1997) 2991.

[34] A.A. Nikolopoulos, B.W.L. Jang, J.J. Spivey, Appl. Catal. A 296 (2005) 128.

[35] K. Weissermel, H.-J. Arpe, Industrial Organic Chemistry, 4th ed., Wiley-VCH, 2003.

[36] P.Y. Chen, S.J. Chu, N.S. Chang, T.K. Chuang, L.Y. Chen, Stud. Surf. Sci. Catal. 46 (1989) 231.

[37] P.Y. Chen, S.J. Chu, W.C. Lin, K.C. Wu, C.L. Yang, Stud. Surf. Sci. Catal. 83 (1994) 481.

[38] P.P. Yang, Y.C. Shang, J. Wang, J.F. Yu, T.H. Wu, React. Kinet. Catal. Lett. 91 (2007) 391.

[39] T.J. Huang W.O. Haag, US Patent 4339606, 1982.

[40] L. Melo, G. Giannetto, L. Cardozo, A. Llanos, L. Garcia, P. Magnoux, M. Guisnet, F. Alvarez, Catal. Lett. 60 (1999) 217.

[41] L. Melo, G. Giannetto, F. Alvarez, P. Magnoux, M. Guisnet, Catal. Lett. 44 (1997) 201.

[42] L. Melo, A. Llanos, L. Garcia, P. Magnoux, F. Alvarez, M. Guisnet, G. Giannetto, Catal. Lett. 51 (1998) 207.

[43] P.Y. Chen, S.J. Chu, C.C. Chen, N.S. Chang, W.C. Lin, T.K. Chuang, US Patent 5059724, 1991.

[44] Y. Diaz, L. Melo, M. Mediavilla, A. Albornoz, J.L. Brito, J. Mol. Catal. A 227 (2005) 7.

[45] P.P. Yang, Y.C. Shang, J.F. Yu, J. Wang, M.L. Zhang, T.G. Wu, J. Mol. Catal. A 272 (2007) 75.

[46] S.-M. Yang, Y.M. Wu, Appl. Catal. A 192 (2000) 211.

[47] C.U. Pittman, Y.F. Liang, J. Org. Chem. 45 (1980) 5048.

[48] Y. Watanabe, Y. Matsumura, Y. Izumi, Y. Mizutani, J. Catal. 40 (1975) 76.

[49] Y. Higashio, T. Nakayama, Catal. Today 28 (1996) 127.

[50] Y.Z. Chen, B.J. Liaw, H.R. Tan, K.L. Shen, Appl. Catal. A 205 (2001) 61.

[51] M. Martínez-Ortiz, D. Tichit, P. Gonzalez, B. Cog, J. Mol. Catal. A 201 (2003) 199.

[52] N.N. Das, S.C. Srivastava, Bull. Mater. Sci. 25 (2002) 283.

[53] Y.Z. Chen, C.M. Hwang, C.W. Liaw, Appl. Catal. A 169 (1998) 207.

[54] N. Das, D. Tichit, R. Durand, P. Graffin, B. Coq, Catal. Lett. 71 (2001) 181.

[55] L.M. Gandia, M. Montes, Appl. Catal. A 101 (1993) L1.

[56] S. Narayanan, R. Unnikrishnan, Appl. Catal. A 145 (1996) 231.

[57] C. Della Pina, E. Falletta, M. Rossi, M. Gargano, P. Giannoccaro, R. Ciriminna, M. Pagliaro, Appl. Catal. A 321 (2007) 35.

[58] E.F. Kozhevnikova, I.V. Kozhevnikov, J. Catal. 238 (2006) 286.

[59] F. Delbecq, P. Sautet, J. Catal. 152 (1995) 217.

[60] R.L. Augustine, Catal. Rev. 13 (1976) 285.

[61] P.N. Rylander, Hydrogenation Methods, in: C.O. Methcohn, A.R. Katrizky, C.W. Rees (Eds.), Best Synthetic Methods, Academic Press, New York, 1988, 70.

[62] J. Wisniak, M. Herskowitz, D. Roffe, S. Smilovitz, Ind. Eng. Chem. Prod. Res. Dev. 15 (1976) 163.

[63] W.K. O'Keefe, M. Jiang, F.T.T. Ng, G.L. Rempel, Chem. Eng. Sci. 60 (2005) 4131.

[64] I.V. Kozhevnikov, J. Mol. Catal. A 262 (2007) 86.

[65] A. Corma, S. Iborra, A. Velty, Chem. Rev. 107 (2007) 2411.

[66] A. Stolle, B. Ondruschka, W. Bonrath, Eur. J. Org. Chem. (2007) 2310.

[67] D.M. Roberge, D. Buhl, J.P.M. Niederer, W.F. Hölderich, Appl. Catal. A 215 (2001) 111.

[68] A.I. Allahverdiev, G. Gunduz, D.Y. Murzin, Ind. Eng. Chem. Res. 37 (1998) 2373.

[69] G.A. Rudakov, Chemistry and Technology of Camphor; Nauka, Moscow, 1976.

[70] A. Severino, A. Esculcas, J. Rocha, J. Vital, L.S. Lobo, Appl. Catal. A 142 (1996) 255.

[71] A. Severino, J. Vital, L.S. Lobo, Stud. Surf. Sci. Catal. 78 (1993) 685.

[72] C.M. Lopez, F.J. Machado, K. Rodriguez, B. Mendez, M. Hasegawa, S. Pekerar, Appl. Catal. A 173 (1998) 75.

[73] A.I. Allahverdiev, S. Irandoust, D.Y. Murzin, J. Catal. 185 (1999) 352.

[74] A.I. Allahverdiev, S. Irandoust, B. Andersson, D.Y. Murzin, Appl. Catal. A 198 (2000) 197.

[75] O. Akpolat, G. Gunduz, F. Ozkan, N. Besun, Appl. Catal. A 265 (2004) 11.

[76] G. Gunduz, R. Dimitrova, S. Yilmaz, L. Dimitrov, Appl. Catal. A 282 (2005) 61.

[77] G. Gunduz, R. Dimitrova, S. Yilmaz, L. Dimitrov, M. Spassova, J. Mol. Catal. A 225 (2005) 253.

[78] R. Dimitrova, G. Gunduz, M. Spassova, J. Mol. Catal. A 243 (2006) 17.

[79] C. Breen, Appl. Clay Sci. 15 (1999) 187.

[80] N. Besun, F. Ozkan, G. Gunduz, Appl. Catal. A 224 (2002) 285.

[81] M.K. Yadav, C.D. Chudasama, R.V. Jasra, J. Mol. Catal. A 216 (2004) 51.

[82] C. Volzone, O. Masini, N.A. Comelli, L.M. Grzona, E.N. Ponzi, M.I. Ponzi, Mater. Chem. Phys. 93 (2005) 296.

[83] M.C. Costa, R.A. Johnstone, D. Whittaker, J. Mol. Catal. A 104 (1996) 251.

[84] T. Yamamoto, T. Matsuyama, T. Tanaka, T. Funabiki, S. Yoshida, Phys. Chem. Chem. Phys. 1 (1999) 2841.

[85] T. Yamamoto, T. Matsuyama, T. Tanaka, T. Funabiki, S. Yoshida, J. Mol. Catal. A 155 (2000) 43.

[86] O. Chimal-Valencia, A. Robau-Sanchez, V. Collins-Martinez, A. Aguilar-Elguezabal, Bioresour. Technol. 93 (2004) 119.

[87] M.A. Ecormier, A.F. Lee, K. Wilson, Microporous Mesoporous Mater. 80 (2005) 301.

[88] M.A. Ecormier, K. Wilson, A.F. Lee, J. Catal. 215 (2003) 57.

[89] H. Pines, R.C. Olberg, V.N. Ipatieff, J. Am. Chem. Soc. 74 (1952) 4872.

[90] J.P. Bain, R.E. Fuguitt, W.Y. Gary, US Patent 2741645, 1956.

[91] A. Stanislaus, L.M. Yeddnapalli, Can. J. Chem. 50 (1972) 113.

[92] L.G. Wideman, BR Patent 8301541, 1983.

[93] V. Krishnasamy, V. Mohan, J. Indian Chem. Soc. 60 (1983) 359.

[94] P.A. Weyrich, H. Trevifio, W.F. Hölderich, W.M.H. Sachtler, Appl. Catal. A 163 (1997) 3144.

[95] H. Jaramillo, L.A. Palacio, L. Sierra, Stud. Surf. Sci. Catal. 142B (2002) 1291.

[96] D.W. Bonniface, J.R. Fryer, P. Landon, J.D. Scott, W.D.S. Scott, M.J.Watson, G. Webb, J.M. Winfield, Green Chem. 1 (1999) 9.

[97] J.D. Scott, M.J. Watson, N.P. Ewing, WO 95/27688 (1995).

[98] T. Yokoyama, N. Yamagata, Appl. Catal. A 221 (2001) 227.

[99] D. Gulkova, M. Kraus, J. Mol. Catal. 87 (1994) 47.

[100] B.M. Reddy, I. Ganesh, J. Mol. Catal. A 151 (2000) 289.

[101] Z.L. Wang, H.C. Ma, W.C. Zhu, G.J. Wang, React. Kinet. Catal. Lett. 76 (2002) 271.

[102] V.S. Kumar, S.S. Reddy, A.H. Padmasri, B.D. Raju, I.A. Reddy, K.S.R. Rao, Catal. Commun. 8 (2007) 899.

[103] J. Sloczynski, J. Janas, T. Machej, J. Rynkowski, J. Stoch, Appl. Catal. B 24 (2000) 45.

[104] G.D. Piero, F. Trifiro, A. Vaccari, J. Chem. Soc. Chem. Commun. 1984, 656.

[105] M.C.J. Bradford, M.V. Konduru, D.X. Fuentes, Fuel Process. Technol. 83 (2003) 11.

[106] F. Simard, U.A. Sedran, J. Sepulveda, N.S. Figoli, H.I. De Lasa, Appl. Catal. A 125 (1995) 81.

[107] K.D. Jung, O.S. Joo, Catal. Lett. 84 (2002) 21.

[108] J. M. Campos-Martin, A. Guerrero-Ruiz, J.L.G. Fierro, J. Catal. 156 (1995) 208.

[109] W.S. Epling, G.B. Hoflund, D.M. Minahan, Appl. Catal. A 183 (1999) 335.

[110] M. Ohta, Y. Ikeda, A. Igarashi, Appl. Catal. A 258 (2004) 153.

[111] M. Ohta, Y. Ikeda, A. Igarashi, Appl. Catal. A 266 (2004) 229.

[112] Z.F. Wang, J.Y. Xi, W.P. Wang, G.X. Lu, J. Mol. Catal. A 191 (2003) 123.

[113] Y.Y. Wu, H.M. Bai, J.Z. Zhou, C.X. Chen, X. Xu, Y.F. Xu, G.R. Qian, Appl. Clay Sci. 42 (2009) 591.

[114] M. delArco, V. Rives, R. Trujillano, P. Malet, J. Mater. Chem. 6 (1996) 1419.

[115] S.R. Naidu, A.K. Banerjee, N.C. Ganguli, S.P. Sen, J. Res. Inst. Catal., Hokkiadio Univ. 21 (1973) 172.

[116] A.M. El-Awad, B.M. Abu-Zied, J. Mol. Catal. A 176 (2001) 213.

[117] Y. Ogino, M. Oba, H. Uchida, Bull. Chem. Soc. Jpn. 32 (1959) 284.

[118] Y. Ogino, M. Oba, H. Uchida, Bull. Chem. Soc. Jpn. 32 (1959) 616.

[119] M. Fujiwara, H. Ando, M. Tanaka, Y. Souma, Bull. Chem. Soc. Jpn. 67 (1994) 546.

[120] X.J. Tang, J.H. Fei, Z.Y. Hou, H. Lou, X.M. Zheng, React. Kinet. Catal. Lett. 94 (2008) 3.

[121] C.Y. Shiau, S. Chen, J.C. Tsai, S.I. Lin, Appl. Catal. A 198 (2000) 95.

[122] K. Tanabe, in: J.R. Anderson, M. Boudart (Eds.), Catalysis Science and Technology, Springer, 1981, Chapter 5.

[123] I. Melian-Cabrera, M.L. Granados, J.L.G. Fierro, Catal. Lett. 79 (2002) 165.

[124] Y. Ogino, M. Oba, H. Uchida, Bull. Chem. Soc. Jpn. 33 (1960) 358.

Chapter 2. Experimental

2.1. Introduction

This chapter will focus on the preparation of Pd doped Zn-Cr oxide and bulk Zn-Cr-Cu oxide, which are used in this study as redox/acid multifunctional catalysts for the synthesis of MIBK from acetone and hydrogen, and p-cymene from α-pinene. Following the discussion on catalyst preparation, the characterisation techniques that have been used to determine water content, surface area and porosity, and acidity of the catalysts will be described in detail. Finally, a description of the reaction procedure and the experimental setup will be provided.

2.2. Chemicals and solvents

All chemicals were ordered and purchased from Aldrich and hydrogen gas from BOC Gases Ltd. In brief, the chemicals used in our experiments were acetone and hydrogen (H_2) as reactants for MIBK synthesis, α-pinene for the p-cymene synthesis, water as a solvent for bulk oxide preparation, benzene as a solvent for Pd supported on bulk oxides, decane as a standard for gas chromatography (GC) in the liquid phase, $Zn(NO_3)_2.6H_2O$, $Cr(NO_3)_3.9H_2O$, $Cu(NO_3)_2.3H_2O$, and NH_4OH for the preparation of oxide catalysts and, finally, $Pd(OAc)_2$ for the preparation of Pd doped catalysts.

2.3. Catalyst preparation

2.3.1. Preparation of Zn-Cr mixed oxide catalysts

A series of Zn-Cr mixed oxides with a Zn/Cr atomic ratio of 1:30-20:1 was prepared by co-precipitation of Zn^{II} and Cr^{III} hydroxides using a procedure adopted from that reported in the literature [1]. Co-precipitation was performed by adding 10 wt% aqueous ammonium hydroxide (dropwise) to a stirred aqueous mixture of $Zn(NO_3)_2.6H_2O$ and $Cr(NO_3)_3.9H_2O$ ($[Zn^{II}] + [Cr^{III}] = 0.2$ M) at 70°C until a pH of 7 was achieved. This was followed by ageing of the suspension for 3 hours at 70°C. The precipitates were then filtered off, washed with deionised water until ammonia-free, dried in air at 100-110°C overnight and finally calcined under nitrogen flow for 5 h at 300°C, to create Zn-Cr oxides as black powders. The oxides were pelleted and ground into powder, with a particle size of 45-180 μm.

2.3.2. Preparation of palladium doped Zn-Cr mixed oxide catalysts

The Pd-doped Zn-Cr mixed oxide catalysts were prepared by impregnating Zn-Cr oxides with a 0.02 M solution of $Pd(OAc)_2$ in benzene, at room temperature, followed by evaporation of the solvent in a rotary evaporator and the subsequent reduction of Pd^{II} to Pd^0 by a hydrogen flow (30 mL/min) at 250°C for 2 h. The catalysts were then stored in a desiccator over P_2O_5 at room temperature.

2.3.3. Preparation of Zn-Cr-Cu mixed oxide catalysts

The ZnO-Cr_2O_3-CuO mixed oxides with a variation of the atomic ratio of Zn-Cr-Cu (from 1:1:2 to 1:1:0.1) and Cu-Cr with atomic ratio of 1:1 were prepared via co-precipitation of $Zn(NO_3)_2.6H_2O$, $Cr(NO_3)_3.9H_2O$ and $Cu(NO_3)_2.3H_2O$ using a procedure adapted from that reported in section 2.3.1.

2.4. Techniques

2.4.1. Thermogravimetric analysis (TGA)

The thermal stability of the catalysts was measured using thermogravimetric analysis (TGA) by monitoring the change in the mass of catalyst material following a gradual increase in the temperature. Catalyst samples of between 30-50 mg were placed on a high precision balance, equipped with a Perkin Elmer TGA 7 instrument, and then heated electrically at a linear rate under a nitrogen gas flow. The results were presented as thermogravimetric curves, showing the change in weight percentage as a function of temperature; or as a derivative thermogravimetric weight loss (DTG) curve which can be used to demonstrate a clear observation of weight loss at a certain point.

Thermogravimetric experiments were performed using a heating rate of 20°C per minute to raise the temperature from room temperature to 700°C, under a nitrogen gas flow. Figures 2.1 shows a typical example of a thermogravimetric curve for 0.1% Pd/Zn-Cr (1:1), after pre-treatment at 300°C for 5 h under nitrogen gas flow.

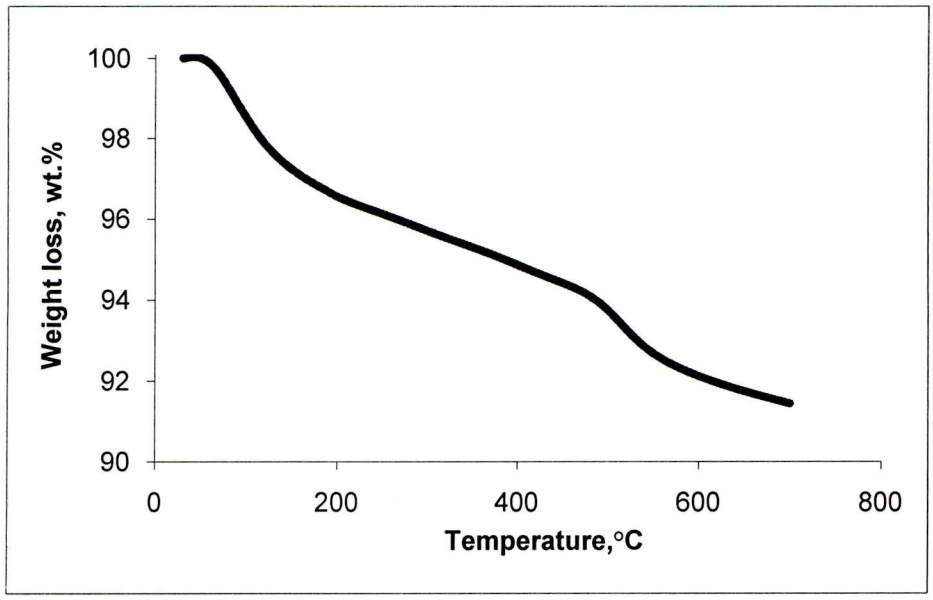

Figure 2.1 Thermogravimetric analysis of 0.1 wt%Pd/Zn-Cr (1:1). Heating rate: 20 °C/min.

2.4.2. Surface area and porosity analysis

The experiments were carried out using the Micromeritics ASAP 2000 adsorption apparatus. Typically, 200-250 mg of the catalyst sample was heated under vacuum to 150°C in a furnace for 1 h and then packed, accurately, into a sample tube and evacuated under vacuum (10^{-3} Torr) on the Micromeritics ASAP 2000 analyzer at 250°C for 3 h, to remove all gases within the pores. After outgassing, the sample was allowed to cool to room temperature before the sample tube was immersed in liquid nitrogen. Finally, the gas pressure was allowed to reach equilibrium. Subsequently, a series of 55 successive nitrogen doses were performed to obtain an adsorption isotherm. After analysis, the samples were reweighed to adjust the computer data based on any change of mass during the pre-treatment process.

2.4.3. Fourier Transform Infrared Spectroscopy (FTIR)

Samples for analysis were prepared by first drying a small amount of sample under vacuum at 150°C for 1 h, after which 10 mg of catalyst was mixed with 100 mg of KBr and ground thoroughly to create a diffusely scattering matrix that lowered absorption and hence increased throughput of the beam and enhanced resolution for analysis. After dilution with KBr, catalyst samples were loaded into the environmental chamber and pre-treated at 100°C and 20 mtorr for 1 h. Following this, the background DRIFT spectra were recorded at 100°C and 20 mtorr. The samples were then exposed to pyridine vapour at 15 torr pressure and 100°C for 0.5 h, followed by pumping out, at 100°C and 20 mtorr, for 0.5 h. The DRIFT spectra of the adsorbed pyridine were recorded at 100°C and 20 mtorr against the background spectra and displayed in the absorbance mode, i.e. $\log_{10}$ (1/R), where R is the reflectance. Variations of catalyst concentration from 5 – 50 wt% in KBr did not affect the spectra of adsorbed pyridine, apart from their intensity and signal-to-noise ratio, indicating that dilution with KBr did not change the catalysts.

2.4.4. Powder X-ray diffraction

Powder X-ray diffraction (XRD) patterns of catalysts were recorded on a PANalytical Xpert diffractometer with a monochromatic Co $K_{\alpha 1}$ radiation with λ = 1.789 Å, at 40 kV and 40 mA. Typically, powdered samples of Zn-Cr and Zn-Cr-Cu, prepared by drying a small amount of the samples under vacuum at 100°C for 1 h, were then placed on a sample holder and exposed to X-ray radiation at room temperature. The patterns were recorded in the range of 2θ, between 10° and 80°, and attributed using JCPDS database for comparison with previously studied solids.

2.4.5. Inductive coupled plasma atomic emission spectroscopy (ICP-AES)

Plasma emission spectroscopy is a commonly used technique for quantitative determination of most elements, over a wide concentration range of chemical samples. In this technique, plasma is produced by ionising argon gas through the influence of strong electrical field, either by radio frequency or using direct current [2].

Sample to be analysed, usually in the form of a solution, is introduced into plasma, which has a characteristic toroidal shape at high temperatures between 6000°C and 8000°C. The sample is then excited by thermal energy, causing the outer orbital electron in the sample atoms and ions to be excited to a higher orbital energy level than their ground state before returning to their ground state after a very short time. This excitation and subsequent de-excitation causes emission of an electromagnetic radiation, which can be analysed by separating the wavelength for each individual element in the sample using a spectrograph. A plot of emission line intensity against concentration produced from the standard calibration solutions of varying concentrations of each individual element gives information about the concentration of a particular element in the sample.

In this study, determination of zinc, chromium, copper and palladium in Zn-Cr and Zn-Cr-Cu oxide catalysts was carried out by Steve G. Apter using a Spectro Ciros CCD Inductively Coupled Plasma (ICP) source linked to an Atomic Emission Spectroscopy (AES) available in the Department of Chemistry of the University of Liverpool.

2.4.6. Elemental analysis

Determination of elements like carbon, hydrogen and nitrogen in organic compounds is one of the most important quantitative applications in gas chromatography.

A milligram sized sample is weighed and introduced into a reactor at ca. 2000°C under a stream of helium gas, temporarily enriched with pure oxygen, followed by frequent flash combustion to obtain quantitative combustion. Finally, the gaseous products so obtained are passed through a Porapak chromatographic column for separation and are then quantified using a GC detector.

In our work, carbon and hydrogen (organic residues on the catalyst surface after reaction) analysis were performed by Steve G. Apter, using a Thermo flash EA1112 apparatus located in the Department of Chemistry of University of Liverpool.

2.4.7. Ultraviolet (UV) spectroscopy

In this study, UV spectroscopy was used for measuring the concentration of pyridine in the calorimetric study of pyridine adsorption on Zn-Cr oxide catalysts. The amount of pyridine in a solution of cyclohexane was measured with a VARIAN Cary 50 UV spectrophotometer, in a 1 cm quartz cuvette, at a wavelength of 250 nm. The value of the molar extinction coefficients (ε), obtained by plotting the absorbance against concentration (see Figure 1 in appendix (I)), was 1818 L/mol cm at $\lambda = 250$ nm.

2.4.8. Differential scanning calorimetry (DSC)

A differential scanning calorimeter is a widely used technique for catalysts characterisation [3]. This technique combines differential scanning calorimetry with thermogravimetric analysis to give information about the physical and chemical transformations of materials, such as crystallisation, phase changes, sublimation, adsorption, desorption, decomposition, oxidation, reduction, surface reactivity and calcinations.

The differential scanning calorimeter is built around two open refractory tubes crossing the heating furnace with the detection unit, designed according to the Calvet principle, in the medium part of the tubes (Figure 2.2). Temperature must be kept constant in both the sample and the reference chambers in the DSC to measure the heat flow into each. This is achieved by placing separate heating elements in the sample and the reference chambers.

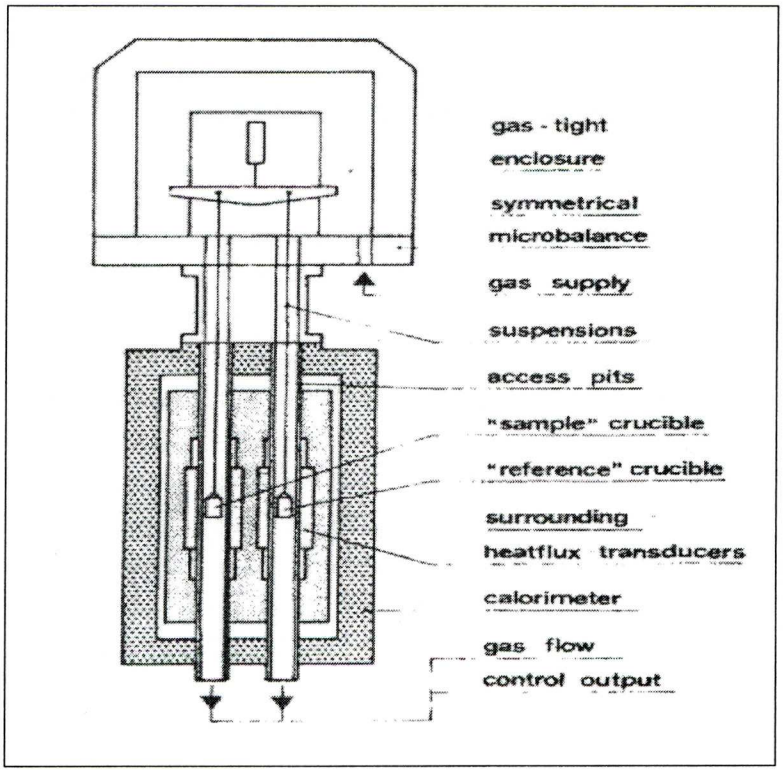

Figure 2.2 TG-DSC schematic cross section [3].

In this work, acidity and total number of Brønsted and Lewis acid sites in Zn-Cr oxides were measured by passing a continuous flow of NH_3 gas over a catalyst samples in a flow system using a Setaram TG-DSC 111 differential scanning calorimeter. The nitrogen and ammonia gases used were passed through molecular sieve traps before entering the system, to achieve a purity of around 99.99%.

Samples for analysis (60-80 mg) were placed in the DSC cell and pretreated at 300°C for 1 h under 35 mL/min N_2 flow, followed by weight stabilization at 100°C for 1 h. Analysis was then performed by adding ammonia in the gas flow for 1 h, with NH_3:N_2 (1:1) molar ratio in a flow of 35 mL/min. Following this, the sample was purged of physisorbed NH_3 molecules by keeping the sample under a nitrogen flow for 1 h in order to reach the adsorption equilibrium. From the sharp weight gain and heat release recorded, the acidity and the number of acid sites can be obtained.

A pulse method was used to measure the differential heats of NH_3 adsorption (molar heat for each dose of adsorbate). Catalyst samples (60-80 mg) were placed in the calorimeter and pre-treated under a flow of helium (30 mL/min) at 300°C for 1 h. Temperature was then lowered to 100°C while under a flow of He. After the sample weight stabilisation at 100°C (about 2 h), analysis was performed by adding successive pulses of 2 mL of ammonia into the He flow using a loop fitted in a 6 port valve. Sufficient time (about 20 min) was allowed after each pulse for the adsorption equilibrium to be reached. The weight gain and the corresponding heat of adsorption were recorded, from which the differential adsorption heat was obtained.

2.4.9. Microcalorimetry

Calvet calorimetry is one of the most important techniques for measuring thermal phenomena in chemical reactions. In this study, a Setaram C80 heat flux Calvet type microcalorimeter was used to measure the heat of adsorption of pyridine on Zn-Cr (1:1) and (1:10) oxides in a cyclohexane slurry (used as a solvent in the liquid phase).

The setup consisted of two stainless steel mixing vessels (sample and reference) adapted with stirrers. A Teflon membrane was used to separate the sample chamber (2.5 cm^3 volume) from the upper volume (Figure 2.3). Both sample and reference vessels were placed in a calorimetric block that controlled temperature with an accuracy of $\pm 0.01^{\circ}C$.

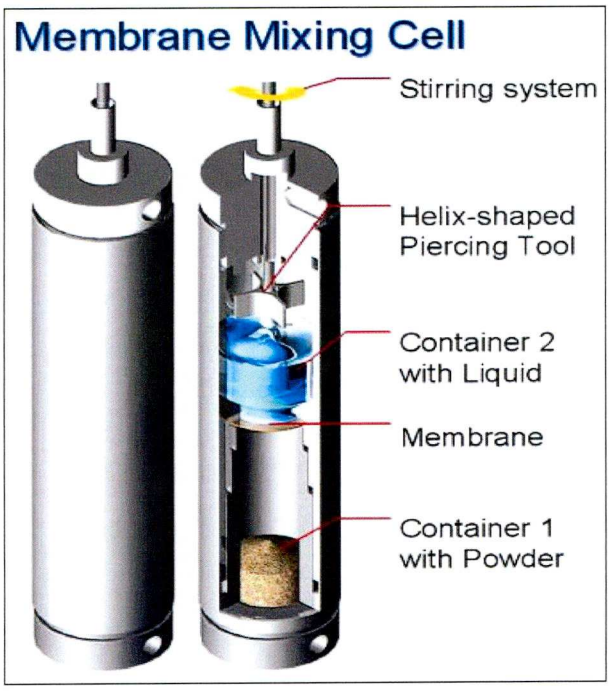

Figure 2.3 SETARAM C80 membrane mixing vessel [4].

Prior to measurements, samples were pre-treated at $200^{\circ}C$ under vacuum. Unless stated otherwise, measurements were carried out in an isothermal mode of

operation at 50°C. Sample analysis was performed under a dry nitrogen atmosphere. A fresh catalyst oxide sample (0.5 g) was used for each adsorption measurement. The weighed sample was placed into 1 mL anhydrous cyclohexane in the sample chamber (2.5 cm^3), and heated at 50°C for 30 min to remove absorbed gas. The sample chamber was then covered with a Teflon membrane and locked within an upper volume body (2.9 cm^3). The reference vessel was filled in the same manner, but without catalyst. In both vessels the upper volume was then filled with pyridine solution in cyclohexane (1 mL) and locked. Both vessels were loaded into the calorimeter and allowed to thermally equilibrate, which usually required 3-4 h. Once equilibrium was attained, the experiment was initiated by bringing pyridine into contact with the catalyst sample, which was done by activating the stirrers and breaking off the membranes.

The total amount of unadsorbed pyridine was obtained by UV-VIS spectroscopy using a Varian Cary 50 spectrophotometer in a 1 cm quartz cuvette, at a pyridine absorption band of 250 nm (ε = 1818 L/mol cm). The amount of adsorbed pyridine was determined using the Ad-Cal method developed by Drago [5, 6].

2.4.10. Metal dispersion from hydrogen adsorption

Numerous methods have been used for metal dispersion measurements [7-12]. These include H_2 titration [7-10], H_2 and O_2 chemisorption [8, 11] and the direct adsorption of carbon monoxide [10]. Dispersion, D, is defined as the fraction of metal at the surface, $D = metal_s/metal_{total}$. The most sensitive method for this type of analysis is hydrogen-oxygen titration because the amount of H_2 adsorbed in this way is higher than

that for the direct chemisorption of H_2 or O_2 adsorption [8]. In addition, the direct adsorption of carbon monoxide has several disadvantages [12], namely:

(1) There may be more than one adsorption stoichiometry for CO.

(2) CO is readily adsorbed by some supports.

(3) The adsorption mode may vary with dispersion.

In our work, the palladium dispersion in catalysts was determined by hydrogen chemisorption measured by the pulse technique, using a Micromeritics TPD/TPR 2900 instrument fitted with a thermal conductivity detector (TCD) and connected to the computer used for data analysis. Analysis was carried out at a furnace temperature of 100°C and a pressure of 1.3 bar, in order to avoid the undesirable adsorption of hydrogen into the palladium bulk [7, 8].

Prior to adsorption of H_2, the catalyst samples were treated in a H_2 flow (20 mL/min) at 250°C for 1 h to ensure that palladium was reduced to palladium metal. It was then exposed to air for 1 h at room temperature to adsorb oxygen on the Pd surface at a Pd_s-O_{ad} ratio of 1:1, where Pd_s is a surface Pd atom and O_{ad} is adsorbed oxygen. When the sample was ready for analysis, approximately 50 mg of the catalyst sample from each experiment was packed into a sample tube, and was used for volumetric H_2 titration in a Micromeritics TPD/TPR 2900 analyzer.

After TCD baseline stabilisation at 100°C (about 20 min), under N_2 flow, analysis was performed by using successive pulses of 50 µl of H_2 (heated to 75°C) into the sample tube using N_2 as the carrier gas for H_2. A sufficient time of 3 minutes was allowed for adsorption equilibrium to be reached after each pulse. Pulses were carried out until adsorption was completed. Equation (2.1) shows the stoichiometry of H_2 titration.

$$Pd_sO_{ad} + 1.5\ H_2 \rightarrow Pd_sH_{ad} + H_2O \qquad (2.1)$$

The ratio of H_{ad}/Pd_s and O_{ad}/Pd_s have been determined as 1:1 and hence H_{ad}/O_{ad} must also be 1:1 [8]. From the unadsorbed hydrogen peaks observed by the TCD detector, the integrated areas under the peaks were used to calculate the Pd dispersion using equation shown below:

$$D = \frac{A_r \times V_{ads\ at\ 273\ K}}{S \times 22414 \times C_{Pd}} \qquad (2.2)$$

In eq. 2.2, A_r is the relative atomic mass of Pd = 106.42, V_{ads} is the volume of H_2 (mL) adsorbed onto the surface at 273 K, S is a stoichiometric ratio of H_2/Pd_s in equation (2.7) (S = 1.5), 22414 represents the volume (mL) of one mole of H_2 gas at 273 K and C_{Pd} is the Pd content in the sample (g). In this study, V_{ads} at 273 K was calculated using equation (2.3).

$$V_{ads\ at\ 273\ K} = \sum \{0.05 - [(\frac{PA_{ads}}{PA_{av}}) \times 0.05]\} \times (\frac{273}{348}) \qquad (2.3)$$

In eq. (2.3), 0.05 represents the volume (mL) of H_2 gas in each pulse, PA_{ads} is the peak area with H_2 adsorption and PA_{av} is the mean average peak area of four pulses with no adsorption.

2.4.11. Gas chromatography-mass spectrometry (GC-MS)

Mass spectrometry is a very important technique which has been used in the identification of a particular organic compound present in an unknown mixture and also to distinguish between close peaks on GC chromatograms.

The sample for analysis by GC-MS is vaporised using high vacuum and is ionised by a high energy electron beam to produce many positively charged molecular radicals of various sizes. Detection of these radicals can then be achieved by accelerating them in an electric field and then deflecting them in a magnetic field, after which each particular ion gives a peak in the mass spectrum depending on its mass/charge ratio, as shown schematically in Figure 2.4.

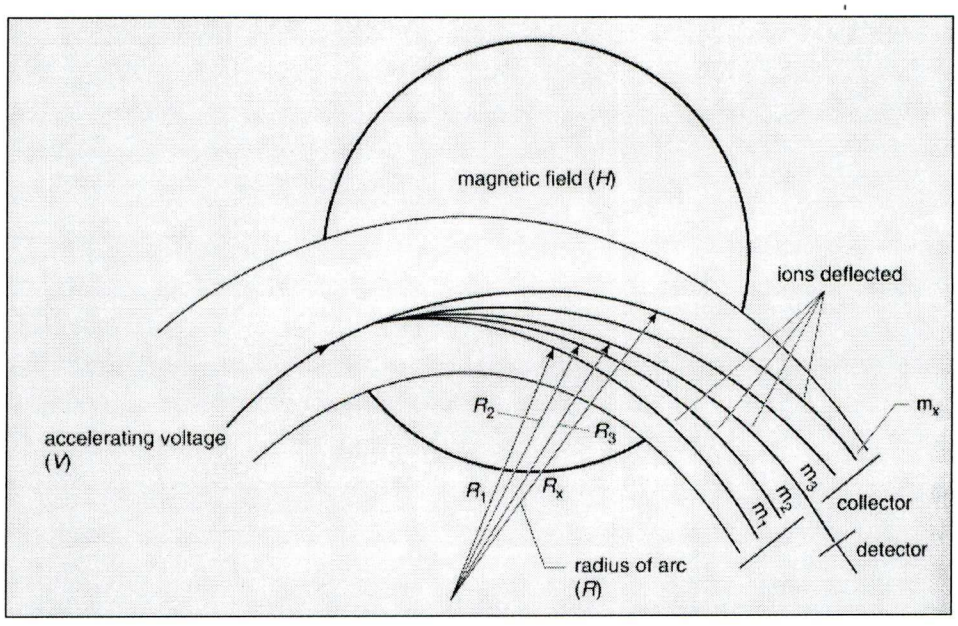

Figure 2.4 Positively charged ions are deflected to varying degrees by an applied magnetic field according to their mass [13].

In this work, a TRIO-1000 GC/MS spectrometer was employed for identification of products, both in MIBK and p-cymene synthesis over Zn-Cr mixed

oxide catalysts. Samples were then analysed by Moya McCarron and Alan Mills. An ZB-WAX capillary column was used for the GC-MS analysis.

2.4.12. Gas chromatography

In this study, a Varian Star 3400 CX gas chromatograph was used for product analysis in both the gas and the liquid phases. The gas and liquid phase columns were equipped with the Varian Star 3400 CX gas chromatograph and a flame ionisation detector was connected to a computer with the Varian Star software. For MIBK synthesis, a polar HP-INNOWAX capillary column (30 m length x 0.25 mm internal diameter x 0.5 μm film thickness) fitted with an offline GC and a non-polar BP5 capillary column (30 m length x 0.25 mm internal diameter x 0.5 μm film thickness) fitted with an online GC were used for product separation in the liquid and gas phase processes, respectively. For p-cymene synthesis, a ZB-1701 capillary column (30 m length x 0.25 mm internal diameter x 0.5 μm film thickness) fitted with an online GC was used for product separation in the gas phase process. Moreover, all of these columns contained a polyethylene glycol (PEG) stationary phase used for product separation, with the products progressing through to the detector at differing times, depending on the interaction of each component with the column. The rate of passage of the components can be affected by the boiling points and the polarity of the components.

For online product analysis in the gas phase processes, the sample being analysed fills the 250 μl loop connected to a Valco valve from where it is injected into the capillary column for separation. It is then directly detected on the FID. For the liquid phase analysis in the offline GC, a 0.2 μl of the sample mixture was directly

injected into the gas chromatograph by micro-syringe, and vaporised into a heated (split/splitless) glass-lined injection port and swept through to a heated FID capillary column.

For product analysis in the MIBK synthesis, helium gas with a flow rate of 2 mL/min and nitrogen gas with a flow rate of 30 mL/min were used as the carrier and the make-up gases, respectively. On the other hand, for the product analysis of p-cymene synthesis, nitrogen was used as carrier and make-up gas with a flow rate of (2 mL/min) and (30 mL/min), respectively.

The injector and detector temperatures were set to 230°C. Temperature of the column oven was programmed for each type of synthesis separately. Hydrogen, with a flow rate of 30 mL/min, introduced from the column into the eluate, is burnt in air (300 mL/min) added into the base of the detector to form a stable, noise-free flame. Products were identified by comparison with authentic samples and by gas chromatography-mass spectrometry (GC-MS) using a TRIO-1000 GC-MS spectrometer with a ZB-WAX capillary column.

2.4.13. GC calibration

For both MIBK and p-cymene synthesis, each known product was calibrated using the internal standard method. Different known concentrations of analyte with the same concentration of decane as an internal standard for the GC were diluted in an appropriate solvent. The solutions were then injected into the GC using a 0.2 µl injection. The effluent of the column was analysed using an FID detector and the results were then plotted on the computer as a GC chromatogram. From this chromatogram, the calibration factor (K), which is the correlation of the peak areas with

the concentration of a particular organic component, can be calculated using equation (2.4).

$$\frac{M}{M_0} = K \times \frac{S}{S_0} \qquad (2.4)$$

In eq. (2.4), the gradient of the straight line produced in the linear plot of the molar ratio of the analysed compound and the internal standard (*M/Mo*) against the ratio of the area counts of the corresponding peaks (S/S_o), is the relative calibration factor, *K*.

In both MIBK and p-cymene synthesis, if some of unknown by-products were not available or there were numerous by-products with low peak areas, then it may be assumed that the isomers or compounds of similar structural types will have similar calibration constants and, therefore, the relative peak areas can be compared [13].

The relative molecular mass, the boiling points, the GC retention times and the molar calibration factors for the compounds (internal standard: decane in liquid phase processes and acetone in gas phase processes) involved in the conversion of acetone to MIBK are given in Table 2.1. The retention times and the molar calibration factors were measured by GC under the temperature programme shown in Figure 2.5. A typical GC trace for the MIBK synthesis in the gas phase processes is shown in Figure 2.6. The calibration plots (equation (2.4)) for this system are shown in (see Figures 2-7 in appendix (II)).

Table 2.1 GC retention times and calibration factors for MIBK synthesis.

Compound[a]	Molecular weight (g/mol)	Boiling point (°C)	Liquid sample		Gaseous sample	
			Retention time (min)	Calibration factor	Retention time (min)	Calibration factor
Acetone	58.1	56	1.8-2.1	5.01	0.9-1.1	1.00
IP	60.1	82	2.2-2.4	4.75	-	1.00
C_3	40 & 42	-47 &-42	1.3-1.7	3.34	0.5-0.8	0.67
MIBK	100.2	117	2.6-2.9	1.98	2.1-2.3	0.43
DIBK	142.3	163	3.9-4.1	1.43	4.2-4.4	0.27
MO	98.2	129	3.6-3.8	2.31	2.7-2.9	0.48
MS	120.2	166	4.5-4.7	1.06	4.4-4.6	0.22
others			-	1.00	-	0.50

[a] C_3 is propene and propane, IP isopropanol, MO mesityl oxide, MS mesitylene, and others are mainly C_{9+} acetone condensation products (mostly 2,6,8-trimethylnonane-4-one).

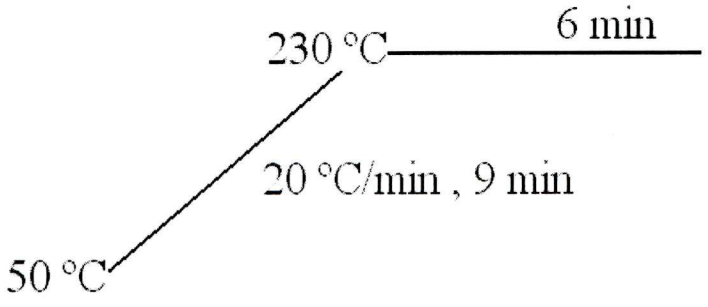

Figure 2.5 Temperature programme for the GC column.

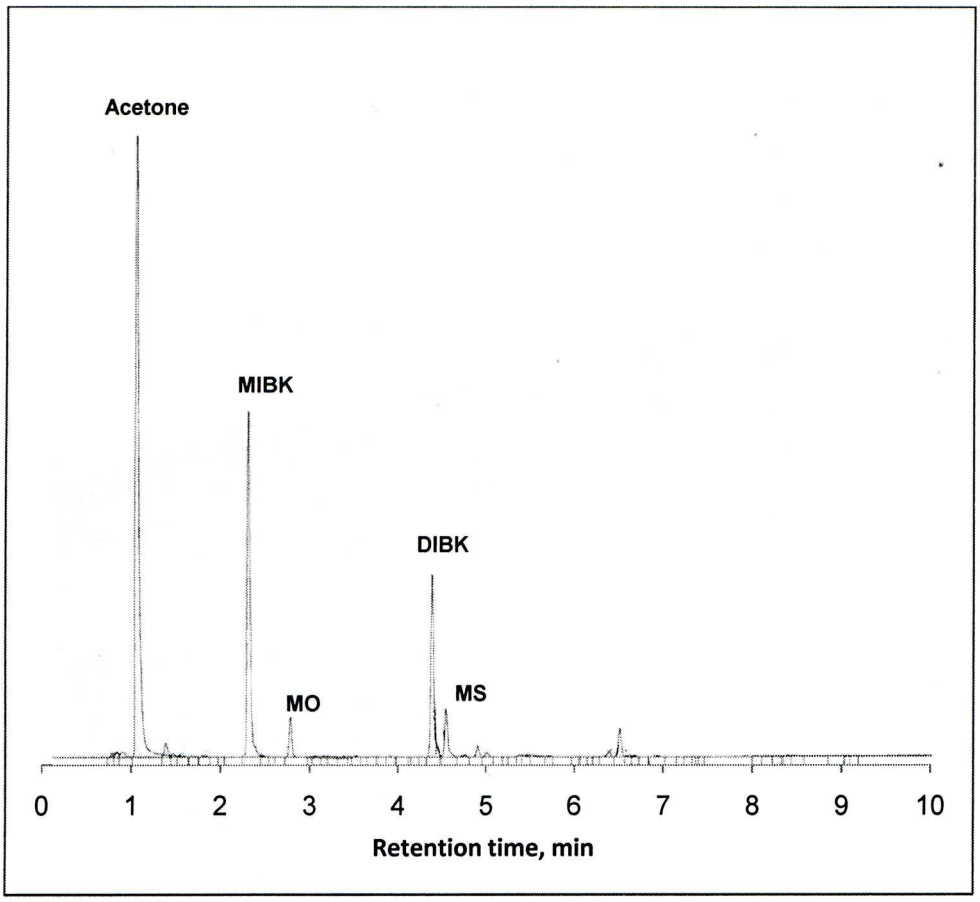

Figure 2.6 GC trace for the gas phase conversion of acetone to MIBK over 0.3 wt% Pd/Zn-Cr (1:1) catalyst.

The calibration data for the gas phase conversion of α-pinene to p-cymene are given in Table 2.2. The temperature programme for the GC column is shown in Figure 2.7. A typical GC trace for the gas phase thermal conversion of α-pinene to p-cymene is given in Figure 2.8.

Table 2.2 GC retention times and calibration factors for p-cymene synthesis.

Compound	Molecular weight (g/mol)	Boiling point (°C)	Gaseous sample	
			Retention time (min)	Calibration factor
α-pinene	136.24	156	3.0-3.1	1.00
p-cymene	134.22	177	6.3-6.4	1.00
camphene	136.24	159	3.5-3.6	1.00
limonene	136.24	176	5.3-5.4	1.00
terpinolene	136.24	184	6.4-6.5	1.00
others	-	-	-	1.00

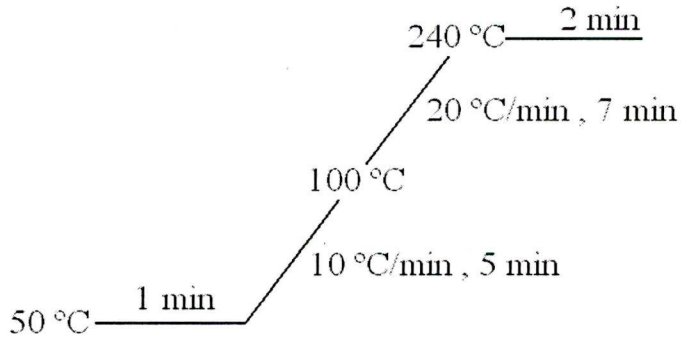

Figure 2.7 Temperature programme for the GC column.

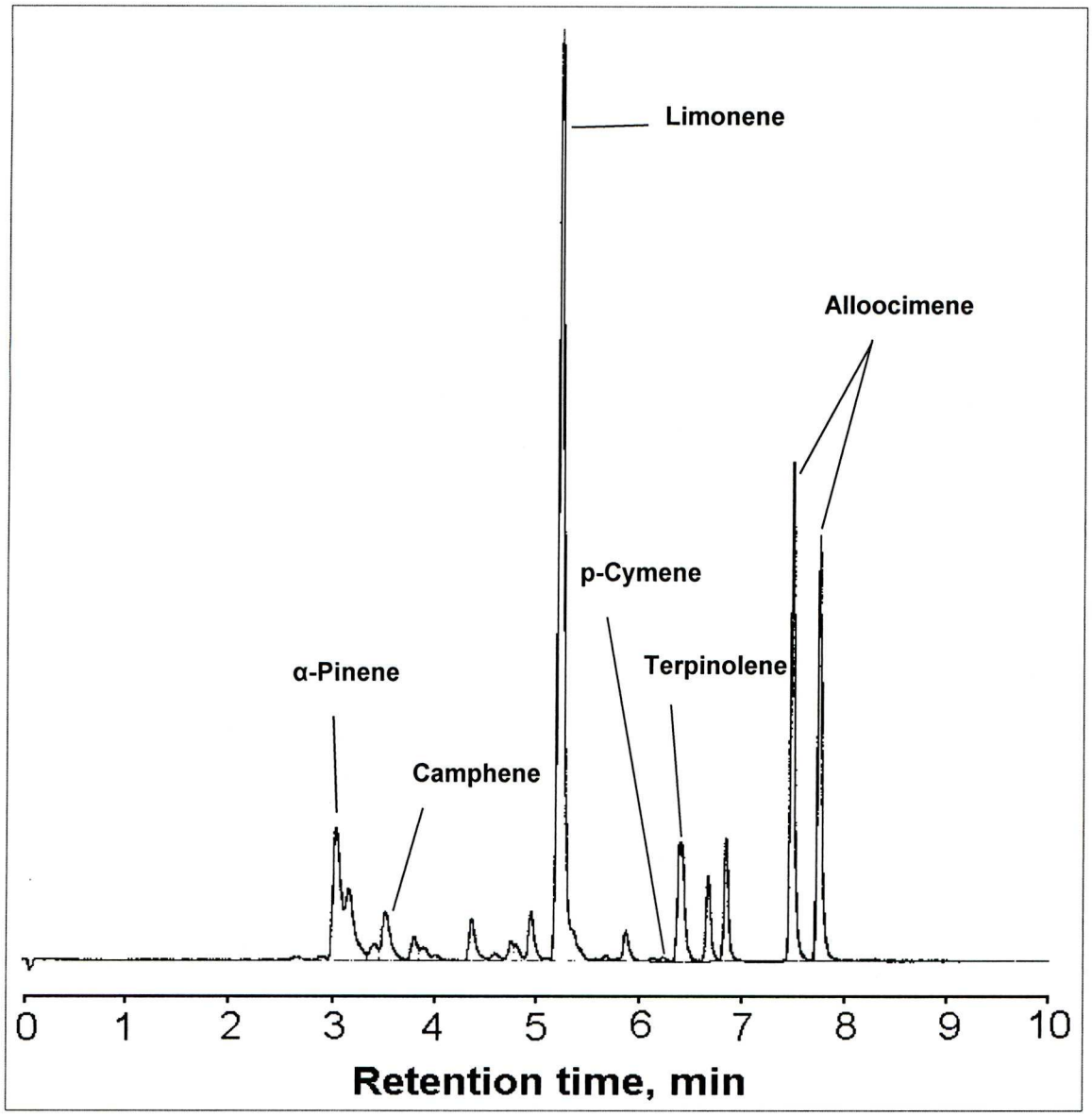

Figure 2.8 GC trace for the gas phase thermal conversion of α-pinene to p-cymene.

2.5. Reaction studies

2.5.1. Gas phase reactions

The catalytic tests were performed under atmospheric pressure in a Pyrex glass fixed-bed microreactor (21 cm in length and 0.9 cm internal diameter) with on-line GC analysis (Varian Star 3400 CX gas chromatograph equipped with a 30 m x 0.25 mm BP5 capillary column for MIBK synthesis and a 30 m x 0.25 mm ZB-1701 capillary

column for p-cymene synthesis and a flame ionisation detector). The reactor was placed in a vertical, tubular furnace. Unless stated otherwise, the catalyst bed contained 0.2-0.3 g of a catalyst powder (45-180 μm particle size for MIBK synthesis and <180 μm particle size for p-cymene synthesis). This was placed in the reactor between two layers of Pyrex glass wool. In some cases, the catalyst was diluted with acid-washed sand, which was itself inactive in the reaction. The temperature in the reactor was controlled by a Eurotherm controller using a thermocouple placed at the top of the catalyst bed. The gas feed was fed into the reactor from the top. Acetone or α-pinene was supplied to the gas flow by bubbling a flow of H_2 or N_2 (10-30 mL/min, controlled by Brooks mass flow controllers) through a stainless steel saturator containing acetone or α-pinene which was kept at a certain temperature to maintain the chosen acetone or α-pinene vapour pressure for the MIBK or p-cymene synthesis processes, respectively. All gas lines were made of stainless steel. The downstream lines and sampling valves were heated at 175°C to prevent product condensation. Prior to reaction, the catalysts were pre-treated with hydrogen (10-30 mL/min) at 300°C for 0.5 h. At regular time intervals, the downstream gas flow was analysed by the on-line GC. The liquid products from the MIBK synthesis were collected in an ice trap and also analysed by the off-line GC using a 30 m x 0.25 mm HP-INNOWAX capillary column. The products were identified by GC and GC-MS using authentic samples. Figure 2.9 shows a diagram of the reactor setup used for the MIBK and the p-cymene synthesis in the gas phase.

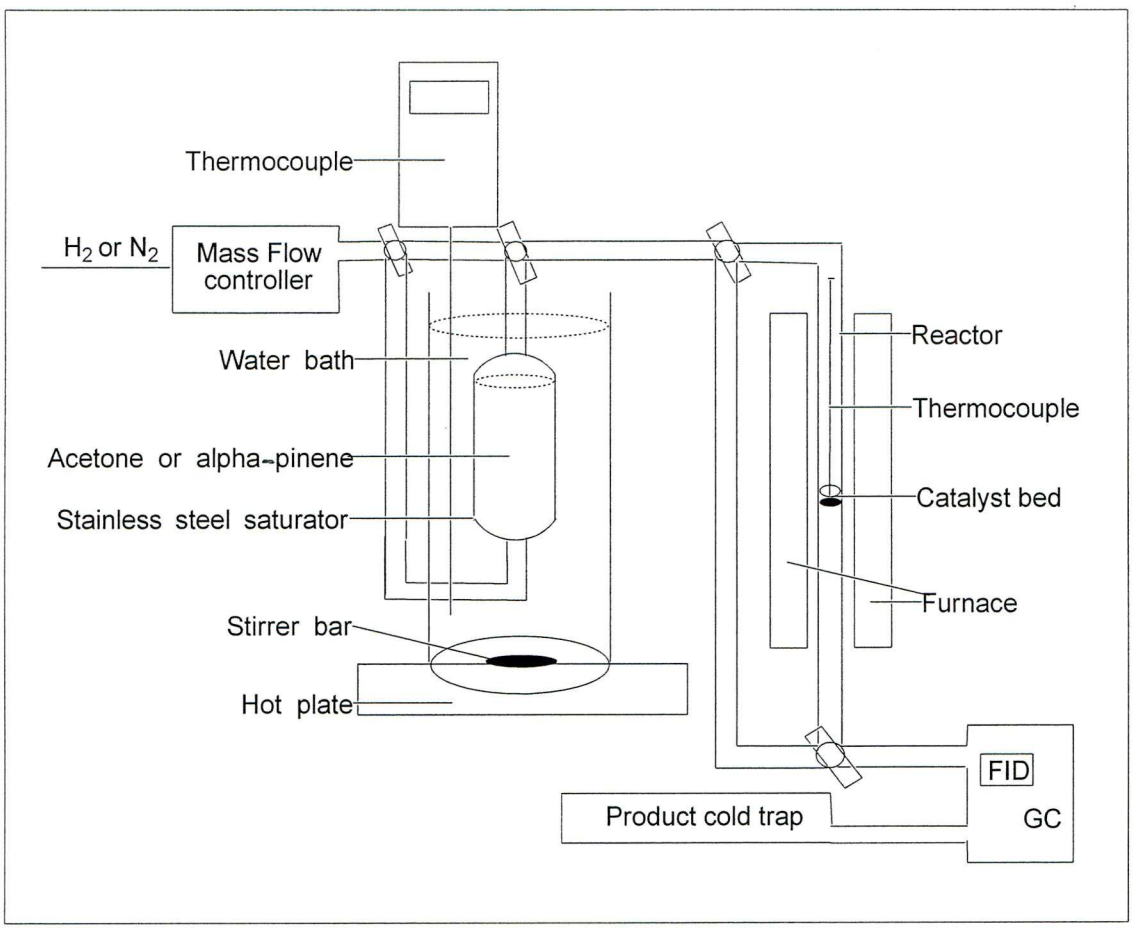

Figure 2.9 A diagram of the reactor setup used for gas phase processes.

The reaction activation energy, E_a, was measured under differential conditions at an acetone conversion ≤ 10% using 0.02 g catalyst samples diluted with 0.2 g of sand. If the reactor is operating in differential conditions, the rate becomes approximately linearly proportional to the change in conversion. Therefore the activation energy can be calculated directly from the incremental change in conversion [14, 15].

The vapour pressures of α-pinene and acetone increase with increasing saturator temperatures and these data are shown in Tables 2.3 and 2.4 respectively. From the vapour pressure data of these reactants, the ratio of H_2 to acetone or N_2 to α-pinene were determined, and therefore the gas hourly space velocity (GHSV in h^{-1}) and

the contact times of substrate across the catalyst for the gas phase reactions could be calculated. N_2 was also used for flushing the pipes clear of reactants and products.

Table 2.3 The vapour pressure of α-pinene at saturation temperatures used in experiments (calculated from reference book [16]).

α-Pinene temperature (°C)	Vapour pressure (kPa)
50	2
82	10

Table 2.4 The vapour pressure of acetone at saturation temperatures used in experiments (calculated from reference book [16]).

Acetone temperature (°C)	Vapour pressure (kPa)
0	9
30	37
37	50
44	65

2.5.2. Liquid phase reactions

The liquid-phase synthesis of MIBK was carried out in a 45-mL Parr 4714 stainless steel autoclave, equipped with a pressure gauge and a magnetic stirrer. Tests using the glass-lined autoclave revealed no effect of the stainless steel on the reaction with Pd/Zn-Cr catalysts. However, the reaction with Zn-Cr oxides in the absence of Pd was carried out in the glass-lined reactor to avoid any effect of Pd contamination. Typically, reaction mixture contained 2.0 g of acetone, 0.30 g of decane (internal GC standard) and 0.20 g of the catalyst. The stirring speed was between 400 to 1000 rpm unless stated otherwise. The autoclave was purged three times with H_2 then pressurised

with H_2 and placed in an oil bath which was preheated to the reaction temperature. Judging from the resulting pressure, most of the acetone remained liquid under such conditions. After reaction completion, the reactor was cooled with ice to 0°C, depressurised into a gas bag (balloon) with a stopcock to collect gaseous products (propene and propane) and then opened. The reaction mixture was taken out of the autoclave and separated from the catalyst by centrifugation. Products were identified by GC-MS and quantified using gas chromatography (Varian Star 3400 CX instrument equipped with a flame ionisation detector and a 30 m x 0.25 mm HP-INNOWAX capillary column). Figure 2.10 shows a diagram of the equipment setup for the liquid phase reactions.

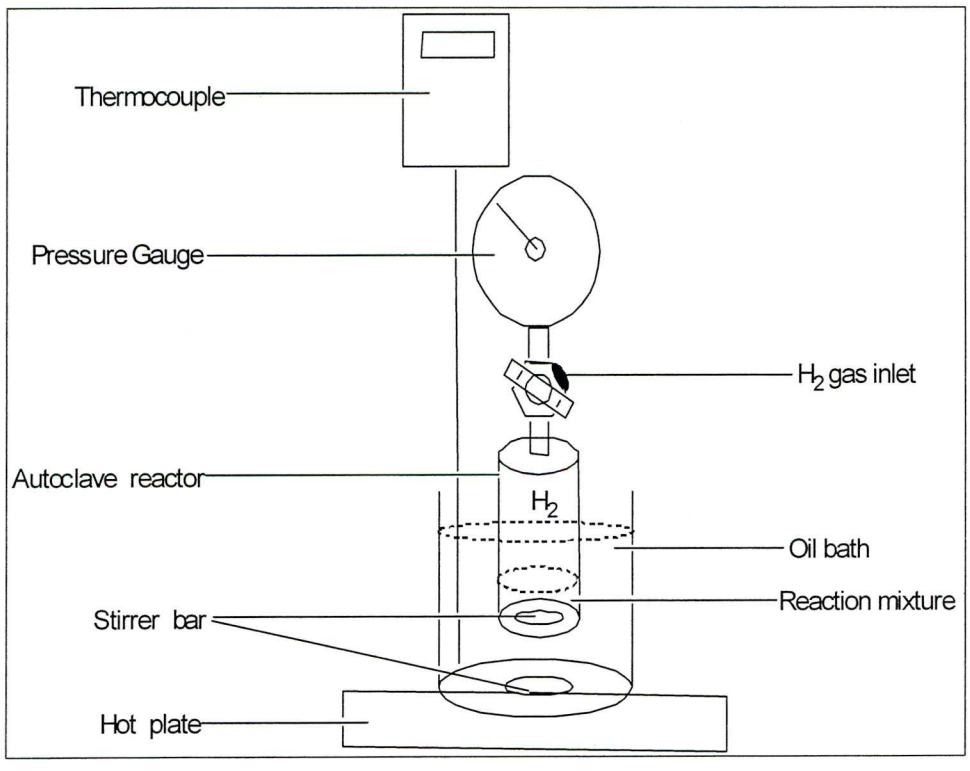

Figure 2.10 The reactor setup used for liquid phase processes.

The reaction time course was studied in a Parr 4590 stainless steel reactor of 25 mL volume equipped with an overhead stirrer (600 rpm) which allowed taking of

aliquots of the reaction mixture during the reaction, whilst maintaining a constant hydrogen pressure.

2.6. Calculation of reaction results

2.6.1. Calculation of reaction results in the gas phase processes

In the gas phase processes, the yield of each individual product (Y_p), total conversion (C) and selectivity of a particular product ($S_{P,S}$) were calculated using equations (2.5) – (2.7) respectively.

$$Y_p = \frac{S_P \times K_g \times A}{(\sum S_P \times K_g \times A)} \times 100 \qquad (2.5)$$

$$C = \sum Y_P \qquad (2.6)$$

$$S_{P,S} = \frac{Y_p}{C} \times 100 \qquad (2.7)$$

In equations (2.5) – (2.7), S_p is the relative area of the product peak(s), K_g is the calibration factor of the product relative to the acetone or α-pinene as the internal standard in gas phase reaction, A is the stoichiometry factor of the product relative to the reactant and $(\sum S_P \times K_g \times A)$ is a summation for all products including unreacted acetone or α-pinene.

The gas hourly space velocity (*GHSV*) and catalyst contact time (C_t) were calculated using equations (2.8) – (2.9) respectively.

$$GHSV(h^{-1}) = \frac{F \times 60}{V_{cat}} \tag{2.8}$$

$$C_t(s) = \frac{1}{GHSV(h^{-1})} \times 3600 \tag{2.9}$$

In equation (2.8), F is the gas flow of acetone over the catalyst (mL/min) and V_{cat} is the volume of catalyst (mL).

The activation energy (E_a) was derived using the natural log derivation of the Arrhenius expression, by plotting the natural logs of the conversion against the inverse of the temperature and then a straight line was obtained, allowing E_a/R to be determined. The Arrhenius expression and the derived equation are shown in equations (2.10) and (2.11) respectively, where k is the reaction rate constant, A is the pre-exponential factor, E_a is the activation energy, R is the gas constant and T is the temperature (K).

$$k = Ae^{\frac{-E_a}{RT}} \tag{2.10}$$

$$ln(k) = \frac{E_a}{R} \times \frac{1}{T} + ln\,(A) \tag{2.11}$$

2.6.2. Calculation of reaction results in the liquid phase processes

In the liquid phase processes, the percentage yield of C_3 gases (Y_g) as well as the products in liquid mixture (Y_p) were calculated using equation (2.12) and (2.13) respectively.

$$Y_g = \frac{(V_r + V_b)\, S_g}{22414\, S_o\, M_{acetone}} \times 100 \qquad (2.12)$$

In eq. (2.12), V_r is the volume of autoclave reactor (mL), V_b is the volume of the balloon (mL), S_g is the GC area count for C_3 gases injected from the gas sample collected from the balloon, S_o is the mean GC area count from five injections of the same volume of pure propene gas, 22414 mL is the volume of one mole of gas at 273 K and $M_{acetone}$ is the initial number of moles of the reactant acetone.

$$Y_P = \frac{K_{decane} \times S_P \times M_{decane} \times A}{M_{acetone} \times S_{decane}} \times 100 \qquad (2.13)$$

In equation (2.13), K_{decane} is the calibration factor of the product relative to the decane internal standard, S_P is the relative area of the product peak(s), M_{decane} is the moles of decane added to the reaction mixture, A is the stoichiometry factor of the product relative to the reactant, $M_{acetone}$ is the moles of acetone charged in the reaction mixture and S_{decane} is the relative area of the decane peak.

The individual product selectivities (Y_p) and the total conversion (C) were calculated using equation (2.5) and (2.6) presented in section 2.6.1 respectively.

References

[1] E.F. Kozhevnikova, I.V. Kozhevnikov, J. Catal. 238 (2006) 286.

[2] J. Mendham, R.C. Denney, J.D. Barnes, M.J.K. Thomas, Vogel's Textbook of Quantitative Chemical Analysis, Pearson Education Ltd., 2000.

[3] P.L. Parlouer, Thermochim. Acta, 103 (1986) 21.

[4] www.setaram.com/images/photos/thumb_cellule_55-3.jpg.

[5] C.W. Chronister, R.S. Drago, J. Am. Chem. Soc. 115 (1993) 4793.

[6] R.S. Drago, J.A. Dias, T.O. Maier, J. Am. Chem. Soc. 119 (1997) 7702.

[7] J.E. Benson, H.S. Hwang, M. Boudart, J. Catal. 30 (1973) 146.

[8] G. Prelazzi, M. Cerboni, G. Leofanti, J. Catal. 181 (1999) 73.

[9] J.E. Benson, M. Boudart, J. Catal. 4 (1965) 704.

[10] S.E. Wanke,.N. A. Dougharty, J. Catal. 24 (1972) 367.

[11] K.C. Taylor, J. Catal. 38 (1975) 299.

[12] M.A. Aramendia, V. Borau, C. Jimenez, J.M. Marinas, A. Moreno, Colloids. Surf. A 106 (1996) 161.

[13] L.M. Harwood, C.J. Moody, J.M. Percy, Experimental Organic Chemistry: Standard and Microscale, Blackwell Science, 2001.

[14] C. Perego, S. Peratello, Catal. Today. 52 (1999) 133.

[15] H. Purnama, T. Ressler, R.E. Jentoft, H. Soerijanto, R. Schlogl, R. Schomacker, Appl. Catal. A 259 (2004) 83.

[16] D.R. Lide, Handbook of Chemistry and Physics, 84th edition, CRC press, 2003-2004.

Chapter 3. Catalyst characterisation

3.1. Introduction

This chapter describes the results and discussion of the characterisations of the prepared catalysts involved in this study. A range of techniques was used in order to determine the elemental composition, the catalyst crystallinity, the thermal stability, the surface area and porosity, the palladium dispersion on the catalyst surfaces and the acidity. The catalysts under consideration include bulk Zn-Cr and Zn-Cr-Cu oxides and palladium-doped Zn-Cr oxides.

3.2. Inductively coupled plasma atomic emission spectroscopy (ICP-AES)

Inductively coupled plasma atomic emission spectroscopy (ICP-AES) was used to measure zinc, chromium and copper content within the Zn-Cr and Zn-Cr-Cu oxide catalysts, as well as to determine palladium content supported on Zn-Cr oxide catalysts. The oxide samples were dissolved in a strong, concentrated acidic mixture, with 1 eq conc. HNO_3 and 1 eq HF. Tables 3.1 and 3.2 present the results of ICP elemental analysis and show, in general, a good agreement between the stoichiometry involved in the preparation of the samples and the values obtained by ICP analysis.

Table 3.1 ICP-AES analysis of Pd/Zn-Cr oxide catalysts.

Catalyst	Zn/Cr molar ratio		Pd content (%wt.)
	Theoretical	Experimental	Experimental
0.3%Pd/Zn-Cr (1:30) oxide	0.03	0.03	0.19
0.3%Pd/Zn-Cr (1:10) oxide	0.10	0.07	0.25
0.1%Pd/Zn-Cr (1:1) oxide	1.00	0.85	0.10
0.3%Pd/Zn-Cr (1:1) oxide	1.00	0.85	0.25
1.0%Pd/Zn-Cr (1:1) oxide	1.00	0.85	0.68
0.3%Pd/Zn-Cr (10:1) oxide	10.00	9.29	0.26
0.3%Pd/Zn-Cr (20:1) oxide	20.00	19.10	0.27

Table 3.2 ICP-AES analysis of Zn-Cr-Cu oxide catalysts.

Catalyst	Zn/Cr molar ratio		Cu/Cr molar ratio	
	Theoretical	Experimental	Theoretical	Experimental
Cr-Cu (1:1) oxide	-	-	1.0	1.04
Zn-Cr-Cu (1:1:0.1) oxide	1	0.87	0.1	0.13
Zn-Cr-Cu (1:1:0.2) oxide	1	0.91	0.2	0.22
Zn-Cr-Cu (1:1:0.5) oxide	1	0.85	0.5	0.63
Zn-Cr-Cu (1:1:0.8) oxide	1	0.82	0.8	0.88
Zn-Cr-Cu (1:1:1) oxide	1	0.84	1.0	1.10
Z Zn-Cr-Cu (1:1:2) oxide	1	0.93	2.0	2.38

The densities of Zn-Cr and Zn-Cr-Cu oxide materials are summarised in Tables 3.3 and 3.4 respectively. In Zn-Cr oxide catalysts, the Cr-rich catalysts had a density of

1.38–1.44 g/cm^3, whereas the Zn-rich ones were lighter, with a density of 0.77–1.30 g/cm^3. In Zn-Cr-Cu oxide catalysts, the density decreases with increasing copper content from 1.66 g/cm^3 for Zn-Cr-Cu (1:1:0.1) oxide to 0.46 g/cm^3 for Zn-Cr-Cu (1:1:2) oxide. This means that the densities depend on the ratio between zinc, chromium and copper in these oxides (Table 3.4 and Figure 3.1).

Table 3.3 Densities of Pd/Zn-Cr oxide catalysts.

Catalyst	Catalyst density (g/cm^3)
0.3%Pd/Zn-Cr (1:30)	1.38
0.3%Pd/Zn-Cr (1:10)	1.39
0.3%Pd/Zn-Cr (1:1)	1.44
0.3%Pd/Zn-Cr (10:1)	1.30
0.3%Pd/Zn-Cr (20:1)	0.77

Table 3.4 Densities of Zn-Cr-Cu oxide catalysts.

Catalyst	Catalyst density (g/cm^3)
Cr-Cu (1:1) oxide	1.42
Zn-Cr-Cu (1:1:0.1) oxide	1.66
Zn-Cr-Cu (1:1:0.2) oxide	1.47
Zn-Cr-Cu (1:1:0.5) oxide	1.21
Zn-Cr-Cu (1:1:0.8) oxide	1.15
Zn-Cr-Cu (1:1:1) oxide	1.10
Zn-Cr-Cu (1:1: 2) oxide	0.46

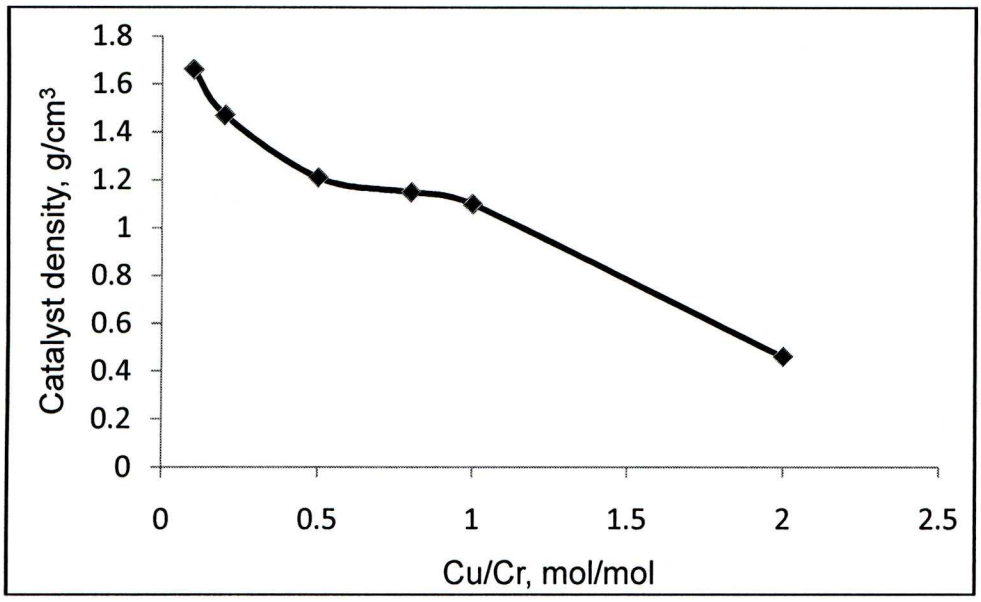

Figure 3.1 Densities of Zn-Cr-Cu oxide catalysts.

3.3. Powder X-ray diffraction

The XRD diffraction measurements for Zn-Cr and Zn-Cr-Cu mixed oxide catalysts were carried out using the experimental procedure described in Section 2.4.4. The XRD patterns are shown in Figures 3.2 and 3.3 for Zn-Cr and Zn-Cr-Cu oxides pretreated under nitrogen for 5 h at 300°C, respectively, and in Figure 3.4 for Zn-Cr-Cu oxides pretreated under hydrogen for 2 h at 300°C. The main purpose of the XRD studies was to determine the composition of the catalysts.

3.3.1. XRD for Zn-Cr oxides

Figure 3.2 shows XRD patterns of Zn-Cr mixed oxide catalysts with a Zn/Cr atomic ratio from 1:30 – 20:1. These catalysts were prepared by coprecipitation of Zn^{II} and Cr^{III} hydroxides, followed by calcination at 300°C. Zn-rich oxides with a molar ratio Zn/Cr = 10:1 – 20:1 were crystalline and exhibited the XRD peaks at 2θ = 37.08°, 40.21°, 42.37°, 55.85°, and 66.83° attributed to the ZnO phase with a crystallite sizes of

about 58 and 48 nm for Zn-Cr (10:1) and (20:1) respectively, as estimated from the XRD line width at $2\theta = 42.37°$ using the Scherrer equation.

In contrast, Cr-rich oxides (Zn/Cr = 1:1 – 1:30) were amorphous materials. The XRD measurements showed no ZnO crystalline phase due to the high chromium content in these oxides. From the XRD patterns of Zn-Cr oxides, Simard *et al.* and Bradford *et al.* have both observed that when the Cr/Zn ratio is increased from 0.5 to 15 (calcinated at 350°C) and from 0 to 1.9 (calcinated at 700°C) respectively, the content of ZnO decreased and $ZnCr_2O_4$ increased. Further increase in chromium content of the catalyst results in the appearance of Cr_2O_3 and a concomitant decrease in $ZnCr_2O_4$ content [1, 2]. Moreover, in Cr-rich oxides, Cr_2O_3 was not observed in the XRD pattrens. This indicates that Cr_2O_3 is completely dispersed and exists in the amorphous phase [3]. In addition to that, $ZnCr_2O_4$ crystalline phase was not observed in the XRD pattrens after calcination at 300°C, indicating that the formation of $ZnCr_2O_4$ depends on the calcination temperature and on the ratio between Zn and Cr, as well as on the way the catalyst is prepared [1-7].

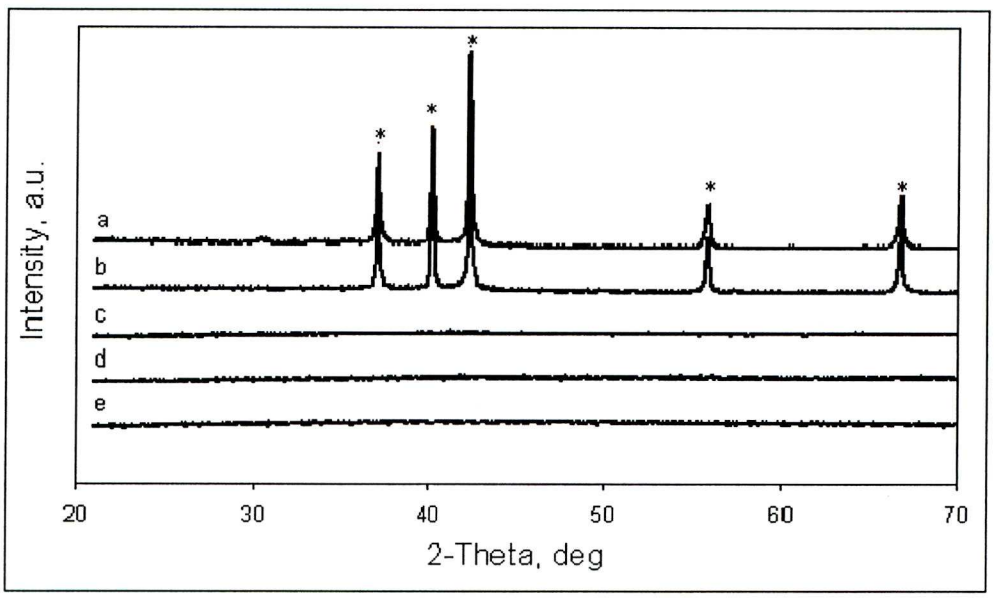

Figure 3.2 XRD pattrens for Zn-Cr oxides calcined at 300°C: (a) Zn-Cr (20:1), (b) Zn-Cr (10:1), (c) Zn-Cr (1:1), (d) Zn-Cr (1:10), (e) Zn-Cr (1:30). ZnO pattern is asterisked.

The same results with regard to XRD measurements for Zn-Cr (1:10) oxide were reported by Kozhevnikova *et al.* They prepared and characterised Zn-Cr (1:10) at 300°C and 350°C and found that the Zn-Cr oxide is amorphous after calcination at 300°C and crystalline after calcination at 350°C. Crystalline Zn-Cr (1:10) oxide was found to have a smaller surface area and a lower catalytic activity in MIBK synthesis than the amorphous Zn-Cr (1:10) [7].

3.3.2. XRD for Zn-Cr-Cu oxides

Figure 3.3 shows the XRD patterns for the Zn-Cr-Cu (a-d) and Cr-Cu (e) oxide catalysts. These catalysts were prepared using the same preparation method used for the Zn-Cr mixed oxide catalysts and calcined at 300°C.

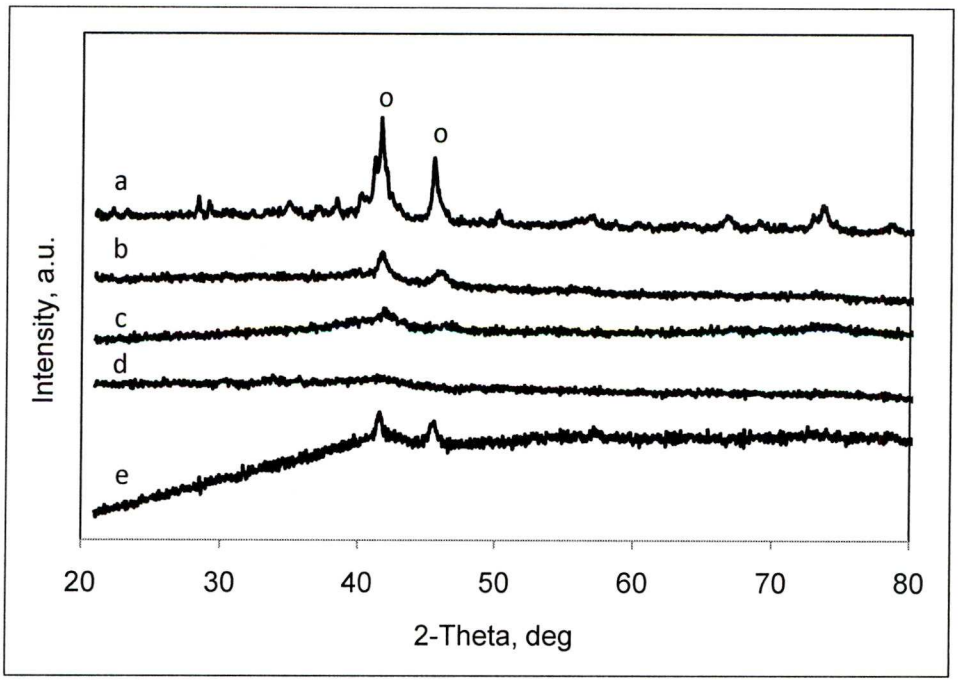

Figure 3.3 XRD pattrens for Zn-Cr-Cu oxides: (a) Zn-Cr-Cu (1:1:2), (b) Zn-Cr-Cu (1:1:1), (c) Zn-Cr-Cu (1:1:0.5), (d) Zn-Cr-Cu (1:1:0.1), (e) Cr-Cu (1:1). CuO pattern is circled.

The XRD measurements for the Zn-Cr-Cu oxide catalysts with various atomic ratios Zn/Cr/Cu ranging from 1:1:0.1 – 1:1:2 and for Cr-Cu (1:1) oxide, exhibited only the characteristic peaks attributable to CuO at $2\theta = 41.5^{o}$ and 45.5^{o}, with a crystallite size of about 23, 16, and 19 nm for Cr-Cu (1:1), Zn-Cr-Cu (1:1:1) and (1:1:2) oxides, respectively. These peaks were observed clearly at high copper content (Zn/Cr/Cu $\geq$ 1:1:0.5, Figures 3.3a and 3.3b). These peaks started to disappear with decreasing copper content (Figure 3.3c) until they were no longer observed in the XRD pattrens of Zn/Cr/Cu (1:1:0.1) (Figure 3.3d). In the XRD pattrens, no peaks attributed to the Cr_2O_3 species were observed, suggesting that Cr_2O_3 exists in amorphous phase [8]. Wang *et al.* have reported similar findings and have noticed that at low percentages ($\leq$40%) the copper species in the catalysts are present as Cu_2O and Cu(0), and no signal of Cr_2O_3 species appears, which indicates that Cr_2O_3 species is completely dispersed and present in amorphous phase [3].

For Zn-Cr-Cu and Cr-Cu samples reduced under hydrogen for 2 h at 300°C, the XRD showed the characteristic peaks at $2\theta = 50.7^{o}$ and 59.7^{o} attributed to Cu(0) (Figure 3.4) with crystallite sizes of about 30, 21, 44 and 44 nm for Cr-Cu (1:1), Zn-Cr-Cu (1:1:0.8), (1:1:1) and (1:1:2) oxides respectively. These results suggest that, when the catalyst samples were pretreated under hydrogen, copper was reduced from Cu(II) to Cu(0). These peaks decrease with decreasing copper content as shown in Figures 3.4 (b-d).

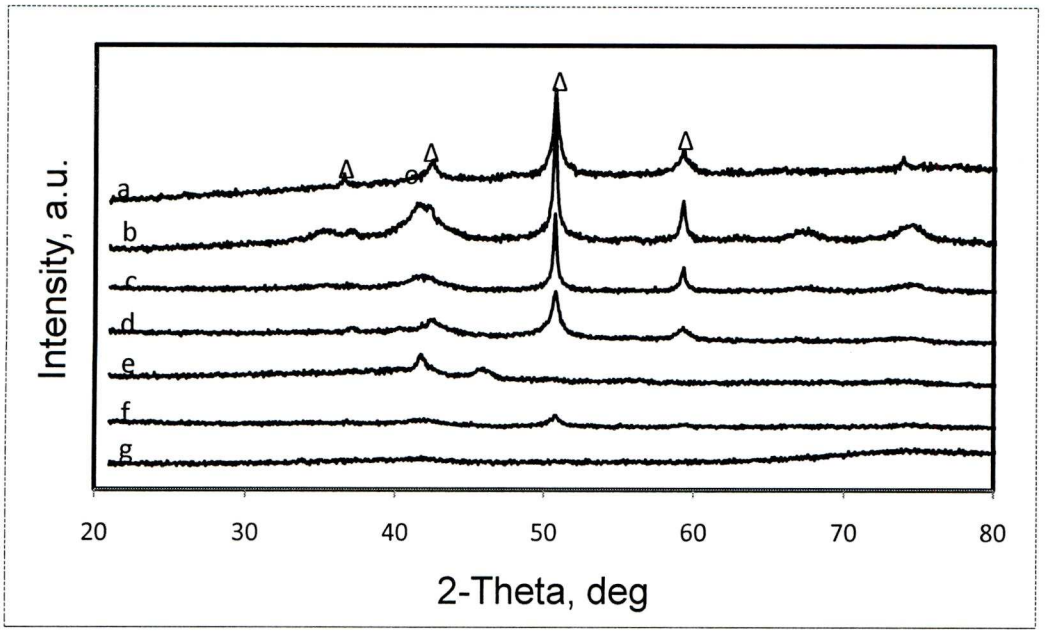

Figure 3.4. XRD pattrens for Zn-Cr-Cu oxides: (a) Cr-Cu (1:1), (b) Zn-Cr-Cu (1:1:2), (c) Zn-Cr-Cu (1:1:1), (d) Zn-Cr-Cu (1:1:0.8), (e) Zn-Cr-Cu (1:1:0.5), (f) Zn-Cr-Cu (1:1:0.2), (g) Zn-Cr-Cu (1:1:0.1), CuO and Cu patterns are circled and triangled, respectively.

3.4. Thermogravimetric analysis (TGA)

In this study, TG analysis (TGA) was performed on Zn-Cr and Zn-Cr-Cu oxide catalysts and was used to determine the H_2O content in the catalysts and their thermal stability. The TG technique was described in Section 2.4.1 and the results are summarised in Tables 3.5 and 3.6 for Zn-Cr and Zn-Cr-Cu oxides, respectively. The thermal behaviour of Zn-Cr and Zn-Cr-Cu oxide catalysts has already been subject of many investigations [1, 7, 9-12]. The results we obtained on the Perkin-Elmer TGA 7 instrument were in good agreement with the results previously obtained by other researchers. Generally, solid Zn-Cr and Zn-Cr-Cu oxides accommodate a small amount of water, depending on catalyst crystallinaty (amorphous or crystalline).

3.4.1. TGA of Zn-Cr oxides

The TG analysis of amorphous and crystalline samples of Zn-Cr oxides and Pd/Zn-Cr was performed in a nitrogen atmosphere after pretreatment at 300°C for 5 h under 30 mL/min of nitrogen flow. It showed two main stages of a monotonous loss of water from the catalysts in the temperature range of 30-600°C (Table 3.5 and Figures 3.5-3.10).

- The first stage took place in the range from room temperature to 250-300°C. It showed an endothermic peak centred between 120-160°C which corresponds to weight loss of about 0.77-4.89%. This was probably due to the removal of physisorbed water from the catalyst surface [9-11], as well as the removal of water resulting from hydroxyl groups condensation [9] to form solid products such as ZnO and CrOOH [10-12].

- In the second stage, a weight loss took place when the temperature was raised from 300 to 600°C, showing a second endothermic peak centred between 500-560°C. This weight loss was attributed to the removal of water resulting from further condensation of hydroxyl groups in CrOOH to form a lower chromium oxide (Cr_2O_3) as well as $ZnCr_2O_4$ [1, 12]. These results can be seen in Figures 3.5-3.10 at temperatures between 300 and 600°C. The amount of water lost decreased with decreasing chromium content in both amorphous and crystalline materials (Figures 3.5-3.7 for Zn-Cr (1:30), Zn-Cr (1:10) and Zn-Cr (1:1) oxides and Figures 3.8-3.9 for Zn-Cr (10:1) and Zn-Cr (20:1) oxides).

Table 3.5 Summary of TGA results for Zn-Cr mixed oxide catalysts.

Catalyst	Temperature range (°C)	Weight loss (%)
Zn-Cr (1:30) oxide	30-300	0.93
	300-600	8.02
Zn-Cr (1:10) oxide	30-300	1.95
	300-600	7.24
Zn-Cr (1:1) oxide	30-300	4.69
	300-600	4.28
Zn-Cr (10:1) oxide	30-300	0.77
	300-600	2.06
Zn-Cr (20:1) oxide	30-300	1.15
	300-600	0.87
0.3%Pd/Zn-Cr (20:1) oxide	30-300	0.82
	300-600	0.91
0.1%Pd/Zn-Cr (1:1) oxide	30-300	4.28
	300-600	4.28
0.3%Pd/Zn-Cr (1:1) oxide	30-300	4.89
	300-600	4.43
1.0%Pd/Zn-Cr (1:1) oxide	30-300	4.56
	300-600	3.96

The TGA results obtained are summarised in Table 3.5. It can be seen that in the amorphous oxides (Zn/Cr = 1:30 – 1:1) the total amount of water (~9 wt%) is higher than that (2.0-2.8%) in the crystalline oxides (Zn/Cr = 10:1 – 20:1). These results are close to those reported in the literature [7] and demonstrate that the amount of water in the catalysts depends on the Zn/Cr ratio as well as on the preparation conditions of Zn-Cr oxides.

In Figure 3.10, the TGA curve for 0.3%Pd/Zn-Cr (1:1) oxide shows the loss of water to be about 9.32%. This weight loss is close to that shown in Figure 3.7, which

clearly indicates that water content is not affected by palladium supported on the Zn-Cr oxide.

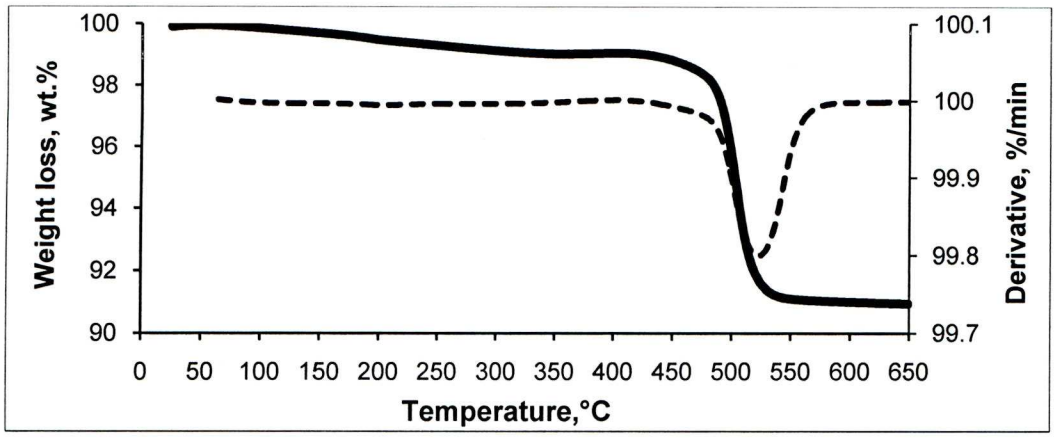

Figure 3.5 TG (solid line) and DTG (dashed line) curves for Zn-Cr (1:30) oxide.

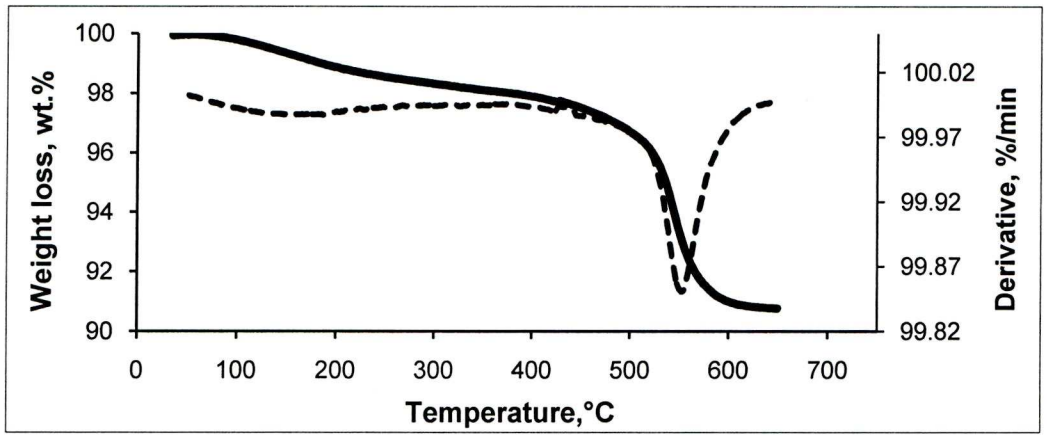

Figure 3.6 TG (solid line) and DTG (dashed line) curves for Zn-Cr (1:10) oxide.

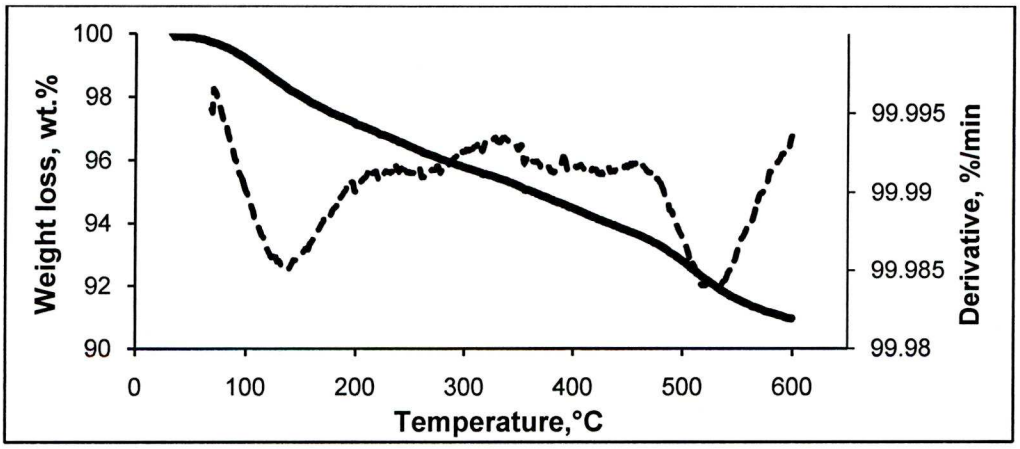

Figure 3.7 TG (solid line) and DTG (dashed line) curves for Zn-Cr (1:1) oxide.

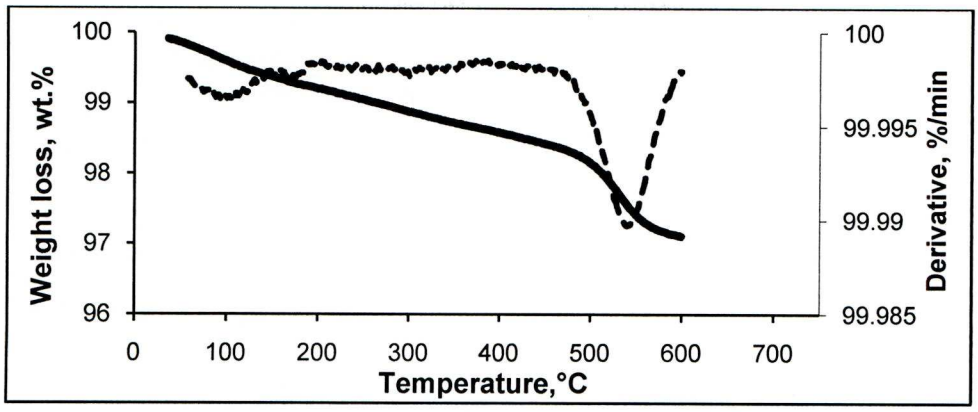

Figure 3.8 TG (solid line) and DTG (dashed line) curves for Zn-Cr (10:1) oxide.

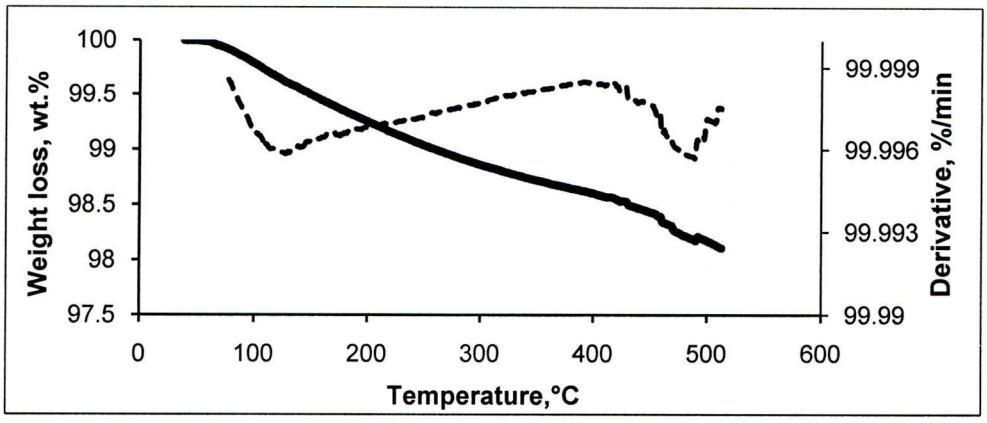

Figure 3.9 TG (solid line) and DTG (dashed line) curves for Zn-Cr (20:1) oxide.

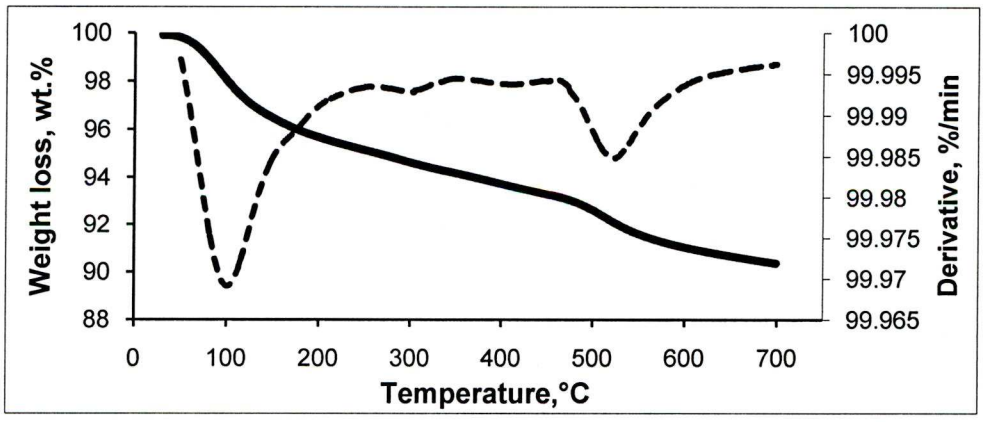

Figure 3.10 TG (solid line) and DTG (dashed line) curves for 0.3%Pd/Zn-Cr (1:1) oxide.

3.4.2. TGA of Zn-Cr-Cu oxides

The experimental procedure for TG analysis of Zn-Cr oxides was also used to determine the amount of water in the Zn-Cr-Cu oxide catalysts. The results of the TG

analysis are presented in Table 3.6, and the TG and DTG curves are also shown in Figures 3.11-3.13. In general, the TG results for Zn-Cr-Cu oxides were close to those obtained for Zn-Cr oxides, showing two endothermic peaks for water loss (Figure 3.11). The first peak was centred between 120-160°C when the temperature was raised from 30 to 300°C. It can be attributed to the loss of physisorbed water on the catalyst surface, as well as to the removal of water that resulted from hydroxyl group condensation to form a metal oxide at higher temperatures [9-11]. The second endothermic peak centred between 550°C and 600°C may be attributed to a further loss of water from hydroxyl group condensation in CrOOH to form ZnO, Cr_2O_3 and $ZnCr_2O_4$ [9, 12].

Table 3.6 Summary of TGA results for Zn-Cr-Cu mixed oxide catalysts.

Catalyst	Temperature rang (°C)	Weight loss (%)
Cr-Cu (1:1) oxide	30-300	2.91
	300-700	5.49
Zn-Cr-Cu (1:1:0.1) oxide	30-300	0.70
	300-700	3.73
Zn-Cr-Cu (1:1:0.2) oxide	30-300	1.38
	300-700	3.94
Zn-Cr-Cu (1:1:0.5) oxide	30-300	1.91
	300-700	4.72
Zn-Cr-Cu (1:1:0.8) oxide	30-300	2.23
	300-700	5.11
Zn-Cr-Cu (1:1:1) oxide	30-300	2.18
	300-700	5.32
Zn-Cr-Cu (1:1:2) oxide	30-300	1.35
	300-700	5.21

Table 3.6 summarises the TGA results obtained. It can be seen that increasing the Cu content in Zn-Cr-Cu oxides has a relatively small effect on the total water content in the oxides, slightly increasing it from 4.43% to 6.56%. Comparison of the results for Cr-Cu (1:1) and Zn-Cr-Cu (1:1:1) oxides shows that Zn has no effect on the water content in these oxides.

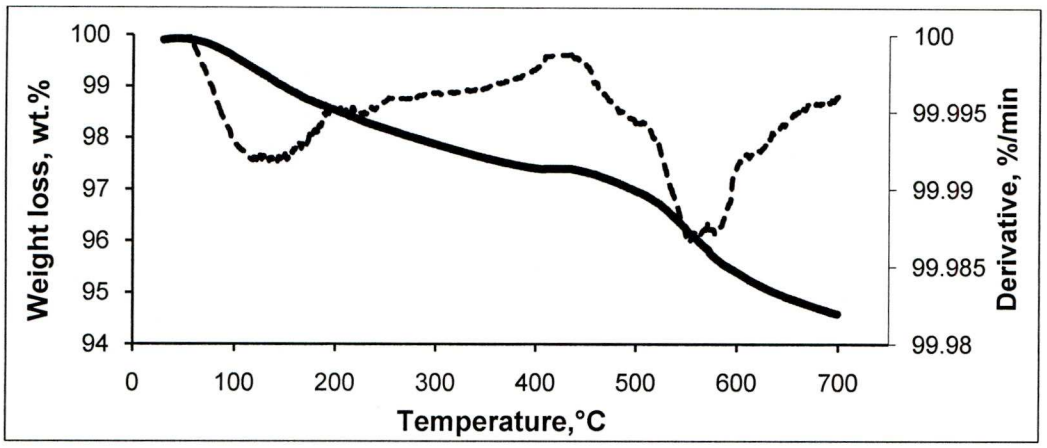

Figure 3.11 TG (solid line) and DTG (dashed line) curves for Zn-Cr-Cu (1:1:0.1) oxide.

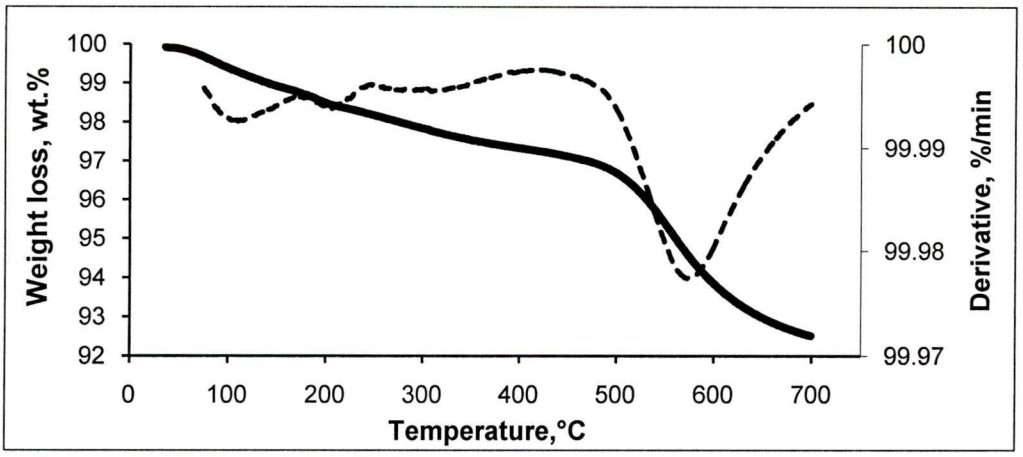

Figure 3.12 TG (solid line) and DTG (dashed line) curves for Zn-Cr-Cu (1:1:1) oxide.

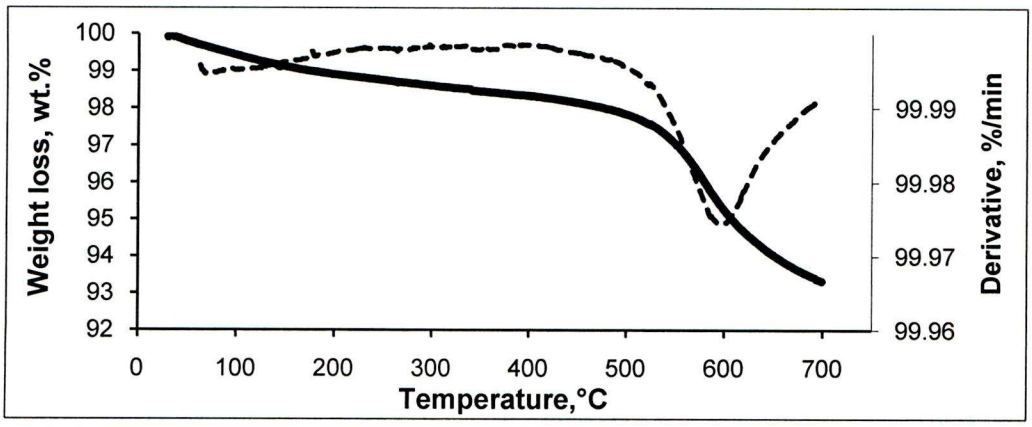

Figure 3.13 TG (solid line) and DTG (dashed line) curves for Zn-Cr-Cu (1:1:2) oxide.

3.5. Surface area and porosity

The measurement of physisorption of nitrogen at 77 K provides very useful data from which information about the catalyst's surface area and porosity can be obtained. For the characterisation of the catalyst's texture, plotting the volume of N_2 adsorbed against its relative pressure to generate the N_2 adsorption isotherm is needed. According to IUPAC classification, this isotherm can be classified into six types of adsorption isotherms, depending on the porous texture of individual solid materials [13-17]. Figure 3.14 shows four different types of adsorption isotherms which are usually found and exhibited by real surfaces in catalyst characterisation [17]. Type I, II, IV and VI isotherms are representative of microporous, macroporous, mesoporous and uniform ultramicroporous solids respectively. Type II and IV isotherms will be illustrated in more detail due to their applications with regard to the catalysts prepared in this study.

- On macroporous solids (type II), the formation of the adsorption monolayer is the main process at low relative pressure, whilst the formation of the adsorption multilayer occurs at high relative pressures. The adsorbate thickness increases with time until condensation pressure has been reached. A strong interaction between adsorbate and

adsorbent causes the pressure of the first monolayer formation to be lower. However, the formation of the adsorption monolayer and multilayer processes always overlap.

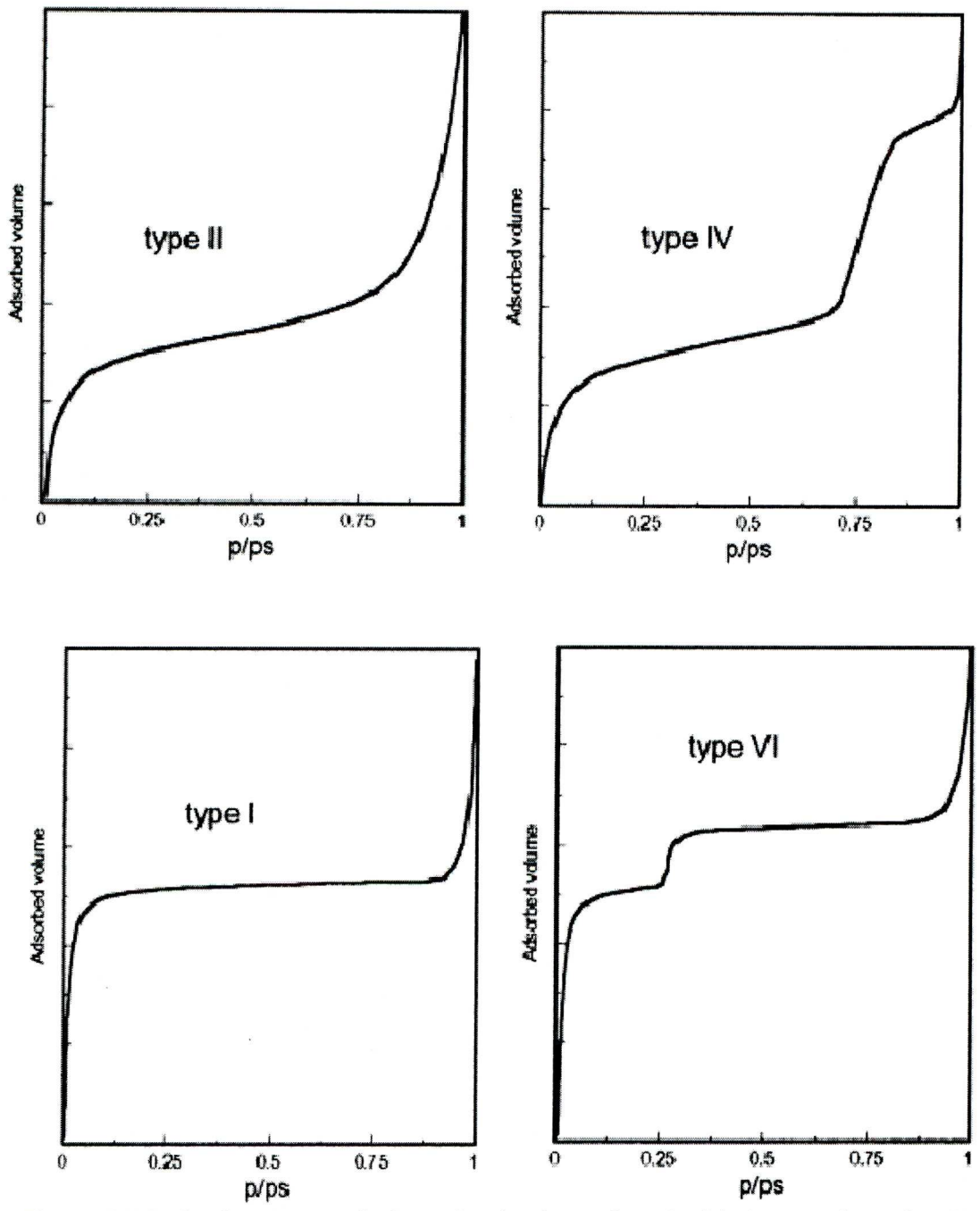

Figure 3.14 The four types of adsorption isotherm found with the N_2 adsorption [17].

- On mesoporous solids (Type IV), the same formation process with regard to the adsorption monolayer occurs at low relative pressures, while at high relative pressures

the formation of adsorption multilayer occurs until condensation takes place, giving a sharp increase in the observed volume of the adsorption gas physisorbed. The larger the mesopores present in the material, the higher the relative pressure at which this process occurs. Adsorption continues as mesopores are filled. Many common catalysts belong to this class of solids.

When the adsorbate reaches saturation, desorption takes place by evaporating the adsorbate from the solid surface and pores. However, on mesoporous solids, this process takes place at lower pressures than those on macroporous solids giving rise capillary condensation leading to a hysteresis loop. Figure 3.15 shows the four hysteresis types that have been recognized in terms of the IUPAC classification [17].

Types H1 and H2 hysteresis isotherms are shown when the sample pores have a uniform or non-uniform size respectively, and are formed when the solid materials consist of particles crossed by closely cylindrical channels or made by aggregates (consolidated) or agglomerates (unconsolidated) that are spheroidal in shape. These hystereses are due to a different size of pore bodies (e.g. ink-bottle shaped pores) and pore mouths or to a different behaviour in terms of adsorption and desorption in near cylindrical pores. Many common mesoporous catalysts exhibit the Type H1 and H2 hysteresis adsorption isotherm [17].

Types H3 an H4 hysteresis are shown when the sample pores have a uniform (type H4) or non-uniform (type H3) size, and are produced with solid materials consisting of aggregates or agglomerate particles forming slit-shaped pores (plates or edged particles analogous to cubes). These hystereses are due to the different behaviour in adsorption and desorption. Active carbon and zeolites are typical examples of catalysts that generate these types of hysteresis isotherms.

Moreover, when solid materials possess blind cylindrical, cone-shaped and wedge-shaped pores, no hysteresis isotherm will be formed. However, due to the usual irregular catalyst pores, only solids with a much reduced hysteresis loop will be observed.

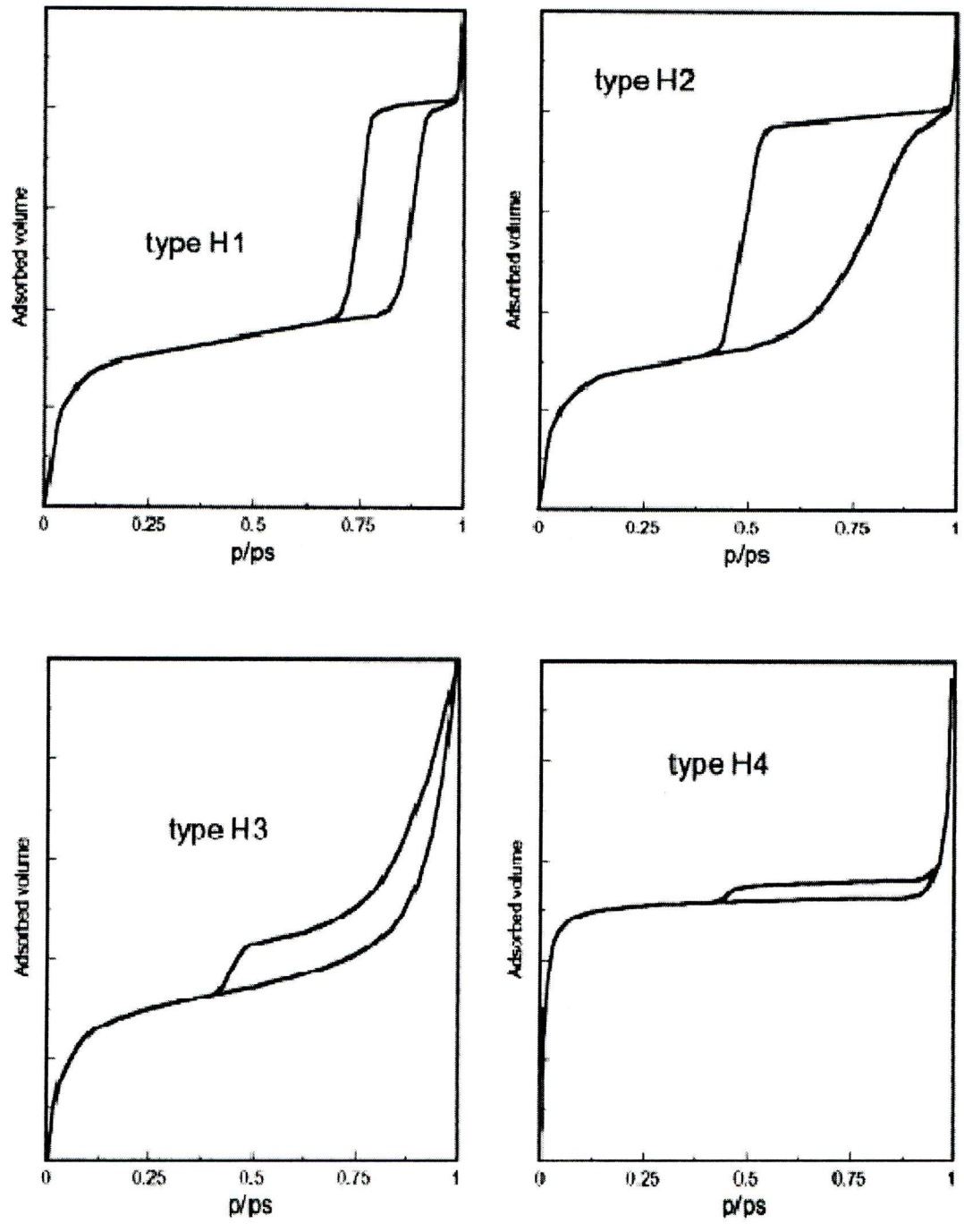

Figure 3.15 The four hysteresis shapes usually observed with N_2 adsorption-desorption isotherms [17].

The total surface area of the prepared catalysts under consideration was calculated using the Brunauer-Emmett-Teller (BET) method [18]. The pore size distribution and the total pore volumes were both determined using the Barrett, Joyner and Halenda (BJH) method [19]. The general procedure for the measurement of the surface area and porosity is described in more detail in Section 2.4.2. The results of the BET surface areas and the porosities of our Zn-Cr and Zn-Cr-Cu oxide catalysts are summarised in Table 3.7 and 3.8, respectively.

Zn-Cr and Zn-Cr-Cu oxide catalysts possess various surface areas depending on the catalyst composition (amorphous or crystalline) as well as on the preparation method and the calcination temperature [1, 2, 6, 7, 20-23].

3.5.1. Surface area and porosity of Zn-Cr oxides

The BET surface area and the porosity of the Zn-Cr oxide catalysts has already been the subject of many investigations. Whenever comparison is possible, our adsorption data for both amorphous and crystalline oxides are in agreement to those obtained by other researchers previously [1, 2, 7, 24-26].

Table 3.7 shows the surface areas of the prepared catalysts. For the amorphous Cr-rich oxides, the surface area increases substantially with increasing chromium content from 132 to 223 m^2/g for Zn-Cr (1:1) and (1:30) respectively. These results are in agreement with those reported in the literature [2, 7]. The larger surface areas and pore volumes (0.11–0.16 cm^3/g) are clearly evident for these oxides, but with smaller average pore diameters (29–33 Å) than for the crystalline Zn-rich oxides (33 – 36 m^2/g, 0.08–0.09 cm^3/g and 91–112 Å respectively) [7, 25]. Ohta *et al.* prepared and characterised the $Pt/ZnO\text{-}Cr_2O_3$ catalyst for the low-temperature dehydrogenation of

isobutene. They found that the larger the surface area, the smaller will be the ZnO crystallite size [6]. These results are in agreement with our BET and XRD results for Zn-rich oxides.

Table 3.7 The texture of Zn-Cr oxides and Pd/Zn-Cr catalysts.

Catalyst	S_{BET} (m^2/g)	Pore diameter[a] (Å)	Pore volume[b] (cm^3/g)
Zn-Cr (1:30) oxide	223	29	0.16
Zn-Cr (1:10) oxide	193	31	0.15
Zn-Cr (1:1) oxide	132	33	0.11
Zn-Cr (10:1) oxide	33	112	0.09
Zn-Cr (20:1) oxide	36	91	0.08
0.3%Pd/Zn-Cr (1:30) oxide	189	36	0.16
0.3%Pd/Zn-Cr (1:10) oxide	180	31	0.14
0.1%Pd/Zn-Cr (1:1) oxide	99	26	0.06
0.3%Pd/Zn-Cr (1:1) oxide	112	35	0.09
1.0%Pd/Zn-Cr (1:1) oxide	107	26	0.07
0.3%Pd/Zn-Cr (10:1) oxide	32	103	0.09
0.3%Pd/Zn-Cr (20:1) oxide	19	87	0.04

[a] Average pore diameter using the BJH method.

[b] Single point total pore volume using the BJH method.

The nitrogen adsorption-desorption isotherm for bulk Zn-Cr (1:30) and for Pd/Zn-Cr oxides catalysts are shown in Figures 3.16 - 3.20 respectively. An isotherm that is of the type IV classification is observed for the amorphous Cr-rich catalyst. This type of isotherm is indicative of a mesoporous material (2 nm < pore diameter < 50 nm)

[17]. This result is in agreement with that of the previous study [27]. The isotherm has a type H2 hysteresis loop and there is also an indication of the presence of narrow (2-5 nm) mesopores, which are of a non-uniform shape. If these pores were wider, type II isotherms would be observed [16], and this is clearly seen for crystalline Zn-Cr oxide isotherms (Figures 3.19 and 3.20). This type of isotherm is characteristic of nonporous or macroporous materials (>50 nm pore diameter) [16, 17]. However, a small hysteresis loop (type H3) with a non-uniform slit-shaped pore distribution was observed according to the IUPAC classification. This indicates the presence of mesoporous solids [16, 17]. These results are in agreement with previous studies [4, 9].

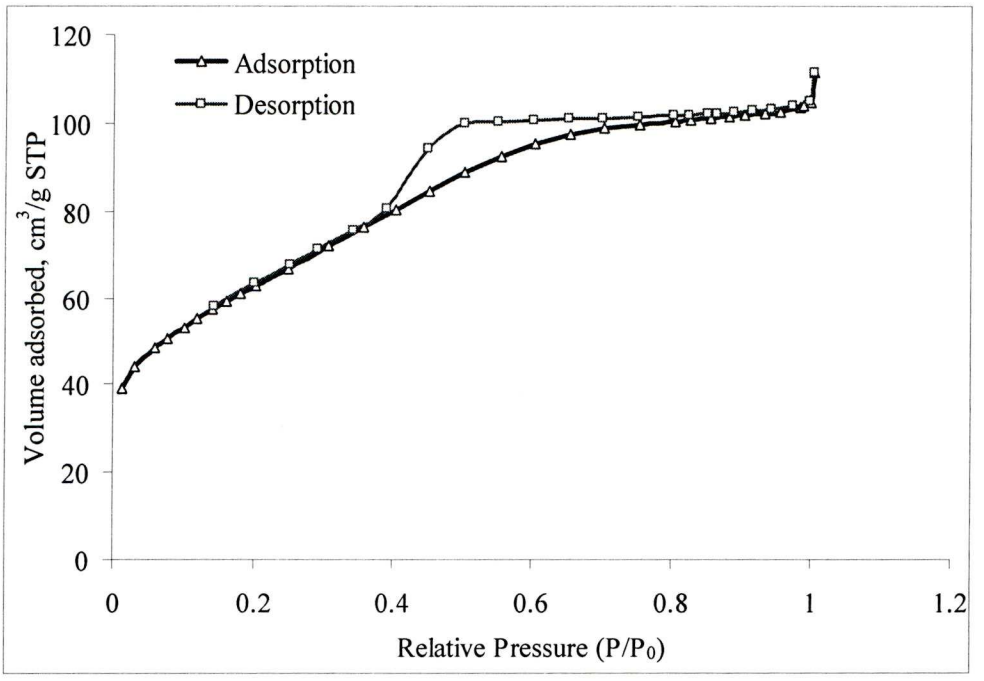

Figure 3.16 N_2 adsorption isotherm for Zn-Cr (1:30) oxide.

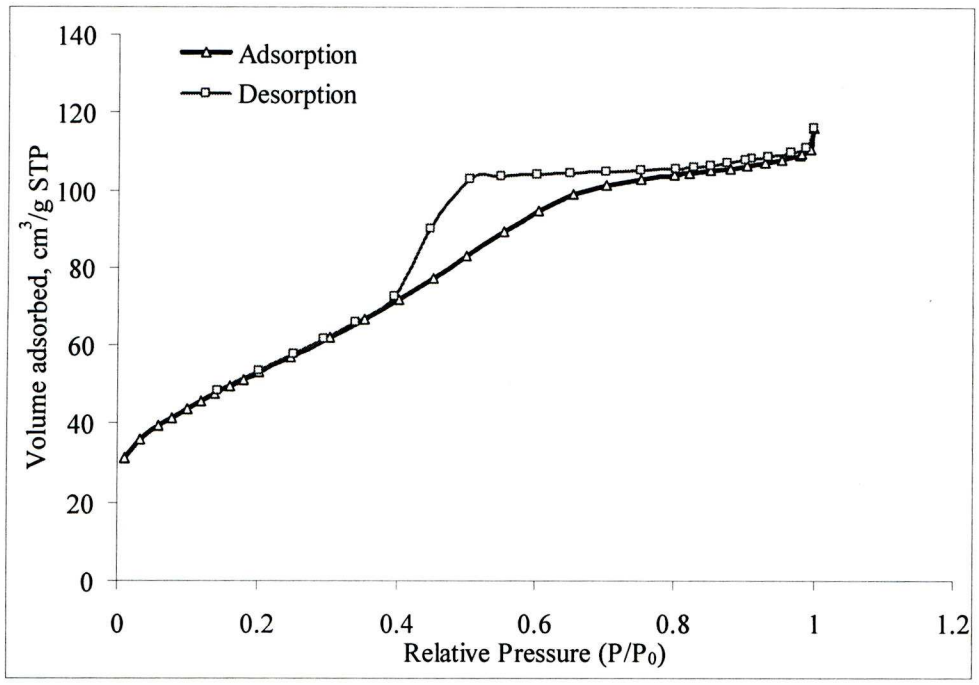

Figure 3.17 N_2 adsorption isotherm for 0.3%Pd/Zn-Cr (1:30) oxide.

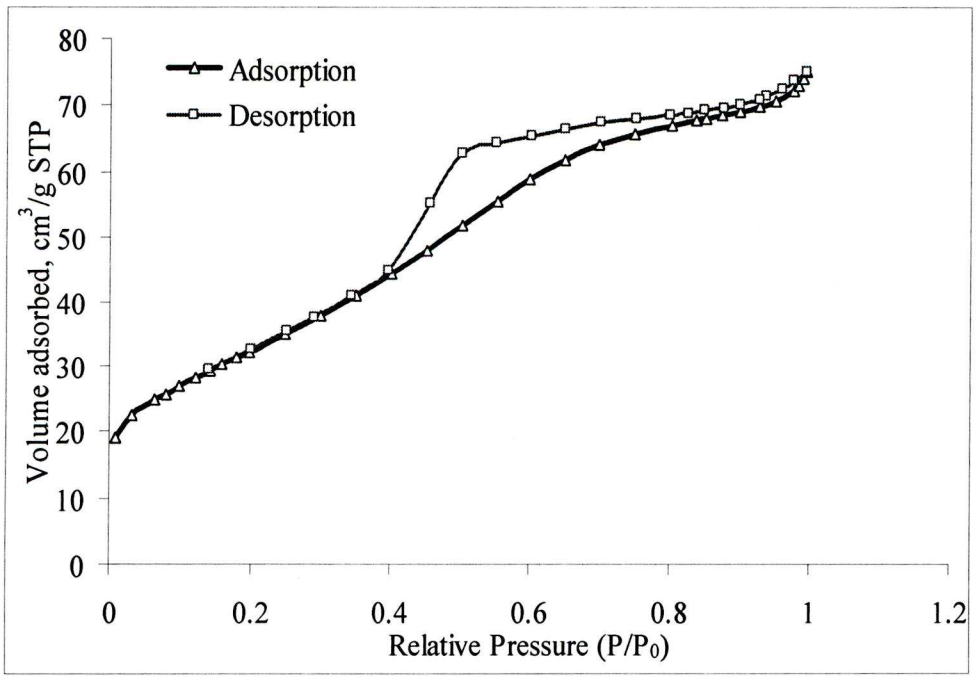

Figure 3.18 N_2 adsorption isotherm for 0.3%Pd/Zn-Cr (1:1) oxide.

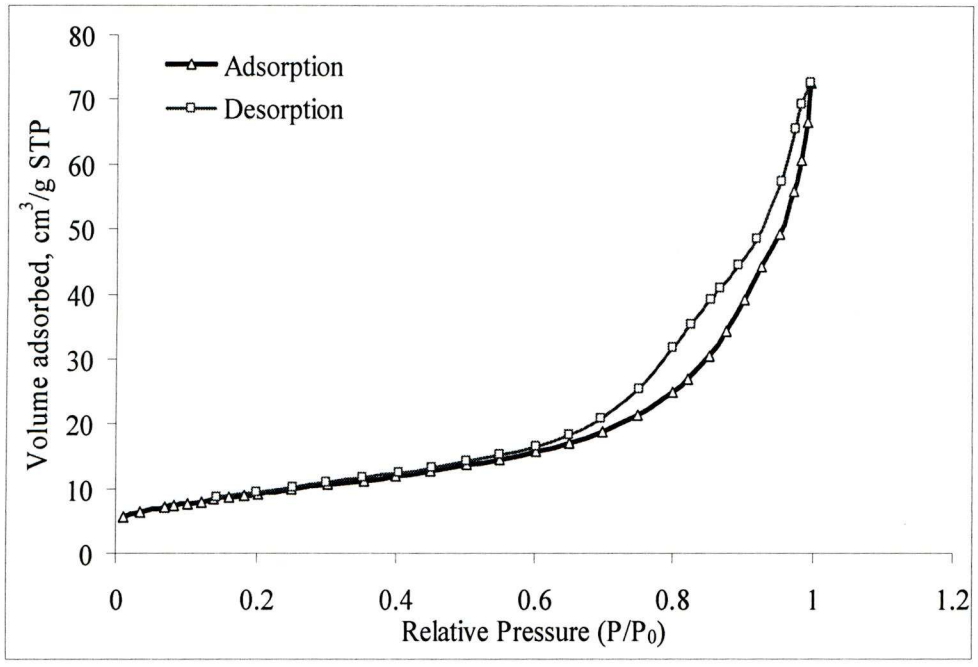

Figure 3.19 N_2 adsorption isotherm for 0.3%Pd/Zn-Cr (10:1) oxide.

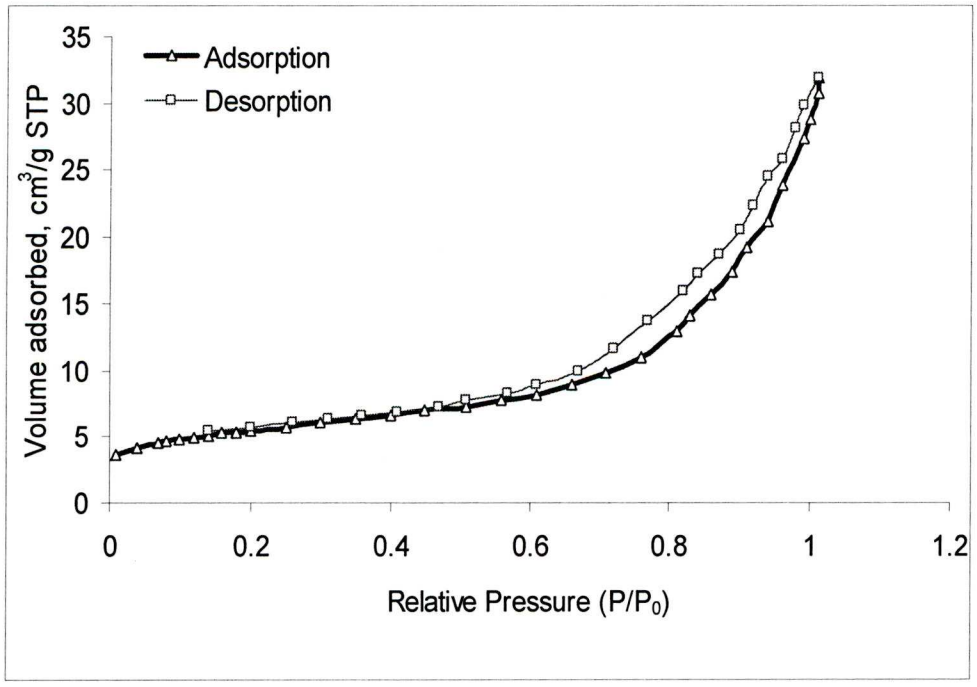

Figure 3.20 N_2 adsorption isotherm for 0.3%Pd/Zn-Cr (20:1) oxide.

Palladium loading did not change the catalyst texture, but decreased the surface area and the pore volume to a small extent, as expected (Table 3.7). This is evidence of

palladium positioned on the surface of the catalysts. This has been observed in previous studies with Pd supported on a Zn-Cr (1:10) bifunctional catalyst [7].

The pore structure of Zn-Cr oxides was found to depend on their Zn/Cr ratio, as evidenced from the pore volume distributions (Figures 3.21 and 3.22). The Cr-rich amorphous oxides had a more regular pore structure in which pores of 35–37 Å diameter dominated, with smaller pores also being present. Pores larger than 40 Å diameter were not found in these oxides. In contrast, the Zn-rich crystalline oxides had a much broader pore size distribution (Figure 3.22). These oxides exhibited a sharp peak at 37–38 Å pore diameter as with the Cr-rich oxides, but also possessed larger pores of up to 1000 Å diameter (Figure 3.22), hence the larger average pore diameter. Zn-Cr (10:1) oxide exhibited a broad peak centred at 91 Å pore diameter. All these results were in agreement with those reported in the literature [26].

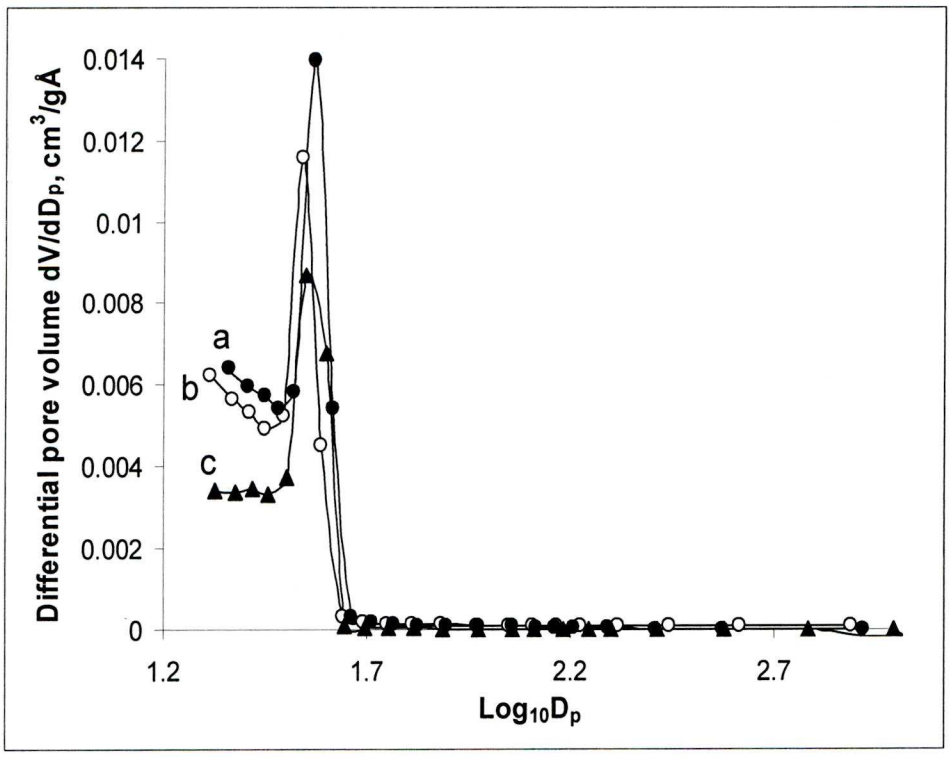

Figure 3.21 Distribution of pore volume as a function of pore diameter, D_p (in Å), for Zn-Cr oxides obtained by BJH method from nitrogen desorption. (a) Zn-Cr (1:10), (b) Zn-Cr (1:30), (c) Zn-Cr (1:1).

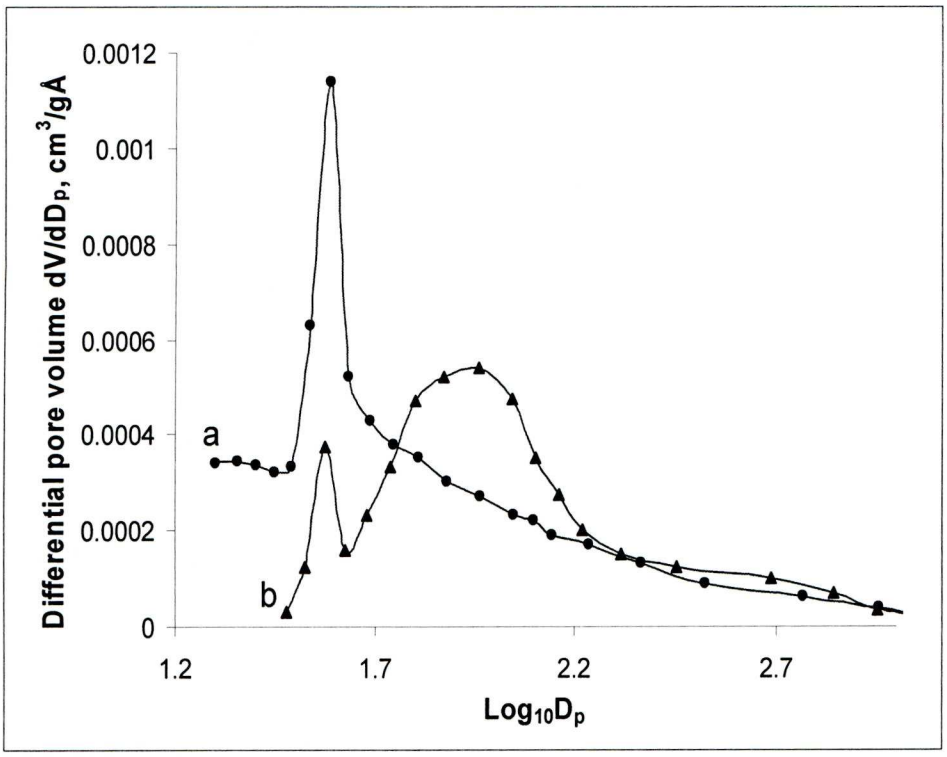

Figure 3.22 Distribution of pore volume as a function of pore diameter, D_p (in Å), for Zn-Cr oxides obtained by BJH method from nitrogen desorption. (a) Zn-Cr (20:1), (b) Zn-Cr (10:1).

3.5.2. Surface area and porosity of Zn-Cr-Cu oxides

The texture of the Zn-Cr-Cu oxide catalysts was characterised by N_2 physisorption at 77 K similarly to the Zn-Cr oxides. In general, the surface areas and the porosities of Zn-Cr-Cu oxides were very close to those found for amorphous Zn-Cr (1:1) oxides. Whenever comparison was possible, our results were in good agreement with those reported previously [20-23, 28].

Table 3.8 shows the data output from the N_2 adsorption isotherms for the bulk Cr-Cu and Zn-Cr-Cu oxide materials, before and after pretreatment under an H_2 gas flow for 2 h at 300°C, as well as that for the palladium doped Zn-Cr-Cu oxide catalysts prepared in this study.

Table 3.8 Catalyst texture from N_2 adsorption measurements.

Catalyst	S_{BET} (m^2/g)	Pore diameter[a] (Å)	Pore volume[b] (cm^3/g)
Cr-Cu (1:1) oxide	89	59	0.13
Zn-Cr-Cu (1:1:0.1) oxide	127	27	0.09
Zn-Cr-Cu (1:1:0.2) oxide	114	28	0.08
Zn-Cr-Cu (1:1:0.5) oxide	104	49	0.13
Zn-Cr-Cu (1:1:0.8) oxide	81	60	0.12
Zn-Cr-Cu (1:1:1.0) oxide	85	70	0.15
Zn-Cr-Cu (1:1:2) oxide	40	119	0.12
Zn-Cr-Cu (1:1:0.1) oxide[c]	80	19	0.04
Zn-Cr-Cu (1:1:0.5) oxide[c]	73	55	0.10
Zn-Cr-Cu (1:1:1.0) oxide[c]	66	71	0.12
0.3%Pd/Zn-Cr-Cu (1:1:1.0) oxide[c]	60	76	0.11
0.1%Pd/Zn-Cr-Cu (1:1:1.0) oxide[c]	72	68	0.12

[a] Average pore diameter using the BJH method.

[b] Single point total pore volume using the BJH method.

[c] After reduction under H_2 for 2 h at 300°C.

As seen from Table 3.8, the Cr-Cu (1:1) oxide had a surface area, pore size and pore volume of 89 m^2/g, 59 Å and 0.13 cm^3/g, respectively. This surface area was close to that obtained by other researchers [21, 28]. For the Zn-Cr-Cu oxides, the surface area decreased with increasing copper content, from 127 m^2/g for Zn-Cr-Cu (1:1:0.1) to 40 m^2/g for Zn-Cr-Cu (1:1:2). In contrast, the catalyst pore sizes increased with increasing copper content, from 27 to 119 Å for Zn-Cr-Cu (1:1:0.1) and (1:1:2), respectively. The

pore volume was between 0.09 and 0.15 cm^3/g and was also found to depend on the copper content.

The pretreatment of catalysts under H_2 for 2 h at 300°C reduced the surface area to some extent. This might be due to sintering of microcrystalline metallic copper [20]. The introduction of palladium into the oxides did not change the catalyst texture, but decreased the surface area and pore volume, as expected (Table 3.8). This is evidence of palladium positioned on the surface of the catalysts. This has been observed in the previous section with Pd supported on Zn-Cr oxide.

The nitrogen adsorption-desorption isotherms for Cr-Cu and Zn-Cr-Cu oxides are shown in Figures 3.23 and 3.24 to 3.27, respectively. In general, these results were close to those observed for Zn-Cr oxides. The isotherm for Cr-Cu and Zn-Cr-Cu oxides can be described as type IV, with a non-uniform shaped pore distribution (type H2 hysteresis loop). This is with the exception of Zn-Cr-Cu (1:1:2) oxide (Figure 3.27) which exhibits a type II isotherm with a non-uniform shaped pore distribution (type H3 hysteresis loop) according to the IUPAC classification [17]. The isotherms indicate that all these oxides are mostly mesoporous materials [16, 17]. However, the exhibition of type II isotherm with Zn-Cr-Cu (1:1:2) oxide is due to a wider range of pore sizes [16].

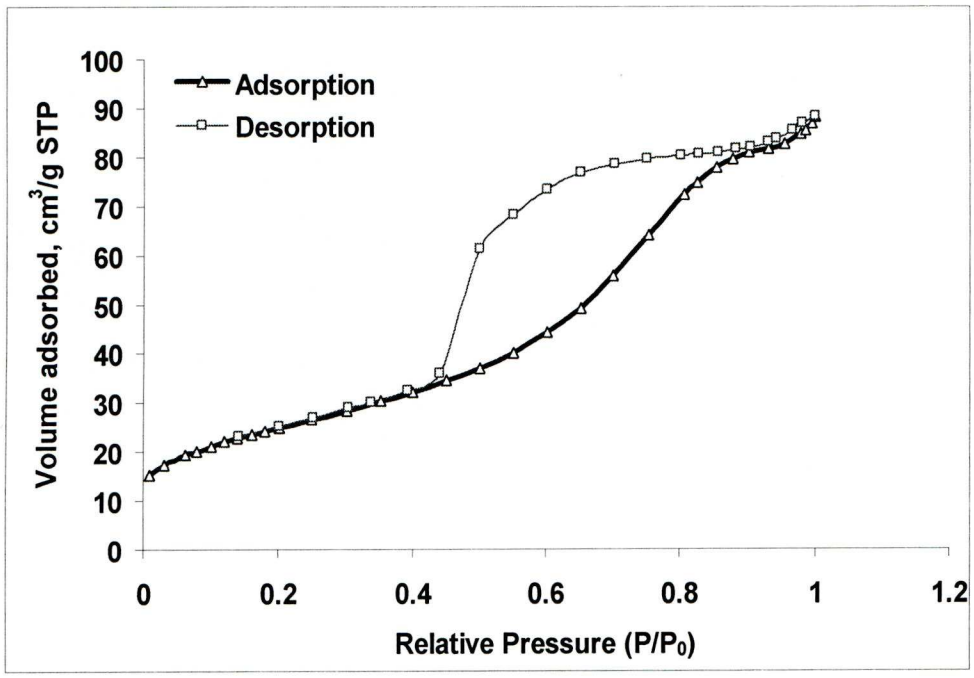

Figure 3.23 N_2 adsorption isotherm for the Cr-Cu (1:1) oxide.

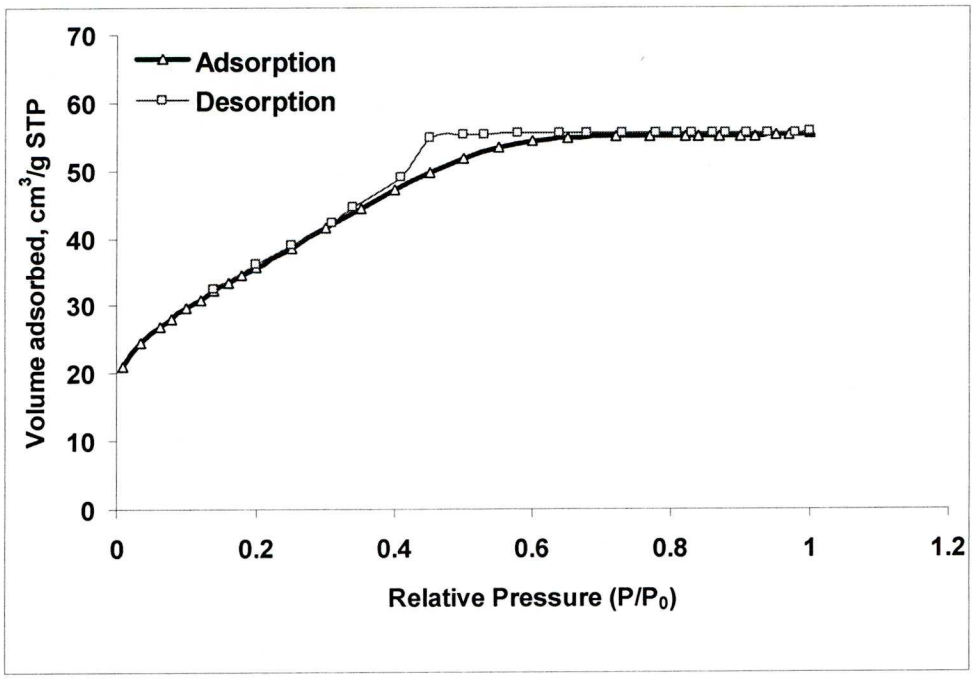

Figure 3.24 N_2 adsorption isotherm for the Zn-Cr-Cu (1:1:0.1) oxide.

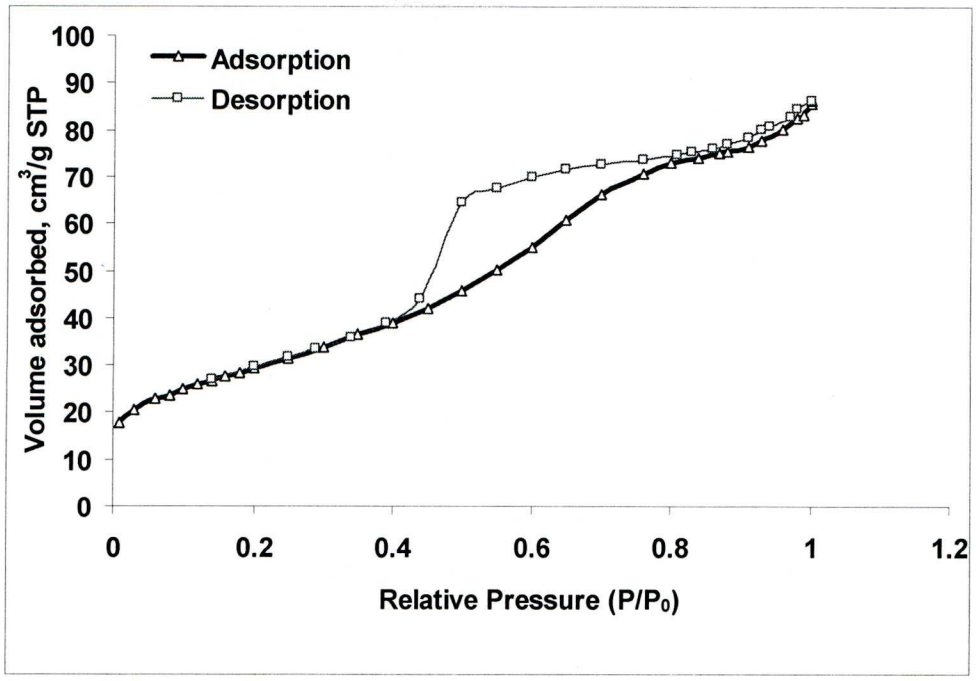

Figure 3.25 N_2 adsorption isotherm for the Zn-Cr-Cu (1:1:0.5) oxide.

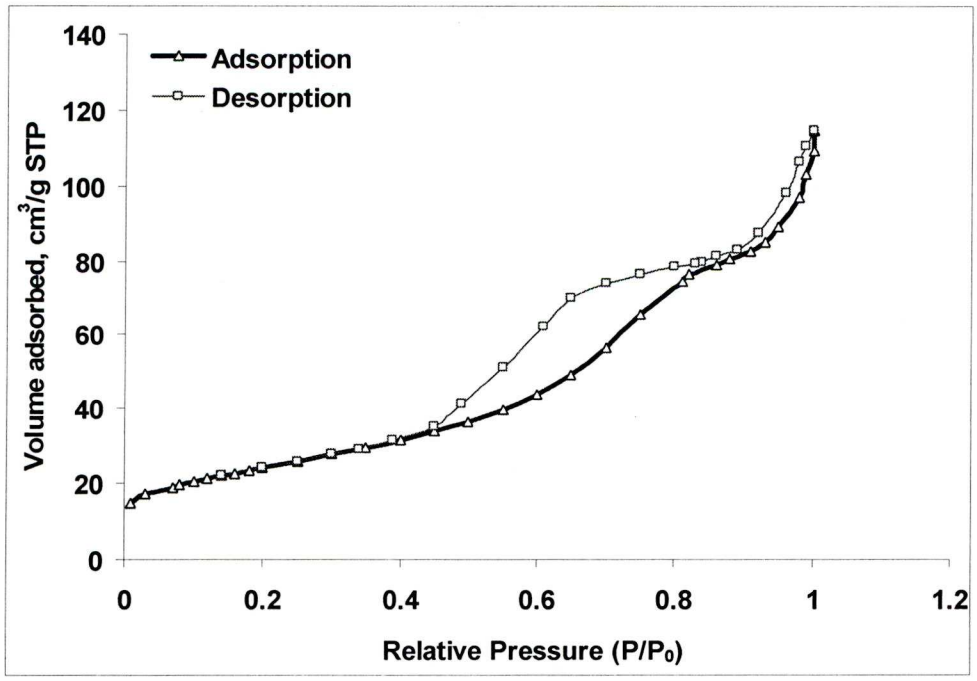

Figure 3.26 N_2 adsorption isotherm for the Zn-Cr-Cu (1:1:1) oxide.

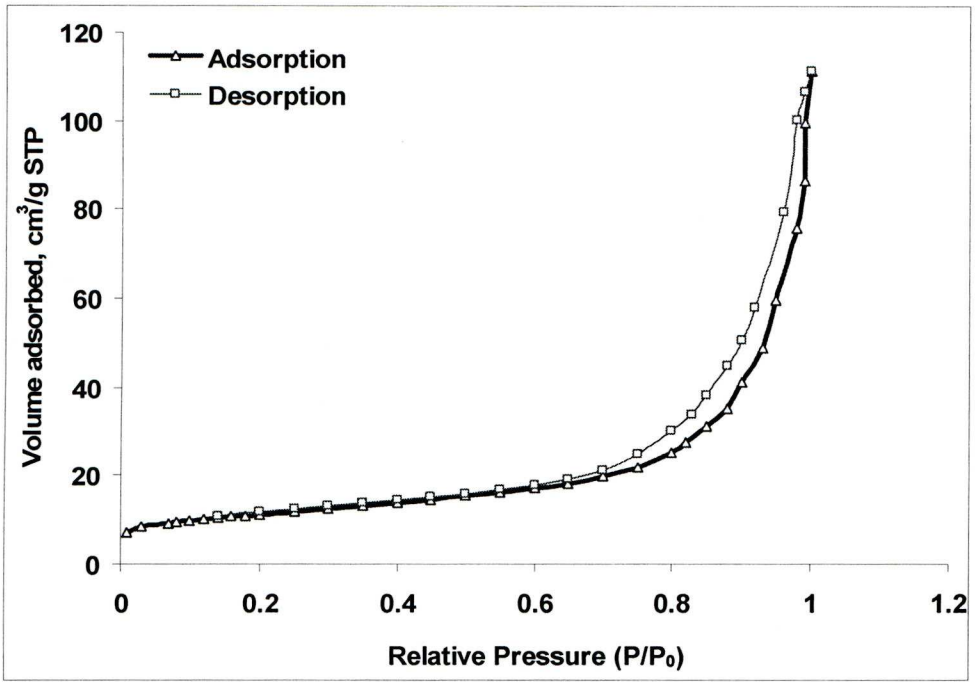

Figure 3.27 N_2 adsorption isotherm for the Zn-Cr-Cu (1:1:2) oxide.

The mesopore-size distributions of the Cr-Cu (1:1) and the Zn-Cr-Cu oxides were derived from the desorption isotherms using the BJH (Barret-Joyner-Halenda) method and are shown in Figures 3.28 and 3.29 respectively. For the Cr-Cu (1:1) oxide, there is a high density of pores in the mesoporous region of between 25 and 80 Å, and the majority of pores are centred at 35 Å. In the Zn-Cr-Cu oxides, the smaller Cu content catalysts (Zn-Cr-Cu (1:1:0.1), (1:1:0.2), (1:1:0.5), and (1:1:0.8) shown in Figures 3.29 (a-d) had a more regular pore structure in which pores of 34–38 Å diameter dominated, with smaller pores also present. In contrast, larger Cu content catalysts had a much broader pore size distribution, in the range of 27-72 and 21-1200 Å, with the broadest distribution being between 36 to 48 Å and 75 to 1200 Å for Zn-Cr-Cu (1:1:1) and (1:1:2) oxides respectively (Figures 3.29 (e) and (f)). It should be noted that the N_2 adsorption technique employed in this study was not able to account for pore sizes of less than 2 Å. However, it is clearly seen from the pore size distribution obtained for

Zn-Cr-Cu (1:1:1) and (1:1:2) oxides that there is a high density of pores present in the mesoporous range (2 nm < pore diameter < 50 nm) [17].

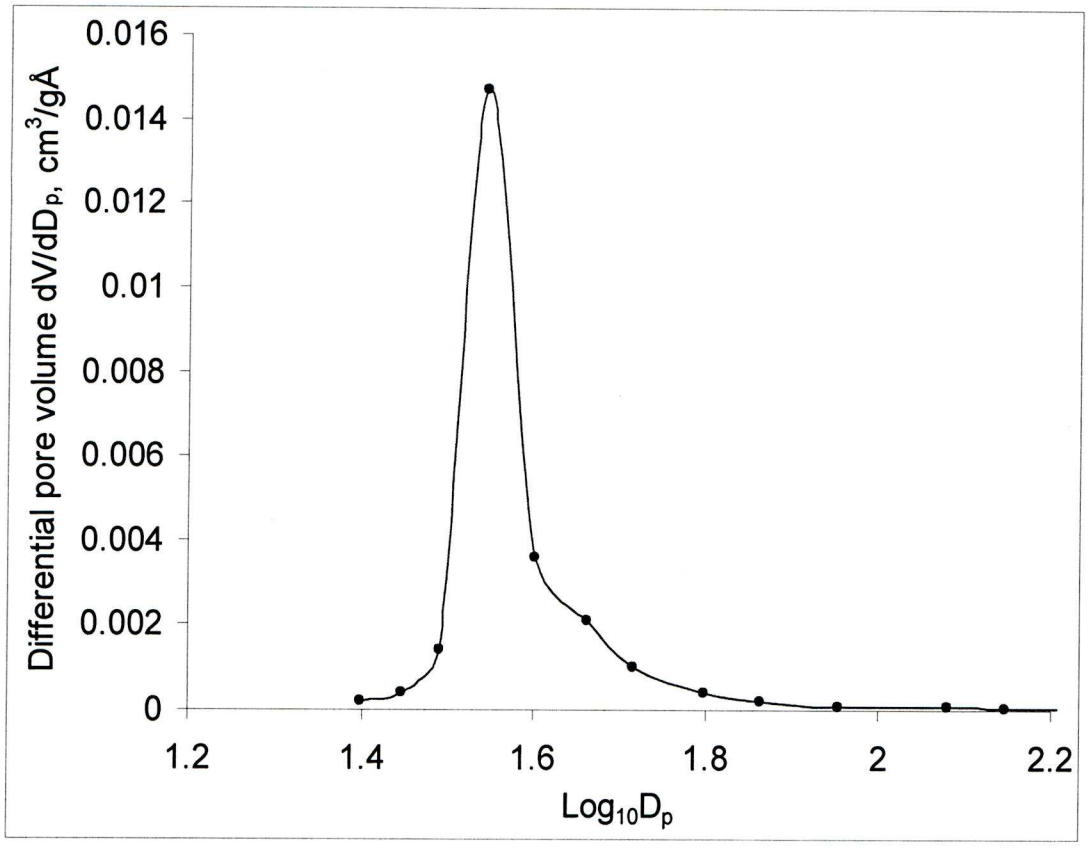

Figure 3.28 Distribution of pore volume as a function of pore diameter, D_p (in Å), for Cr-Cu (1:1) oxide obtained by the BJH method from nitrogen desorption.

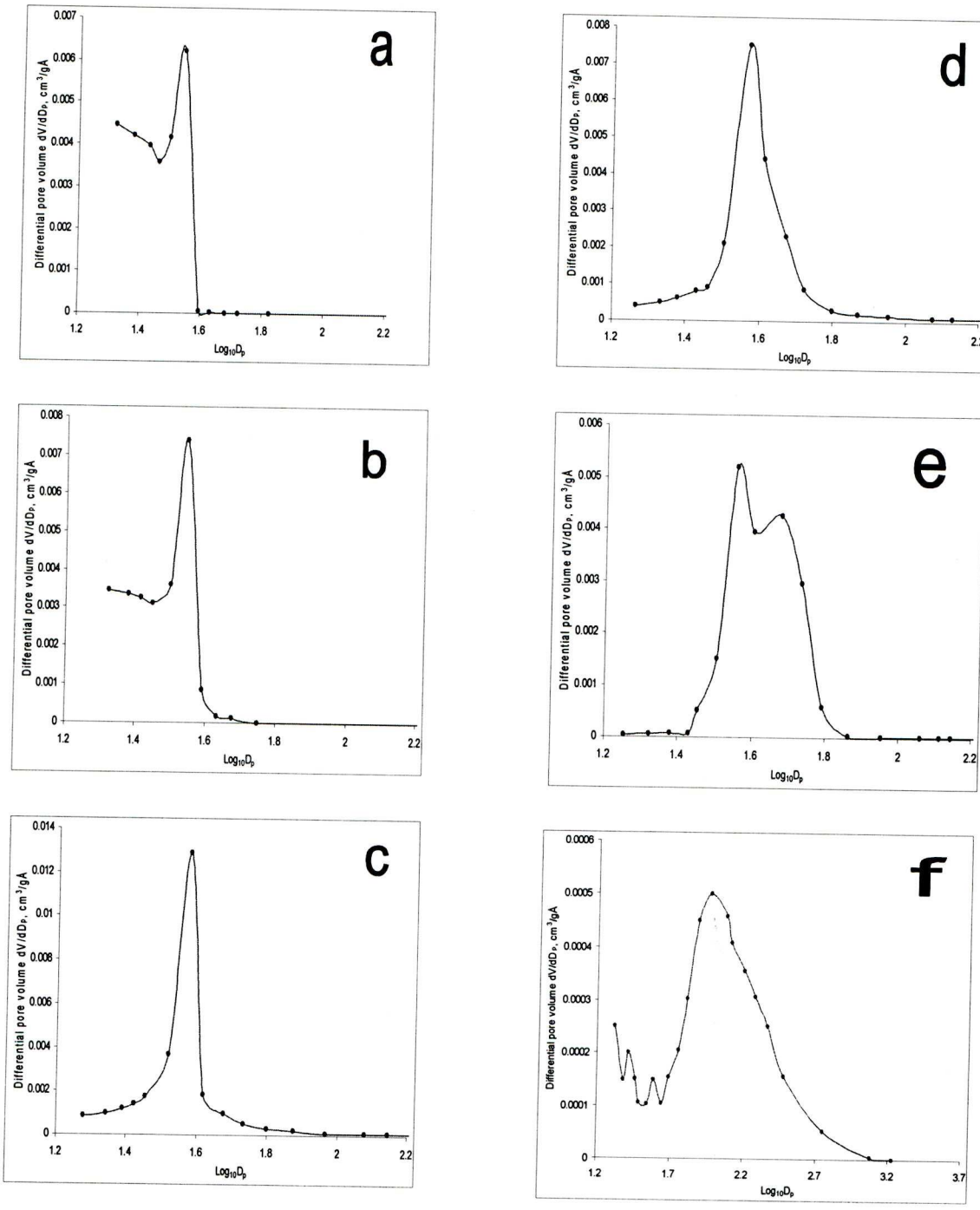

Figure 3.29 Distribution of pore volume as a function of pore diameter, D_p (in Å), for Zn-Cr-Cu oxides obtained by the BJH method from nitrogen desorption. (a) Zn-Cr-Cu (1:1:0.1), (b) Zn-Cr-Cu (1:1:0.2), (c) Zn-Cr-Cu (1:1:0.5) (d) Zn-Cr-Cu (1:1:0.8), (e) Zn-Cr-Cu (1:1:1), (f) Zn-Cr-Cu (1:1:2).

3.6. H_2 adsorption experiments

The catalytic activity of metal-supported catalysts is strongly dependent on the metal dispersion [29-31]. Palladium doping provided hydrogenation activity to Zn-Cr mixed oxide catalysts, which was found to be strongly dependent on the dispersion of palladium as found in this work. The general procedure for the measurement of palladium dispersion by H_2 adsorption is described in Section 2.4.10. The Pd dispersion was calculated using equation (2.2) which is based on the stoichiometry of one hydrogen atom adsorbed per surface palladium atom [32-34]. Palladium particle size was determined using equation $d = 0.9/D_s$ obtained from the literature [32]. It should be noted that the size of supported Pd particles depends on the reduction temperature of Pd(II) [35].

Table 3.9 Dispersion of Pd adsorbed on Zn-Cr oxide.

Catalyst	Dispersion (D_s)[a]	Average Pd particle diameter (nm)[b]
0.3%Pd/Zn-Cr (1:30) oxide	0.83	1.08
0.3%Pd/Zn-Cr (1:10) oxide	0.79	1.14
0.1%Pd/Zn-Cr (1:1) oxide	0.66	1.36
0.3%Pd/Zn-Cr (1:1) oxide	0.37	2.43
1.0%Pd/Zn-Cr (1:1) oxide	0.07	12.90
0.3%Pd/Zn-Cr (10:1) oxide	0.58	1.55
0.3%Pd/Zn-Cr (20:1) oxide	0.58	1.55

[a] Palladium dispersion: $D_s = Pd_s/Pd_{total}$ (average values from at least two measurements).

[b] Particle diameter, calculated using equation $d_s = 0.9/D_s$.

The results of H_2 titration for the Pd-impregnated Zn-Cr oxide catalysts are summarised in Table 3.9 with less than a 10% error margin. At a constant Pd loading of 0.3 wt% on amorphous Zn-Cr oxide, the dispersion decreased with a decrease in the Cr content in the Zn-Cr oxides, from 0.83 for the 0.3%Pd/Zn-Cr (1:30) oxide to 0.37 for the 0.3%Pd/Zn-Cr (1:1) oxide. Consequently, the average Pd particle size increased with decreasing chromium content from 1.08 to 2.43 nm for 0.3%Pd/Zn-Cr (1:30) and 0.3%Pd/Zn-Cr (1:1), respectively. This can be explained by the decrease in the oxide surface area in this direction [35].

With regard to the bulk Zn-Cr (1:1) oxide, introducing Pd to the surface led to Pd dispersion decreasing with increasing Pd loading from 0.1 to 1.0 wt% on the Zn-Cr (1:1) oxide, as expected. This result was in agreement with that reported for similar studies for palladium dispersion on the surface of different supports [29, 36]. Palladium supported on crystalline Zn-Cr (10:1) and Zn-Cr (20:1) oxides had a similar palladium dispersion and palladium particle size (0.58 and 1.55 nm, respectively).

3.7. Acidity of Zn-Cr oxide catalysts

In this section, the results of a calorimetric study of the acidity of the Zn-Cr oxide catalysts are presented and discussed. These results are used for the correlation with activities of the catalysts in the one-step synthesis of MIBK from acetone and hydrogen, as well as the one-step conversion of α-pinene to p-cymene.

The aim of the study described in this Chapter is to characterise the acidity of bulk Zn-Cr oxide in gas-solid and liquid-solid systems, using various calorimetric techniques: differential scanning calorimetry (DSC) of NH_3 adsorption in a gas-solid system and microcalorimetry of pyridine adsorption in a liquid-solid system. The latter

technique, known as the Cal-ad method, was developed by Drago [37, 38]. The FTIR and calorimetric techniques used in this work are described in Chapter 2 (Sections 2.4.3 and 2.4.8-9, respectively).

3.7.1. TG-DSC study of ammonia adsorption (continuous flow and pulse methods)

Table 3.10 TG/DSC for ammonia adsorption on Zn-Cr oxide.

Catalyst	$\Delta H\ (NH_3)^a$ (kJ/mol)	Acid site density[b] (mmol/g)	$\Delta H\ (NH_3)^c$ (kJ/mol)
Zn-Cr (1:30) oxide	-162.5	2.4	-193
Zn-Cr (1:10) oxide	-142.3	1.8	-180
Zn-Cr (1:1) oxide	-94.6	1.2	-155
Zn-Cr (10:1) oxide	-91.4	1.0	-150
Zn-Cr (20:1) oxide	-82.6	0.3	-127

[a, b] Average molar heat of NH_3 adsorption and the number of acid sites obtained in continuous flow of NH_3 using nitrogen as the carrier gas at 100°C.

[c] Differential heat of NH_3 adsorption by pulse method of NH_3 using helium as the carrier gas at 100°C.

Table 3.10 shows the acid properties of Zn-Cr oxides. The total number of acid sites and the average molar heat, as determined from NH_3 adsorption in a gas/solid flow system at 100°C, decreased with a decrease in the Cr content from 2.4 mmol/g and 162.5 kJ/mol for Zn-Cr (1:30) to 0.3 mmol/g and 82.6 kJ/mol for Zn-Cr (20:1) oxide in parallel with the oxide surface area. The results with regard to the density of the acid sites and the average molar heat of Zn-Cr (1:10) were close to that reported in the literature [7]. It should be noted that the calorimetric study using the TG-DSC technique

for the measurement of the NH_3 adsorption on Pd doped Zn–Cr oxide, was not able to provide us with accurate data for analysis.

Figure 3.30 shows the TG-DSC profile for ammonia adsorption on the bulk Zn-Cr (1:30) oxide. During the first 1 h, temperature was increased up to 300°C and held for 1 h to remove physisorbed moisture from the samples. And then, at a time of 2 h, temperature was decreased down to 100°C and held for 1 h to allow equilibrium to be reached. Then a continuous flow of NH_3 gas was introduced over the catalyst samples at a time of 3 h and 40 min, resulting in a weight gain and an exothermic peak of heat flow. Finally, at a time t = 4 h and 40 min, the NH_3 supply was stopped, and a certain time was allowed for physisorbed ammonia to be desorbed in order to reach adsorption equilibrium. From the sharp weight gain and heat release recorded, the average molar heat of adsorption, $-\Delta H_a$, per mole of NH_3 adsorbed, and the numbers of acid sites were obtained.

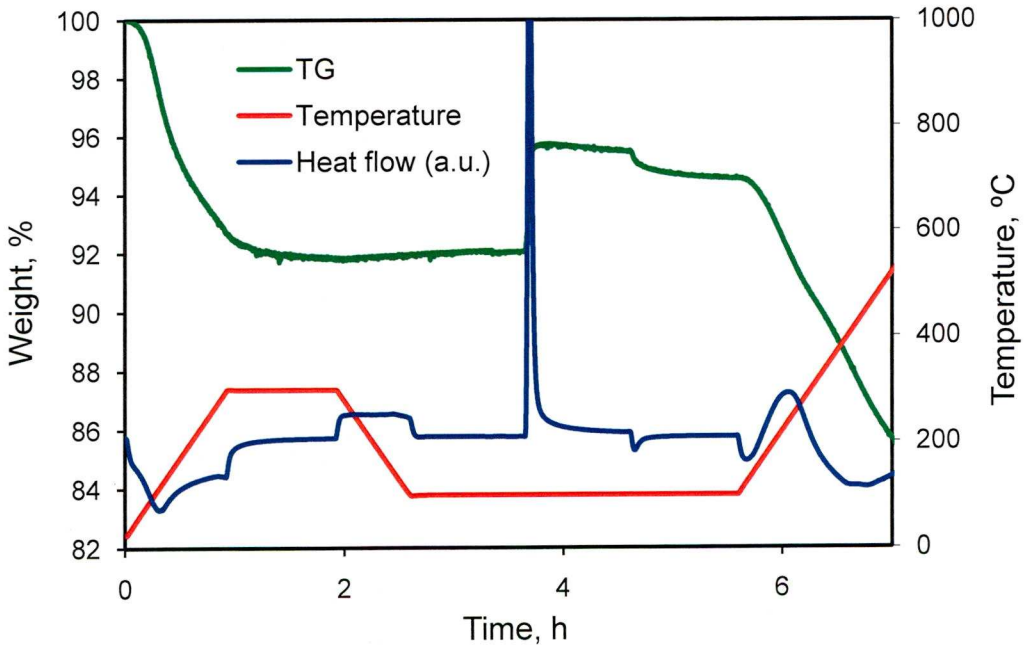

Figure 3.30 TG-DSC for ammonia adsorption on the bulk Zn-Cr (1:30) oxide.

The strength of the acid sites was also characterised by ammonia adsorption calorimetry using the pulse method. Although unable to differentiate between Brønsted and Lewis acid sites, these measurements provide a profile of the adsorption enthalpy (i.e. acid strength) as a function of NH_3 coverage. Figure 3.31 shows the differential adsorption heat as a function of the amount of NH_3 adsorbed by Zn-Cr (1:30), (1:1) and (20:1) oxides. The initial enthalpies of NH_3 adsorption at zero adsorption coverage were obtained for all Zn-Cr oxides. These increase with increasing chromium content, ranging from 127 kJ/mol for Zn-Cr (20:1) to 193 kJ/mol for Zn-Cr (1:30) oxide (Table 3.10). These values are higher than those of the average molar heat, due to the heterogeneity of the acid sites [39]. Both the acid strength and the total number of acid sites increased with increasing the Cr content. Zn-Cr (1:30) oxide possessed the largest number and strength of acid sites (both Brønsted and Lewis). All other oxides possessed only Lewis acid sites of a weaker acid strength (Section 3.7.3).

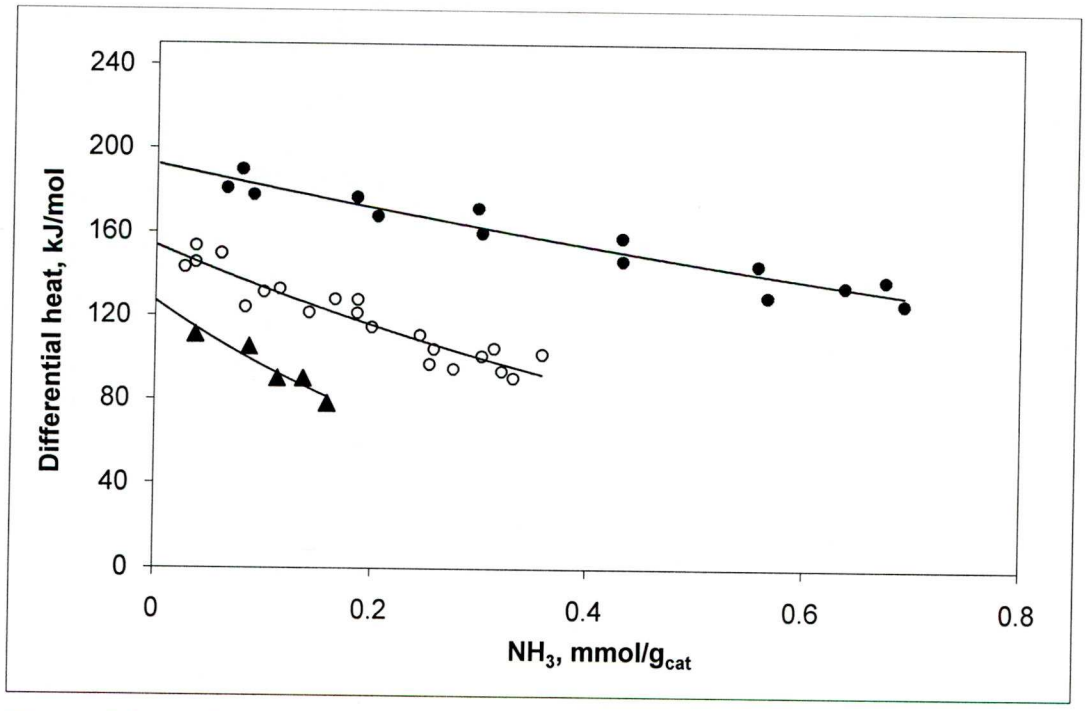

Figure 3.31 Differential heat of NH_3 adsorption on Zn-Cr oxides with Zn/Cr atomic ratio (●) (1:30), (○) (1:1) and (▲) (20:1) at 100°C.

3.7.2. Microcalorimetry of pyridine adsorption

A Setaram C80 microcalorimeter (Section 2.4.9) was used to measure the differential heat of adsorption of pyridine on bulk Zn-Cr (1:1) and (1:10) oxides in the liquid phase using cyclohexane as a solvent in the isothermal mode at 50°C. The calorimetric measurements were carried out at various concentrations of pyridine (10-400 mmol). In most cases, all the pyridine introduced was adsorbed by the bulk Zn-Cr oxide, i.e. no free pyridine was left in solution with lower pyridine concentrations. From the amount of pyridine adsorbed and the total adsorption heat, the differential heat of adsorption per mole of pyridine adsorbed (at zero adsorption), $-\Delta H_a$, was determined.

In microcalorimetric studies, which were performed at equilibrium conditions, in general it is assumed that a base probe adsorbs on the strongest acid sites present in the catalyst [40, 41].

Figure 3.32 shows the heat of pyridine adsorption on the bulk Zn-Cr (1:1) oxide as a function of the amount of pyridine adsorbed. The acid strength measurements gave an initial adsorption enthalpy of 106 and 129 kJ/mol for Zn-Cr (1:1) and (1:10) oxide, respectively. The differential heat of pyridine adsorption for bulk Zn-Cr oxides increased with increasing chromium content in agreement with the acid strength trend. Therefore, the Cal-ad results are fully consistent with those obtained by TG-DSC for Zn-Cr oxides.

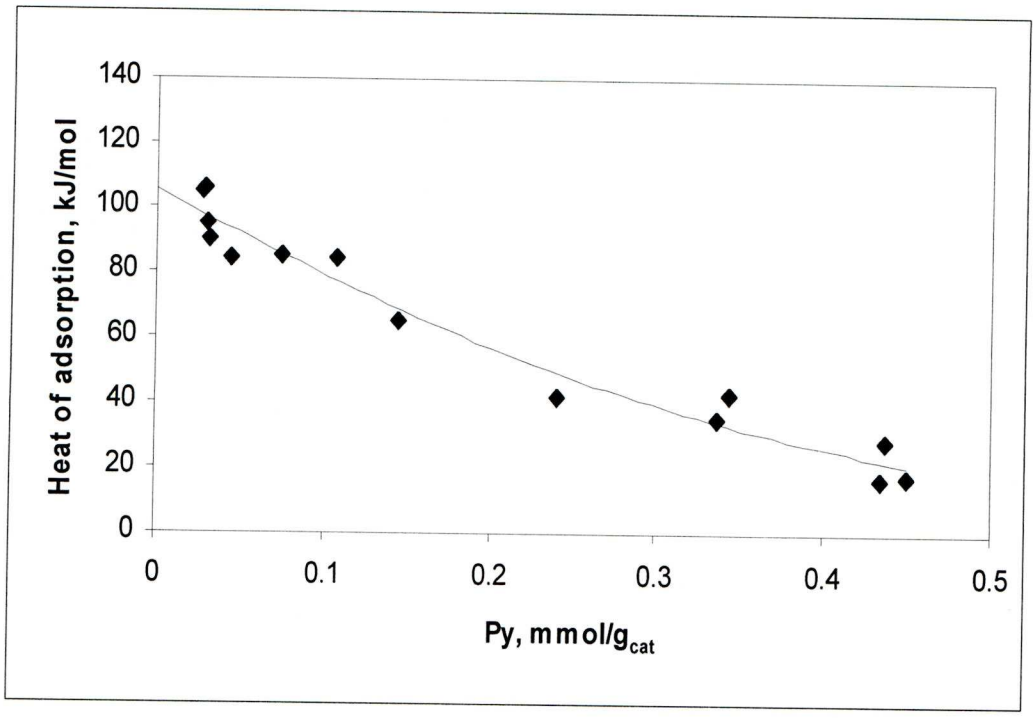

Figure 3.32 Heat of pyridine adsorption on Zn-Cr (1:1) in a cyclohexane slurry at 50°C.

3.7.3. FTIR study of pyridine adsorption

A Nicolet Nexus FTIR spectrometer (Section 2.4.3) equipped with a Controlled Environment Chamber (Spectra-Tech Inc., Model 0030-101) was used to obtain DRIFT spectra of adsorbed pyridine [42]. The fingerprint region of the spectrum (1560-1420 cm^{-1}) was used to obtain information about the nature (Brønsted or Lewis) of acid sites for Zn-Cr oxide catalysts. The details of the measurement of DRIFT spectra are given in Section 2.4.3.

The entire series of Zn-Cr oxides was found to possess Lewis acid sites, as evidenced by the presence of the adsorption band at 1450 cm^{-1} in their spectra (Figure 3.33). Only one oxide, Zn-Cr (1:30) with the largest Cr content, had Brønsted acid sites

strong enough to protonate pyridine, as indicated by the band at 1540 cm^{-1} in the spectrum of this oxide (Figure 3.33 (e)).

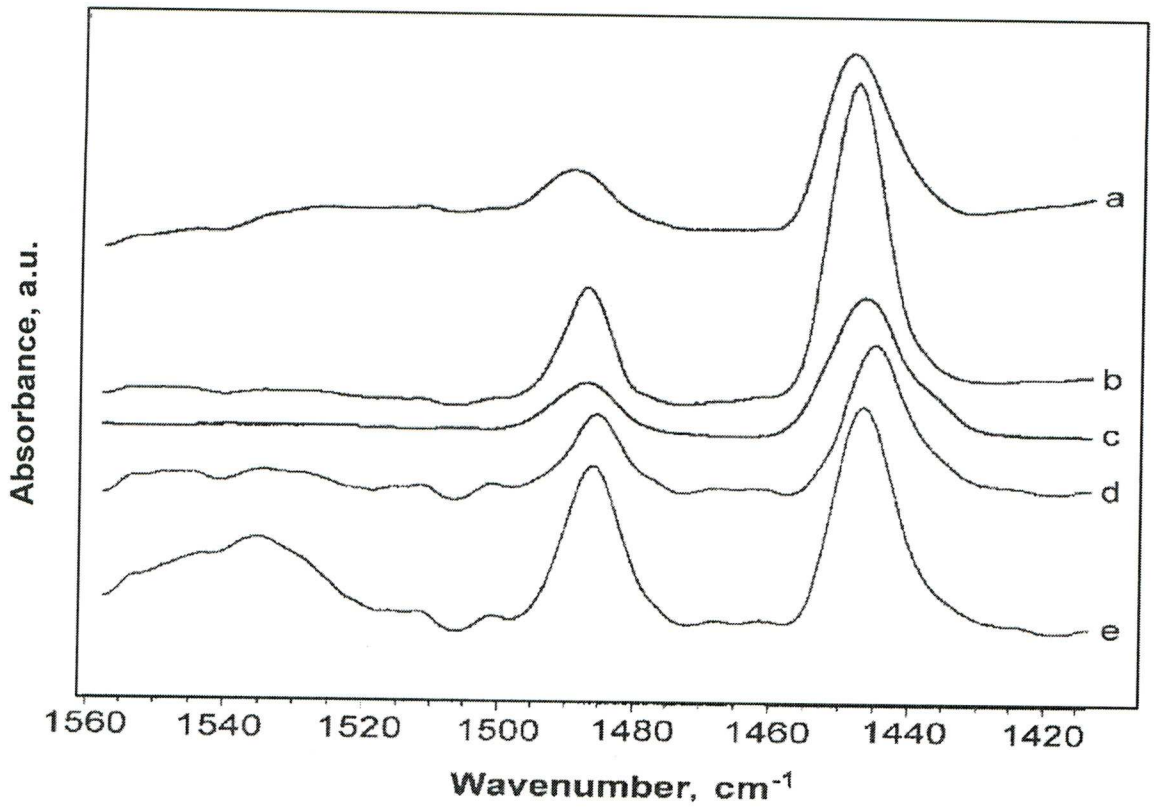

Figure 3.33 FTIR spectra of pyridine adsorbed on Zn-Cr oxides with Zn/Cr atomic ratio (a) 20:1, (b) 10:1, (c) 1:1, (d) 1:10 and (e) 1:30.

3.8. Summary of catalyst characterisation

The XRD measurements for Zn-Cr oxides showed that Zn-rich oxides (Zn/Cr = 10:1-20:1) are crystalline materials, exhibiting the XRD pattern of the ZnO crystalline phase (Figure 3.2). In contrast, Cr-rich oxides (Zn/Cr = 1:1-1:30) were amorphous materials (Figure 3.2). Calcination of Zn-Cr oxides at higher temperatures (>350°C) yields crystalline materials comprising ZnO, $ZnCr_2O_4$ and Cr_2O_3 phases [1, 2, 7]. The crystalline Zn-Cr (1:10) oxide has been found to have a smaller surface area and a lower catalytic activity in MIBK synthesis than the amorphous Zn-Cr (1:10) oxide [7]. On the

other hand, the XRD measurements for Zn-Cr-Cu oxides catalysts (pretreated under N_2 at 300°C) showed that oxides with higher copper content (Zn/Cr/Cu $\geq$ 1:1:0.5) only exhibited the XRD patterns of the CuO crystalline phase (Figure 3.3 (a) and (b)). However, pretreatment under H_2 at 300°C led to a reduction of copper from Cu(II) to Cu(0) as suggested by the XRD patterns of Cu(0) for these catalysts (Figures 3.4(a-d)).

TGA analysis of Zn-Cr, Zn-Cr-Cu oxides and Pd/Zn-Cr catalysts showed a monotonous loss of water in the temperature range of 30-700°C (Figures 3.5-3.10 for Zn-Cr oxides and Figures 3.11-3.13 for Zn-Cr-Cu oxides). In Zn-Cr oxides the amount of water depended on the Zn/Cr ratio: ~9 wt% for the amorphous oxides (Zn/Cr = 1:30 – 1:1) and 2.0 – 2.8 wt% for crystalline (Zn/Cr = 10:1 – 20:1), as shown in Table 3.5. On the other hand, in Zn-Cr-Cu oxides the amount of water depended on the concentration of Cu content, slightly increased from 4.43% to 6.56% with increasing Cu content from 0.1 to 2.0 (in molar ratio), as shown in Table 3.6.

The texture of Zn-Cr and Zn-Cr-Cu oxides was characterised by N_2 physisorption. For Zn-Cr oxides, the amorphous Cr-rich oxides had larger surface areas (132-223 m^2/g) and pore volumes (0.11-0.16 cm^3/g) but smaller average pore diameters (29-33 Å) than the crystalline Zn-rich oxides (33 -36 m^2/g, 0.08-0.09 cm^3/g and 91-112 Å respectively) (Table 3.7). The surface area of the Cr-rich oxides increased substantially with increasing the Cr content. The pore structure of Zn-Cr oxides was found to depend on their Zn/Cr ratio, as evidenced from the pore volume distributions (Figures 3.21 and 3.22). The Cr-rich amorphous oxides had a more regular pore structure in which pores of 35-37 Å diameter dominated, with smaller pores also present. Pores larger 40 Å diameter were not found in these oxides. In contrast, the Zn-rich crystalline oxides had a much broader pore size distribution (Figure 3.22). These oxides exhibited a sharp peak at 37-38 Å pore diameter like the Cr-rich oxides but also

possessed larger pores of up to 1000 Å diameter (Figure 3.22), hence the larger average pore diameter. Zn-Cr (10:1) oxide exhibited a broad peak centred at 91 Å pore diameter. Palladium loading did not change the catalyst texture, slightly decreasing the surface area and pore volume, as expected (Table 3.7). For Zn-Cr-Cu oxides, surface area decreased substantially with increasing the Cu content. In contrast, the catalyst pore sizes increased with increasing copper content, from 27 to 119 Å for Zn-Cr-Cu (1:1:0.1) and (1:1:2), respectively. The pore structure of Zn-Cr-Cu oxides was found to depend on Cu content, as evidenced from the pore volume distributions (Figures 3.29). Oxides with lower Cu content (Zn/Cr/Cu $\leq$ 1:1:0.5) had a more regular pore structure in which pores of 34-38 Å diameter dominated, with smaller pores also present (Figure 3.29 (a-c)). In contrast, oxides with larger Cu content (Zn/Cr/Cu $\geq$ 1:1:0.8) had a much broader pore size distribution (Figure 3.29 (d-f)). These oxides exhibited larger pores of up to 1200 Å diameter.

Palladium dispersion, *D*, in Pd/Zn-Cr catalysts (0.1-1 wt% Pd) was obtained by measuring hydrogen chemisorption. The *D* values are given in Table 3.9. At a constant Pd loading of 0.3 wt%, the dispersion decreased with decreasing the Cr content in Zn-Cr oxides. This can be explained by the decrease in oxide surface area in this direction. As expected, Pd dispersion decreased with increasing Pd loading from 0.1 to 1.0 wt% on Zn-Cr (1:1) oxide.

Table 3.10 shows the acid properties of Zn-Cr oxides. The total number of acid sites, as determined from NH_3 adsorption in a gas/solid flow system at 100°C, decreased with decreasing the Cr content from 2.4 mmol/g (Zn/Cr = 1:30) to 0.3 mmol/g (Zn/Cr = 20:1) in parallel with the oxide surface area. The nature of acid sites (Brønsted or Lewis) was determined by FTIR spectroscopy of adsorbed pyridine [42]. The entire series of Zn-Cr oxides was found to possess Lewis acid sites, as evidenced by the

presence of the adsorption band at 1450 cm^{-1} in their spectra (Figure 3.33). Only one oxide, Zn-Cr (1:30) with the largest Cr content, had Brønsted acid sites strong enough to protonate pyridine, as indicated by the band at 1540 cm^{-1} in the spectrum of this oxide (Figure 3.33 (e)).

The strength of acid sites was characterised by ammonia adsorption calorimetry. Although unable to differentiate between Brønsted and Lewis acid sites, these measurements provide a profile of the adsorption enthalpy (i.e. acid strength) as a function of NH_3 coverage. As an example, Figure 3.31 shows the differential adsorption heat as a function of the amount of NH_3 adsorbed for Zn-Cr (1:30), (1:1) and (20:1) oxides. The initial enthalpies of NH_3 adsorption at zero adsorption coverage were obtained for all Zn-Cr oxides, ranging from -127 to -193 kJ/mol (Table 3.10). The acid strength, as well as the total number of acid sites, increased with increasing the Cr content. Zn-Cr (1:30) oxide possessed the largest number and strength of acid sites (both Brønsted and Lewis). All other oxides possessed only Lewis acid sites of a weaker acid strength.

For Zn-Cr (1:1) and (1:10) oxides, which showed better catalytic performances, the acid strength was also determined in liquid phase using microcalorimetry of pyridine adsorption in cyclohexane slurry. These measurements gave an initial adsorption enthalpy of -106 and -129 kJ/mol for Zn-Cr (1:1) and (1:10) oxide respectively (Table 3.10). Figure 3.32 shows the adsorption heat as a function of the amount of pyridine adsorbed for Zn-Cr (1:1).

References

[1] F. Simard, U.A. Sedran, J. Sepulveda, N.S. Figoli, H.I. Delasa, Appl. Catal. A 125 (1995) 81.

[2] M.C.J. Bradford, M.V. Konduru, D.X. Fuentes, Fuel Process. Technol. 83 (2003) 11.

[3] Z.F. Wang, J.Y. Xi, W.P. Wang, G.X. Lu, J. Mol. Catal. A 191 (2003) 123.

[4] R.M. Gabr, M.M. Girgis, A.M. Elawad, B.M. Abouzeid, Mater. Chem. Phys. 39 (1994) 53.

[5] R.M. Gabr, M.M. Girgis, A.M. Elawad, Mater. Chem. Phys. 30 (1992) 169.

[6] M. Ohta, Y. Ikeda, A. Igarashi, Appl. Catal. A 258 (2004) 153.

[7] E.F. Kozhevnikova, I.V. Kozhevnikov, J. Catal. 238 (2006) 286.

[8] V.S. Kumar, S.S. Reddy, A.H. Padmasri, B.D. Raju, I.A. Reddy, K.S.R. Rao, Catal. Commun. 8 (2007) 899.

[9] M. delArco, V. Rives, R. Trujillano, P. Malet, J. Mater. Chem. 6 (1996) 1419.

[10] S.R. Naidu, A.K. Banerjee, N.C. Ganguli, S.P. Sen, J. Res. Inst. Catal., Hokkiadio Univ. 21 (1973).

[11] Y.Y. Wu, H.M. Bai, J.Z. Zhou, C.X. Chen, X. Xu, Y.F. Xu, G.R. Qian, Appl. Clay Sci. 42 (2009) 591.

[12] A.M. El-Awad, B.M. Abu-Zied, J. Mol. Catal. A 176 (2001) 213.

[13] S.J. Gregg, K.S.W. Sing, Adsorption, Surface Area and Porosity, Academic Press, London, 1982.

[14] K.K. Unger, J. Roquerol, K.S.W. Sing, H. Kral (Eds.), Characterisation of Porous Solids I, Elsevier, Amsterdam, 1988.

[15] J. Roquerol, F. Rodriguez-Reinoso, K.S.W. Sing, K.K. Unger, Characterisation of Porous Solids III, in, Elsevier, Amsterdam, 1994.

[16] G. Attard, C. Barnes, Surfaces, Oxford University Press Inc., New York, 1998.

[17] G. Leofanti, M. Padovan, G. Tozzola, B. Venturelli, Catal. Today. 41 (1998) 207.

[18] S. Brunauer, P.H. Emmett, E. Teller, J. Am. Chem. Soc. 60 (1938) 309.

[19] E.P. Barrett, L.G. Joyner, P.P. Halenda, J. Am. Chem. Soc. 73 (1951) 373.

[20] Z.L. Wang, H.C. Ma, W.C. Zhu, G.J. Wang, React. Kinet. Catal. Lett. 76 (2002) 271.

[21] M. Fujiwara, H. Ando, M. Tanaka, Y. Souma, Bull. Chem. Soc. Jpn. 67 (1994) 546.

[22] X.J. Tang, J.H. Fei, Z.Y. Hou, H. Lou, X.M. Zheng, React. Kinet. Catal. Lett. 94 (2008) 3.

[23] C.Y. Shiau, S. Chen, J.C. Tsai, S.I. Lin, Appl. Catal. A 198 (2000) 95.

[24] B.M. Reddy, I. Ganesh, J. Mol. Catal. A 151 (2000) 289.

[25] Y. Ogino, M. Oba, H. Uchida, Bull. Chem. Soc. Jpn. 32 (1959) 284.

[26] Y. Ogino, M. Oba, H. Uchida, Bull. Chem. Soc. Jpn. 32 (1959) 616.

[27] A.M. Youssef, A.I. Ahmed, S.E. Samra, N.B. El-Assy, E.A. El-Sharkawy, Adsorpt. Sci. Technol. 16 (1998) 175.

[28] Y. Ogino, M. Oba, H. Uchida, Bull. Chem. Soc. Jpn. 33 (1960) 358.

[29] N. Das, D. Tichit, R. Durand, P. Graffin, B. Coq, Catal. Lett. 71 (2001) 181.

[30] A.A. Nikolopoulos, B.W.L. Jang, J.J. Spivey, Appl. Catal. A 296 (2005) 128.

[31] V. Ponec, G.C. Bond, in: B. Delmon, J.T. Yates (Eds.), Catalysis by Metals and Alloys, Stud. Surf. Sci. Catal., vol. 95, Elsevier, Amsterdam, 1995.

[32] J.E. Benson, H.S. Hwang, M. Boudart, J. Catal. 30 (1973) 146.

[33] G. Prelazzi, M. Cerboni, G. Leofanti, J. Catal. 181 (1999) 73.

[34] J.E. Benson, M. Boudart, J. Catal. 4 (1965) 704.

[35] C.A. Muller, M. Maciejewski, R.A. Koeppel, A. Baiker, J. Catal. 166 (1997) 36.

[36] P.P. Yang, Y.C. Shang, J.F. Yu, J. Wang, M.L. Zhang, T.G. Wu, J. Mol. Catal. A 272 (2007) 75.

[37] C.W. Chronister, R.S. Drago, J. Am. Chem. Soc. 115 (1993) 4793.

[38] R.S. Drago, J.A. Dias, T.O. Maier, J. Am. Chem. Soc. 119 (1997) 7702.

[39] E.F. Kozhevnikova, I.V. Kozhevnikov, J. Catal. 224 (2004) 164.

[40] A. Auroux, Top. Catal. 4 (1997) 71.

[41] A.Auroux, Top. Catal. 19 (2002) 205.

[42] K. Tanabe, in: J.R. Anderson, M. Boudart (Eds.), Catalysis Science and Technology, Springer, 1981, Chapter 5.

Chapter 4. One-step synthesis of MIBK from acetone and hydrogen

4.1. Introduction

In this chapter, the results of our study into the one-step synthesis of MIBK from acetone and hydrogen catalysed by Pd/Zn-Cr oxide in both liquid and gas phase systems and Zn-Cr-Cu oxide in the gas phase system are presented and discussed. The output products include propane and propene as gaseous products, isopropanol (IP), MIBK, DIBK, mesityl oxide (MO) and mesitylene (MS) (Scheme 1).

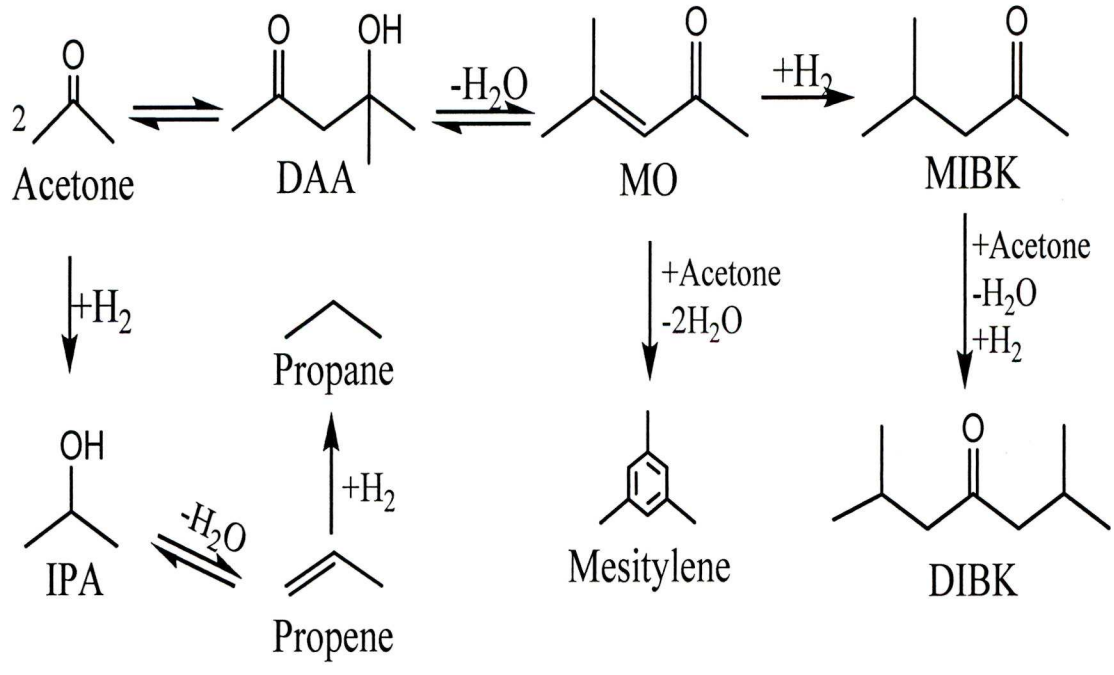

Scheme 1

4.2. Catalyst testing

4.2.1. Gas phase reactions over Pd/Zn-Cr oxide catalysts

Firstly, preliminary investigation with variable reaction parameters was carried out to obtain optimum conditions for one-step synthesis of MIBK. Initially, the reaction was performed thermally in the absence of a catalyst at a temperature of 300°C. It resulted in zero acetone conversion. In the presence of Pd/Zn-Cr catalysts under the same reaction conditions, the acetone conversion increased to 35.7-40.7% with high selectivity to MIBK (53.3-70.2%) and DIBK (18.5-26.4%) (Table 4.1).

4.2.1.1. Effect of Zn/Cr ratio

Representative results at 300°C are given in Table 4.1. Both acid and hydrogenation catalysis effected by Zn-Cr oxide and Pd respectively were required for the reaction to occur. When Zn-Cr (1:10) oxide was used in the absence of Pd, the reaction went with a low conversion of 16.7% and mesityl oxide (the product of acid-catalysed condensation of acetone) was the major product (63.2% selectivity), whereas the selectivity to MIBK was only 15.3% (entry 1). This shows that the Zn-Cr oxide itself mainly acts as an acid catalyst, possessing a weak hydrogenation activity. In the presence of Pd, acetone conversion increased up to 40.5% (entry 3), indicating that the thermodynamically favorable hydrogenation of MO to MIBK on Pd sites drives the process forward.

Table 4.1 Effect of Zn/Cr ratio on the catalytic performance of 0.3%Pd/Zn-Cr in the gas-phase synthesis of MIBK from acetone and hydrogen.[a]

Entry	Catalyst	Conversion (%)	Selectivity (%)[b]						C[c] (wt%)
			MIBK	DIBK	C_3	IP	MO	Others	
1	Zn-Cr (1:10)	16.7	15.3	9.4	0.2	0.0	63.2	12.0	
2	0.3%Pd/Zn-Cr (1:30)	38.7	64.8	18.5	0.7	3.3	3.1	9.6	4.1
3	0.3%Pd/Zn-Cr (1:10)	40.5	58.7	20.7	0.6	4.1	3.0	12.9	4.9
4	0.3%Pd/Zn-Cr (1:1)	39.6	70.2	19.9	0.7	2.5	0.2	6.6	2.6
5	0.3%Pd/Zn-Cr (10:1)	35.7	68.7	18.4	0.7	5.0	0.2	6.9	0.7
6	0.3%Pd/Zn-Cr (20:1)	40.7	53.3	26.4	1.0	3.9	0.0	15.4	

[a] Reaction conditions: 300°C, acetone/H_2 = 37:63 (mol/mol), 10 mL/min H_2 flow, 0.2 g catalyst of 45-180 μm particle size, 3 h time on stream.

[b] C_3 is propene and propane, IP isopropanol, MO mesityl oxide, others are mainly C_{9+} acetone condensation products (mostly 2,6,8-trimethylnonane-4-one).

[c] Carbon content in used catalysts after 6-8 h on stream.

With all Pd/Zn-Cr catalysts, MIBK was the major reaction product, with significant amounts of DIBK also being formed. By-products included C_{9+} acetone condensation products (mainly 2,6,8-trimethylnonane-4-one and some mesitylene) together with small amounts of propene and propane (C_3), mesityl oxide (MO) and isopropanol (IP), in agreement with the previous report [1]. The IP was formed by direct hydrogenation of the C=O group in acetone on Pd. The C_3 was formed by the acid-catalysed dehydration of IP to propene on Zn-Cr oxide, followed by the hydrogenation of propene to propane on Pd. This was confirmed by observing a 70-80% conversion of IP to C_3 with >50% selectivity on 0.3%Pd/Zn-Cr (1:1) under typical reaction conditions (300°C, 0.2 g catalyst, 1 vol% IP in H_2 flow (10 mL/min), 3 h on stream).

The Pd/Zn-Cr catalysts exhibited a good performance stability regardless of their Zn/Cr ratio. Catalyst deactivation was not observed during at least 10 h of

continuous operation (Figure 4.1). The catalysts reached a steady state in 1-2 h and after that performed with constant activity and selectivity.

Coke (0.7–4.9 wt%) was found in the catalysts after the reaction (Table 4.1). Its amount grew with increasing catalyst acidity, with Pd/Zn-Cr (1:30) and Pd/Zn-Cr (1:10) catalysts depositing larger amounts of coke.

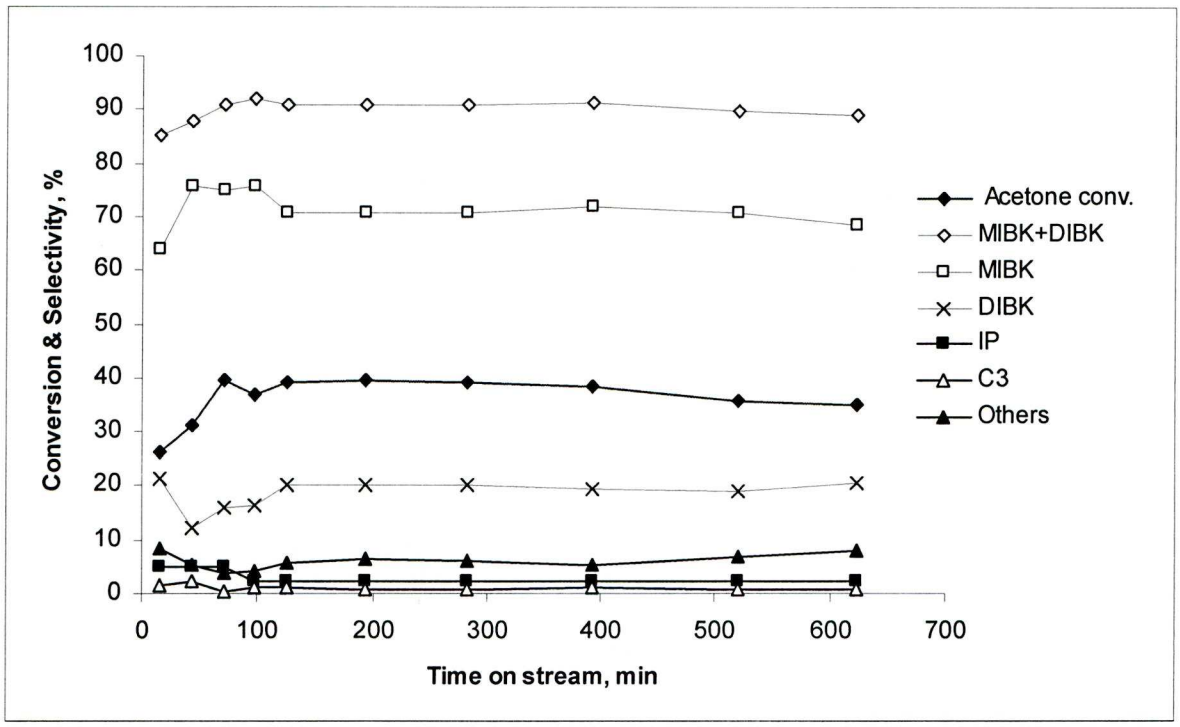

Figure 4.1 Acetone conversion and product selectivities vs. time on stream (0.2 g 0.3%Pd/Zn-Cr (1:1), 10 mL/min H_2 flow, acetone/H_2 = 37:63 mol/mol, 300°C).

Variations of the Zn/Cr ratio (i.e. catalyst acidity) had a very small effect on acetone conversion, but it had a considerable effect on reaction selectivity (Table 4.1 and Figure 4.2). The catalyst 0.3%Pd/Zn-Cr (1:1) possessing an intermediate acid strength and acid site density exhibited the highest MIBK selectivity of 70.2% and 90.1% total selectivity to MIBK + DIBK at 39.6% acetone conversion (Table 4.1, entry 4). This result compares well with the results reported so far [2, 3, 4, 5].

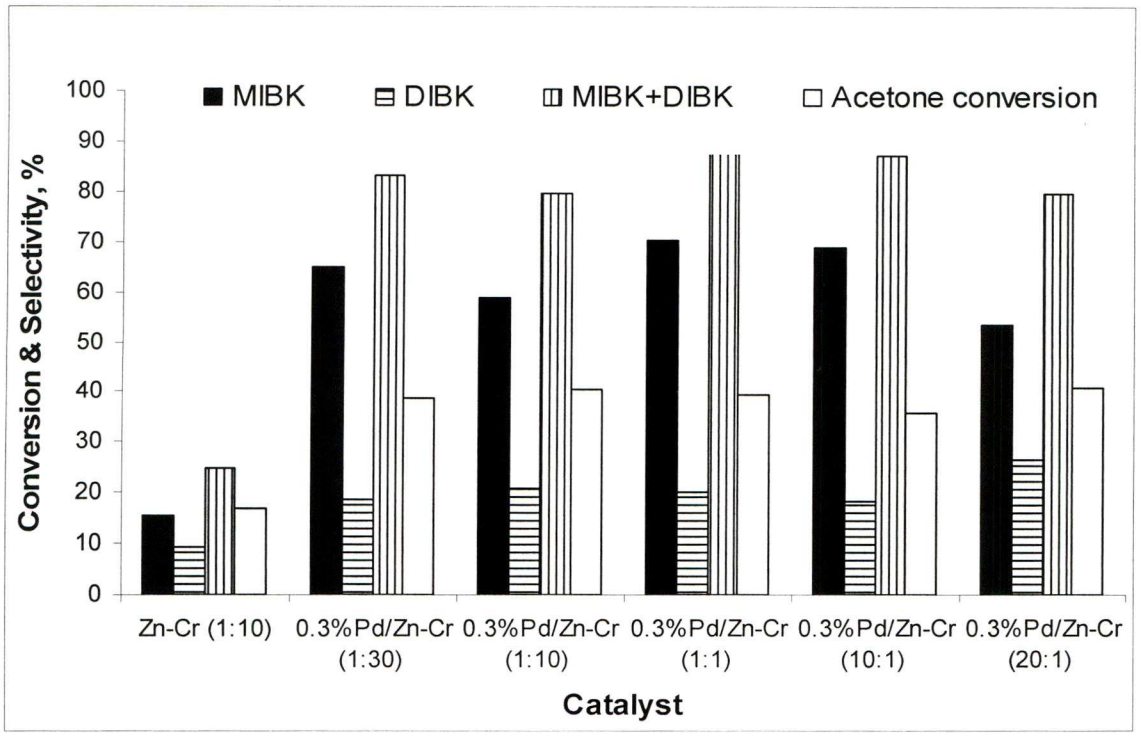

Figure 4.2 Effect of Zn-Cr ratio on the catalytic performance of 0.3%Pd/Zn-Cr in the gas-phase synthesis of MIBK from acetone and hydrogen at 300°C, acetone/H_2 = 37:63 (mol/mol), 10 mL/min H_2 flow rate, 0.2 g catalyst of 45-180 μm particle size and 3 h time on stream.

4.2.1.2. Effect of Pd loading

The introduction of Pd onto the Zn-Cr oxide support had a significant effect on the overall catalyst activity for the direct synthesis of MIBK from acetone and hydrogen at 300°C. This effect was found to depend on the Pd dispersion, *D* (Table 4.2). The conversion of acetone over Pd/Zn-Cr (1:1) scaled directly with the amount of accessible surface palladium, Pd_s, in the catalysts. Thus, the 0.3%Pd/Zn-Cr (1:1) catalyst (*D* = 0.37) possessing 0.11 wt% of Pd_s exhibited an acetone conversion of 34.2%. This value is proportionally higher than that (20.4%) for the catalyst with 0.1% Pd loading (*D* = 0.66, 0.066 wt% Pd_s) and also that (18.9%) for the catalyst with 1% Pd loading (*D* = 0.07, 0.07 wt% Pd_s). The catalysts with 0.1% and 1% Pd loadings, having equal amounts of Pd_s, exhibited almost equal catalytic activity. This result, together with

independence of catalyst activity on the catalyst acidity, indicates that hydrogenation of MO to MIBK is the rate-limiting step in the process. Also this justifies the Pd loading of 0.3 wt% in the catalysts.

Table 4.2 Effect of Pd loading on the catalytic performance of Pd/Zn-Cr (1:1) in the gas-phase synthesis of MIBK from acetone and hydrogen.[a]

Entry	Pd loading (%)	Pd dispersion (D_s)[b]	Conversion (%)	Selectivity (%)					
				MIBK	DIBK	C_3	IP	MO	Others
1	0.1	0.66	20.4	74.4	11.7	3.2	3.8	0.4	6.4
2	0.3	0.37	34.2	70.7	17.0	1.0	4.1	0.2	6.9
3	1.0	0.07	18.9	71.3	13.7	2.4	4.5	0.6	7.6

[a] Reaction conditions: 300°C, acetone/H_2 = 37:63 (mol/mol), 20 mL/min H_2 flow, 0.2 g catalyst of 45-180 μm particle size, 3 h time on stream.

[b] Palladium dispersion: $D_s = Pd_s/Pd_{total}$ (average values from at least two measurements).

4.2.1.3. Effect of contact time

Conversion of acetone increased when contact time was increased from 0.18 s to 0.53 s by changing the H_2 flow rate (Table 4.3). This caused a simultaneous decrease in MIBK selectivity in favour of DIBK, as expected for a consecutive reaction. There was a small difference in MO selectivity at a lower contact time of 0.18 s. The selectivity to IP and C_3 slightly decreased with increasing contact time, and C_{6+} products were not affected by the change in contact time. It should be noted that these tests were carried out under non-differential conditions which smoothed the effect of contact time.

Table 4.3 The effect of contact time on MIBK synthesis[a]

Contact time (s)	H_2 flow	Conversion (%)	Selectivity (%)					
			MIBK	DIBK	C_3	IP	MO	Others
0.53	10	39.6	70.2	19.9	0.7	2.5	0.2	6.6
0.26	20	34.2	70.7	17.0	1.0	4.1	0.2	6.9
0.18	30	30.3	72.2	15.2	1.2	4.3	0.4	6.7

[a] Reaction conditions: 0.2g 0.3 wt% Pd/Zn-Cr (1:1) catalyst of 45-180 μm particle size, at 300°C, acetone/H_2 = 37:63 (mol/mol), and 3 h time on stream.

4.2.1.4. Effect of flow rate at a constant contact time

The purpose of this experiment was to examine the possibility of external mass transfer limitation in the reaction under study. This test was carried out with 0.3%Pd/Zn-Cr (1:1) catalyst by varying the gas flow rate, while keeping a constant contact time of 0.3 s by scaling the catalyst bed in line with the flow rate.

Under such conditions, it was found that the catalytic activity as well as the selectivity to MIBK, DIBK, IP, MO and C_{6+} products did not change (Table 4.4). This indicates that the reaction was not affected by external mass transfer.

Table 4.4 Effect of flow rate on MIBK synthesis at constant contact time[a]

H_2 flow (mL/min)	conversion (%)	Selectivity[b] (%)					
		MIBK	DIBK	C_3	IP	MO	Others
10	32.4	69.2	18.3	1.1	3.2	0.2	8.1
20	34.1	68.5	18.6	0.9	3.4	0.2	8.4
30	34.7	67.1	19.2	1.0	3.6	0.2	9.0

[a] Reaction conditions: 0.3%Pd/Zn-Cr (1:1) catalyst (0.1 – 0.3 g) diluted 50:50 (wt) with sand; the catalyst bed was scaled with H_2 flow rate to keep a constant contact time of 0.3 s; 300°C, acetone/H_2 = 37:63 (mol/mol), 3.5 h time on stream.

4.2.1.5. Activation energy

Activation energy was measured for the gas phase reaction with 0.3 wt% Pd/Zn-Cr (1:1) as a catalyst. Conversion was kept below 10% to ensure differential conditions in the reactor. The temperature range was between 200 – 350°C. Under such conditions selectivity to MIBK was 79-89%. In the differential mode reaction rate is proportional to conversion, which allows using conversion instead of reaction rate in Arrhenius equation.

A conversion of less than 10% was achieved through a combination of using a higher H_2 flow rate and diluting catalyst with sand. In this experiment: the H_2 flow rate = 20 mL/min, acetone/H_2 ratio = 1:2, 0.02 g of catalyst diluted with 0.2 g washed sand and the contact time = 0.03 s.

In the entire temperature range, the reaction obeyed Arrhenius equation with an activation energy of 17.0 kJ/mol (Figure 4.3). The relatively low value of E_a obtained together with the previously observed reaction slowdown upon increasing catalyst particle size [1] suggests that the reaction may be affected by internal mass transfer.

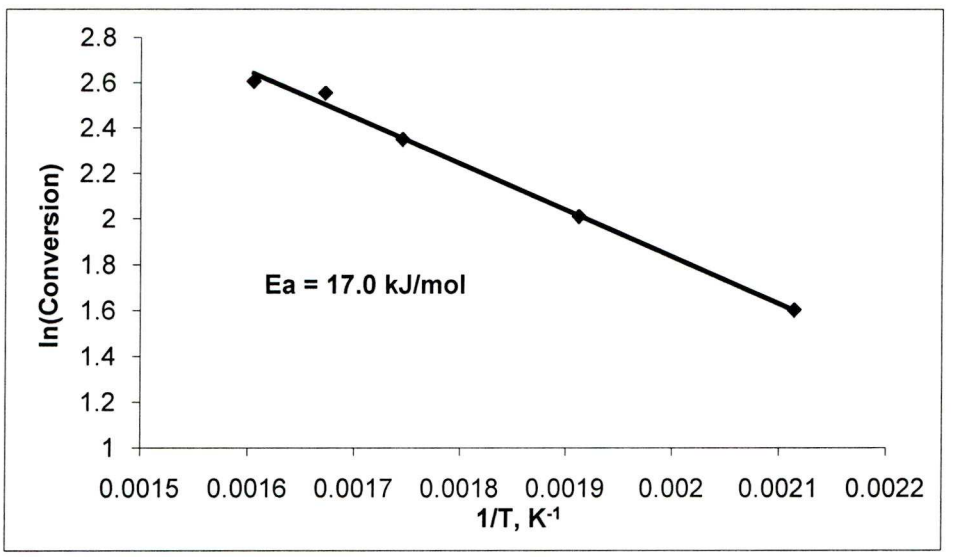

Figure 4.3 Arrhenius plot for MIBK synthesis over 0.3%Pd/Zn-Cr (1:1).

The measurement of activation energy was repeated using another 0.3 wt% Pd/Zn-Cr (1:1) catalyst sample and a higher contact time of 0.07 s by increasing the catalyst amount to 0.05 g. The activation energy was found to be 14.3 kJ/mol which is close to the previous value of 17.0 kJ/mol. These results therefore suggest that there may be internal diffusion limitations in the gas phase synthesis of MIBK over Pd/Zn-Cr (1:1) catalyst.

4.2.2. Liquid-phase reactions over Pd/Zn-Cr oxide catalysts

4.2.2.1. Effect of stirring speed

Figure 4.4 shows the results of influence of the stirring speed on catalytic activity of 0.2 g 0.3%Pd/Zn-Cr (1:1) oxide catalyst in the 45-mL Parr 4714 autoclave at a reaction temperature of 180°C, hydrogen pressure of 7.5 bar and a reaction time of 2 h. The conversion of acetone decreased with a decrease in the stirring speed below 800 rpm from 38.3% at 800 rpm to 31.5% at 600 rpm and then to 24% at 400 rpm. This indicates that the reaction is subject to mass transfer limitations at stirring speed <800 rpm, probably due to slow diffusion of H_2 into the liquid phase. Consequently, the reactions in this reactor were carried out at 800 rpm stirring speed. Under such conditions, acetone conversion and reaction selectivity did not depend on the stirring speed, indicating the absence of mass transfer limitations.

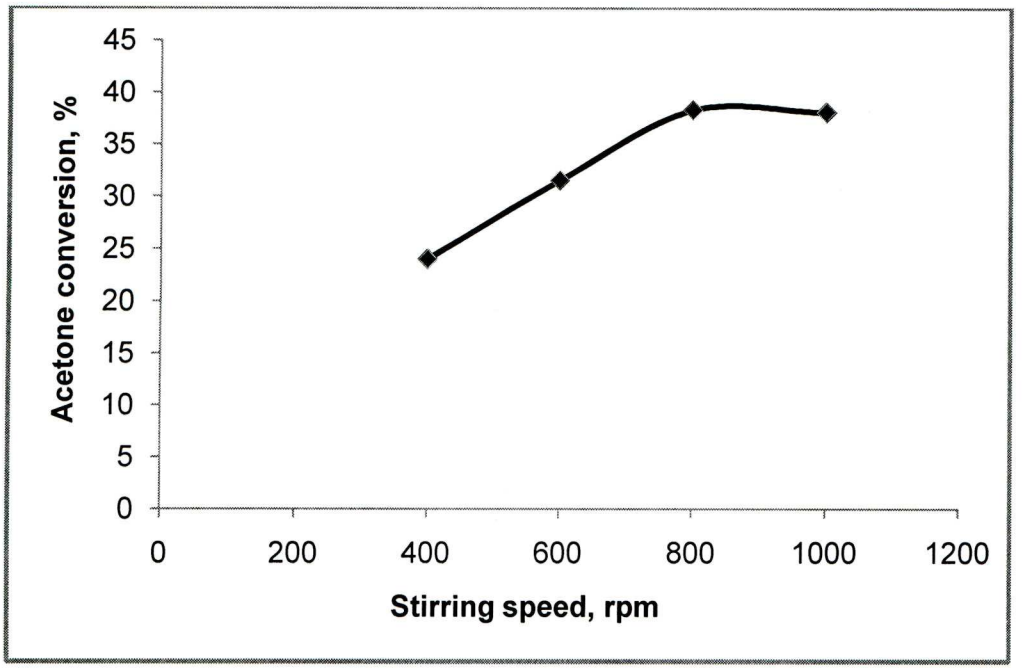

Figure 4.4 Effect of stirring speed on the catalytic performance of 0.3%Pd/Zn-Cr (1:1) in the liquid-phase synthesis of MIBK from acetone and hydrogen (2.0 g acetone, 0.2g 0.3%Pd/Zn-Cr (1:1) catalyst of 45-180 μm particle size, 180°C, 7.5 bar initial H_2 pressure (RT), 2 h).

4.2.2.2. Effect of Zn/Cr ratio

The results for the liquid phase one-step conversion of acetone to MIBK with Pd/Zn-Cr oxide catalysts at a reaction temperature of 180°C are summarised in Table 4.5. As in the gas phase, when Zn-Cr oxide was used without Pd, the reaction went with low conversion (17.3%), and mesityl oxide was the major product (72.9% selectivity), with MIBK selectivity of only 4.9% (entry 1). In the presence of Pd, acetone conversion increased, and MIBK became the main reaction product. In the liquid phase, unlike the gas phase, increasing the Zn/Cr ratio from 1:30 to 20:1 (i.e. decreasing the catalyst acidity) caused the conversion of acetone to decrease from 55.8 to 25.8%. As in the gas phase, the 0.3%Pd/Zn-Cr (1:1) catalyst possessing an intermediate acidity showed the best performance (78.4% MIBK and 90.3% MIBK + DIBK selectivity at 38.3%

conversion) (entry 4). More acidic catalysts 0.3%Pd/Zn-Cr (1:30) and (1:10) were more active but less selective to MIBK and DIBK (entries 2, 3). Less acidic 0.3%/Zn-Cr (10:1) and (20:1) were less active and much less selective, yielding large amounts of IP (entries 5, 6).

Table 4.5 Effect of Zn/Cr ratio on the catalytic performance of Pd/Zn-Cr oxides in the liquid phase.[a]

Entry	Catalyst	Conversion (%)	Selectivity (%)[b]					
			MIBK	DIBK	C_3	IP	MO	Others
1	Zn-Cr(1:1)	17.3	4.9	0.0	1.9	11.1	72.9	9.3
2	0.3%Pd/Zn-Cr(1:30)	55.8	66.5	10.5	1.8	4.5	0.6	16.1
3	0.3%Pd/Zn-Cr(1:10)	41.9	72.5	10.9	1.9	7.1	1.2	6.4
4	0.3%Pd/Zn-Cr(1:1)	38.3	78.4	11.9	1.9	4.7	0.8	2.3
5	0.3%Pd/Zn-Cr(10:1)	34.5	56.3	2.7	2.7	34.3	2.7	1.3
6	0.3%Pd/Zn-Cr(20:1)	25.8	38.9	0.9	1.2	54.6	3.1	1.3

[a] Reactions in 45-mL autoclave, 180°C, 7.5 bar initial H_2 pressure (RT), 2.0 g acetone, 0.20 g catalyst powder of 45-180 μm particle size, 800 rpm stirring speed, 2 h.

[b] C_3 is propene and propane, IP isopropanol, MO mesityl oxide, Others are mainaly C6+ acetone condensation products (mostly 2,6,8-trimethylnonane-4-one).

4.2.2.3. Effect of Pd loading

Table 4.6 shows the effect of Pd loading on the catalytic performance of Pd/Zn-Cr catalysts. Increasing the Pd loading from 0.1% to 1% caused little effect on acetone conversion. As in the gas phase, the highest acetone conversions of around 38.3% were obtained with 0.3% palladium loading at the optimum reaction temperature of 180°C (entry 2). Lower acetone conversion in the range between 34.9% and 36.3% were recorded with Pd loadings of 0.1% and 1.0% (entry 1 and 3). These results may be

explained by the fact that the catalysts with 0.1% and 1% Pd loadings, having equal amounts of Pd_s (0.066 wt% and 0.07 wt%, respectively), exhibited almost equal catalytic activities. However, the 1% Pd catalyst was much less selective, giving a large amount of IP (26.8%) (entry 3). This may be due to the lower dispersions (D=0.07) for 1.0%Pd/Zn-Cr(1:1) and hence larger average Pd particle diameters: 13 nm compared to 2.4 nm for 0.3%Pd/Zn-Cr(1:1). For MIBK synthesis, the co-operation between the hydrogenation and the acid/base functions is required to drive the reaction forward towards the desired product (MIBK). When palladium particle size increases, the average distance between the metal particles and the acid/base sites increases, resulting in a decrease of catalyst activity [6]. Chen *et al.* explained how Pd particles may aggregate when the Pd loading is at higher levels, leading to the covering of basic sites on their Pd/hydrotalcite catalysts [7].

Table 4.6 Effect of palladium loading on the catalytic performance of Pd/Zn-Cr (1:1) at 180°C and 7.5 bar for 2 h and 0.2 g catalyst.

Entry	Pd loading (%)	Conversion (%)	Selectivity (%)[b]					
			MIBK	DIBK	C_3	IP	MO	Others
1	0.1	34.9	75.4	13.1	1.0	3.1	1.3	6.1
2	0.3	38.3	78.4	11.9	1.9	4.7	0.8	2.3
3	1.0	36.3	57.4	8.1	1.1	26.8	3.1	3.5

MIBK selectivities are similar 0.1 and 0.3 wt% Pd loadings, 75.4% and 78.4% respectively. Therefore, only a low Pd loading of 0.1 – 0.3 wt% is sufficient for the hydrogenation of C=C of mesityl oxide to MIBK, as found in previous liquid phase studies with Pd/acid/base catalysts [8, 9]. With 1% Pd loading, the selectivity towards the production of MIBK is reduced significantly to 57.4%, resulting in an increased isopropanol production. This again could be the result of the isopropanol production

being more favourable when distance between Pd and acid/base sites increases with a higher Pd loading.

4.2.2.4. Reaction time course

The time course of reaction with 0.3%Pd/Zn-Cr (1:1) catalyst was studied at a constant H_2 pressure of 7.5 and 20 bar (RT) using a 25-mL Parr 4590 reactor. The results of these experiments are shown in Figures 4.5 and 4.6. In this system, the reaction may be limited by H_2 transfer into the liquid phase due to the lower stirring speed (600 rpm) as well as the lower gas/liquid ratio of about 0.6.

The time course for the reaction at 7.5 bar is shown in Figure 4.5. Zero time is the moment when the temperature in the reactor had reached the preset value of 180°C, which took 20 min to reach while the reaction was going. At zero time, the selectivity to MO was 70.0%, gradually decreasing to 44.2% in 4 h. Simultaneously, the MIBK selectivity was growing from 22.1% to 30.1%, along with the acetone conversion increasing from 17.5% to 23.2%. Therefore, under such conditions, mesityl oxide forms quickly, probably reaching equilibrium, followed by the much slower hydrogenation of MO to MIBK. As expected, increasing the hydrogen pressure to 20 bar (RT) under otherwise similar conditions accelerated the hydrogenation of MO and significantly increased the selectivity to MIBK (Figure 4.6). These results show that under the chosen reaction conditions, the one-step MIBK synthesis over the Pd/Zn-Cr catalyst in the liquid phase is limited by MO hydrogenation due to a slow hydrogen supply.

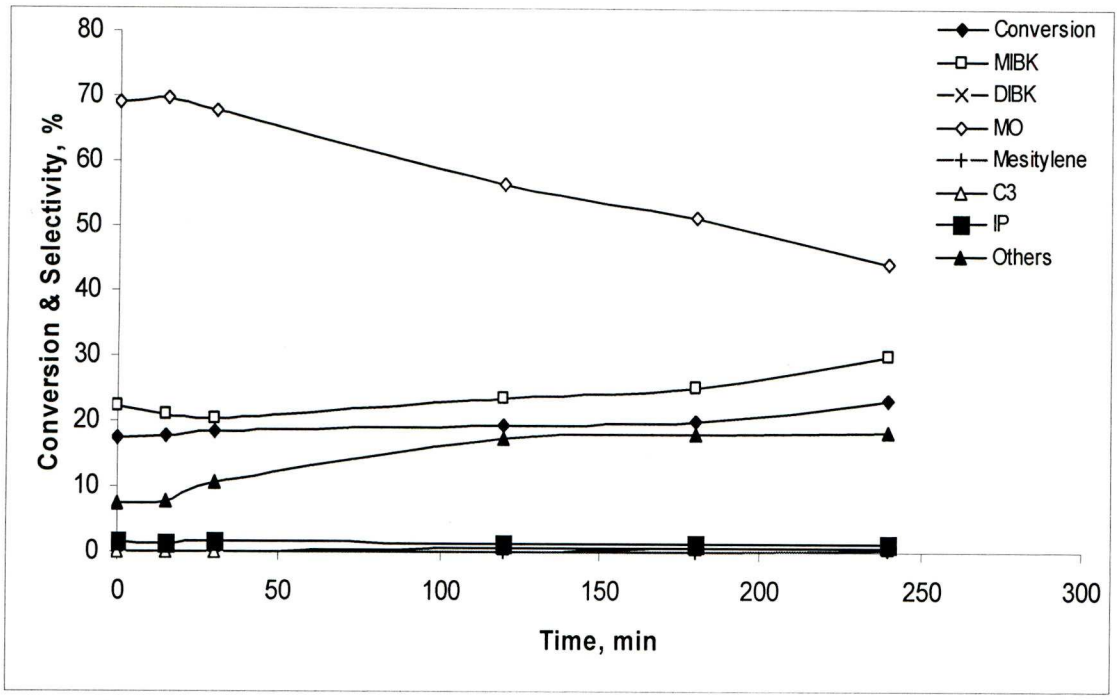

Figure 4.5 Acetone conversion and product selectivities vs. time for MIBK synthesis with 0.3%Pd/Zn-Cr (1:1) catalyst in liquid phase at constant H_2 pressure of 7.5 bar (RT), 180°C.

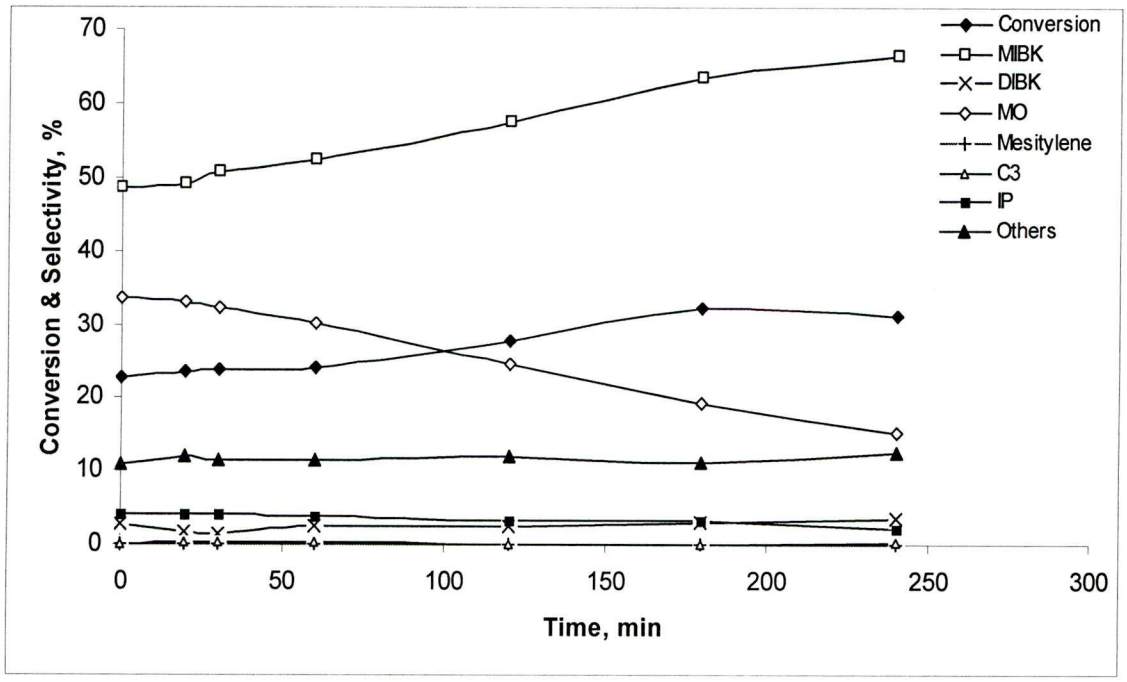

Figure 4.6 Acetone conversion and product selectivities vs. time for MIBK synthesis with 0.3%Pd/Zn-Cr (1:1) catalyst in liquid phase at constant H_2 pressure of 20 bar (RT), 180°C.

4.2.3. Gas phase reactions over Zn-Cr-Cu oxide catalysts

A number of solid acid catalysts comprising Zn-Cr-Cu oxide to be tested in the one-pot synthesis of MIBK from acetone and hydrogen were prepared as described in Section 2.3. These catalysts were characterised by the surface area/porosity analysis (BET surface area, pore size and pore volume), TGA (water content) and ICP (zinc, chromium and copper content). The catalysts, together with the characterisation data, are given in Tables 3.2, 3.4, 3.6 and 3.8 in Chapter 3, as well as in Section 3.3.2 for XRD analysis.

Preliminary investigations with variable reaction parameters were carried out in order to obtain optimum conditions for the reaction with Zn-Cr-Cu oxide catalysts. A reaction temperature of 300°C and a hydrogen flow of 20 mL/min were found to be optimal in terms of acetone conversion and MIBK selectivity in this study and were therefore employed for all reactions studied, except for those that had a change in reactor temperature.

As mentioned at the beginning of this chapter (Section 4.2.1), with bulk Zn-Cr oxides, the reaction went with a low conversion of acetone and MIBK selectivity, with mesityl oxide being the major product, due to the absence of an effective hydrogenation function in the catalyst. This indicates that the Zn-Cr oxide itself mainly acted as an acid catalyst, possessing a weak hydrogenation activity. In the presence of Cu, acetone conversion and MIBK selectivity increased up to 51.6% and 44.5% respectively over Zn-Cr-Cu (1:1:1) oxide (Table 4.7), indicating that the thermodynamically favourable hydrogenation of MO to MIBK on Cu(0) sites drives the process forward to the desired product MIBK.

Table 4.7 The catalytic performance of Zn-Cr-Cu in the gas-phase synthesis of MIBK from acetone and hydrogen.[a]

Catalyst	Conversion (%)	Selectivity (%)[b]						
		MIBK	DIBK	C_3	IP	MO	Mesitylene	Others
Zn-Cr-Cu (1:1:1)	51.6	44.5	28.9	0.8	10.5	0	0	15.3
Cr-Cu (1:1)	49.9	44.1	28.1	1.6	7.6	0	0	18.6

[a] Reaction conditions: 300°C, acetone/H_2 = 37:63 (mol/mol), 20 mL/min H_2 flow, 0.2 g catalyst of 45-180 μm particle size, 3 h time on stream.

[b] C_3 is propene and propane, IP isopropanol, MO mesityl oxide, others are mainly C_{9+} acetone condensation products (mostly 2,6,8-trimethylnonane-4-one).

As can be seen from Table 4.7, acetone conversion slightly increased to 51.6% over Zn-Cr-Cu (1:1:1) oxide compared to 49.9% with Cu-Cr (1:1). This enhancement in the catalyst activity was probably caused by the addition of Zn to the catalyst. Similar results in terms of the improvement of catalyst activity with Zn added to Cu were found in the literature for methanol synthesis [10-12] and for dehydrogenation of isoamyl alcohol [13].

Figure 4.7 shows a typical time course for the direct synthesis of MIBK from acetone and hydrogen over Zn-Cr-Cu (1:1:1) oxide. It can be seen that conversion of acetone decreased slightly from 52.7% recorded after 1 h on stream to 47.7% after 13 h, representative of a slight catalyst deactivation, which was probably caused by catalyst coking [14]. Moreover, sintering of Cu particles resulting from prolonged hydrogen treatment at high temperatures during the reaction could be another reason for this drop in the catalyst activity [3].

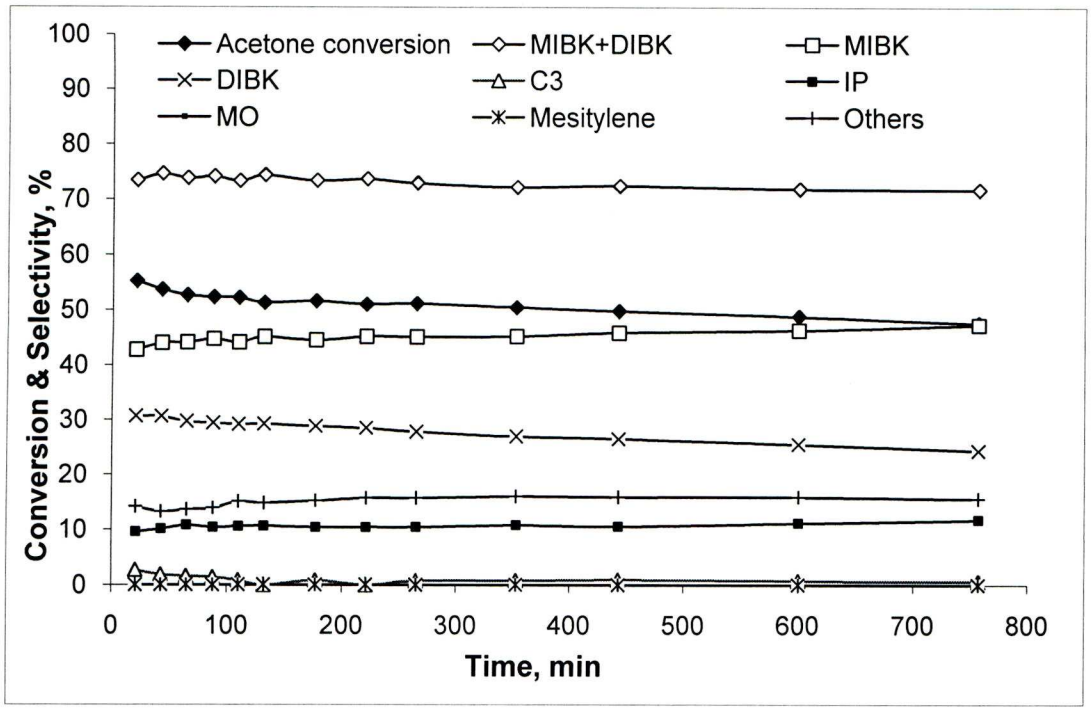

Figure 4.7 Acetone conversion and product selectivities vs. time on stream (0.2 g Zn-Cr-Cu (1:1:1), 20 mL/min H_2 flow, acetone/H_2 = 37:63 mol/mol, 300°C).

4.2.3.1. Effect of Cu content in Zn-Cr-Cu oxide

The results of experiments for the direct synthesis of MIBK from acetone and hydrogen over Zn-Cr-Cu oxides that were carried out with varying Cu content are detailed in Table 4.8. These reactions were carried out for a period of 3 h, at 300°C, under a 20 mL/min H_2 flow rate, acetone/H_2 = 37:63 mol/mol, using 0.2 g catalyst of 45-180 μm particle size. In general, increasing the copper content from 0.1 to 2.0 in molar ratio resulted in a slightly higher catalyst activity, with increasing acetone conversion from 42.6% over Zn-Cr-Cu (1:1:0.1) to 51.6% over Zn-Cr-Cu (1:1:1) and Zn-Cr-Cu (1:1:2) oxide catalysts. As regards to reaction selectivity, the effect of Cu was very small (Table 4.8). With the Cu content increasing, the MIBK selectivity showed a tendency to decrease, whereas the DIBK selectivity slightly increased. The total MIBK + DIBK selectivity was in the range of 72 – 75%.

Table 4.8 Effect of Cu ratio in Zn-Cr-Cu oxide on the catalytic performance of Zn-Cr-Cu in the gas-phase synthesis of MIBK from acetone and hydrogen.

Catalyst	Conversion (%)	Selectivity (%)						
		MIBK	DIBK	C3	IP	MO	Mesitylene	Others
Zn-Cr-Cu (1:1:0.1)	42.6	47.2	24.6	1.9	11.8	0	0	14.4
Zn-Cr-Cu (1:1:0.2)	40.9	45.2	24.8	2.3	12.7	0	0	15.0
Zn-Cr-Cu (1:1:0.5)	47.1	48.1	25.9	1.1	10.2	0	0	14.7
Zn-Cr-Cu (1:1:0.8)	47.3	49.9	24.2	1.2	10.7	0	0	14.1
Zn-Cr-Cu (1:1:1)	51.6	44.5	28.9	0.8	10.5	0	0	15.3
Zn-Cr-Cu (1:1:2)	51.6	46.0	28.5	1.4	8.8	0	0	15.3

4.2.3.2. Effect of reaction temperature

Table 4.9 shows how the results vary with increasing the temperature from 250 to 350°C for Zn-Cr-Cu (1:1:1) oxide as an optimised catalyst in this study. These reactions were carried out for a period of 3 h, under a 20 mL/min H_2 flow rate, acetone/H_2 = 37:63 mol/mol, using 0.2 g catalyst of 45-180 μm particle size.

Table 4.9 Effect of temperature on catalytic performance of Zn-Cr-Cu (1:1:1) oxide.

Temperature (°C)	Conversion (%)	Selectivity (%)						
		MIBK	DIBK	C_3	IP	MO	Mesitylene	Others
250	52.9	37.4	29.2	1.2	16.1	0.0	0.0	16.1
300	51.6	44.5	28.9	0.8	10.5	0.0	0.0	15.3
350	24.1	35.0	5.7	13.4	7.7	17.7	4.8	15.7

Increasing the temperature from 250°C to 300°C had a small effect on catalyst performance. However, a 7.1% increase in MIBK selectivity can be noted at 300°C to

reach 44.5% (Table 4.9). Further increase of the reaction temperature to 350°C caused a significant decline in catalyst performance both in terms of activity (acetone conversion) and selectivity to MIBK and DIBK. Sintering of Cu particles could be the reason for the observed catalyst deactivation and the drop in MIBK selectivity at 350°C [3]. These results warrant the optimum temperature of 300°C for the Zn-Cr-Cu catalyst.

4.2.3.3. Effect of acetone/hydrogen ratio in the gas flow

An investigation into the effect of the acetone/hydrogen molar ratio in the gas flow on the catalytic results was conducted using the Zn-Cr-Cu (1:1:1) oxide which proved to be the more efficient catalyst in the temperature optimisation study. The results from this study are detailed in Table 4.10. At a lower acetone/H_2 molar ratio of 0.10, C_3 gases and over condensation products C_{6+} (others) were the main products with a selectivity of 33.2% and 24.7% for C_3 and C_{6+} respectively, leading to a small MIBK selectivity of 23% .

Table 4.10 Effect of acetone/H_2 molar ratio on the catalytic performance of Zn-Cr-Cu (1:1:1) at 300°C, 20 mL/min H_2 flow rate, 0.2 g catalyst of 45-180 μm particle size and 3 h time on stream.

Acetone/H_2 molar ratio	Conversion (%)	Selectivity (%)						
		MIBK	DIBK	C_3	IP	MO	Mesitylene	Others
0.10	57.1	23.0	10.4	33.2	8.7	0	0	24.7
0.37	51.6	44.5	28.9	0.8	10.5	0	0	15.3
0.50	40.6	55.5	23.6	0.8	7.3	0	0	12.8
0.63	29.5	62.7	16.1	0.8	10.2	0	0	10.2

When the acetone/H_2 molar ratio increased from 0.37 to 0.63, the acetone conversion reduced from 51.6% to 29.5%. Simultaneously, the selectivity to MIBK increased steadily to reach 62.7% at the acetone/H_2 molar ratio of 0.63. At the same time, DIBK and C_{6+} selectivities decreased significantly, with the selectivity to C_3 gases becoming as low as 0.8%. The low levels of C_3 gases at higher acetone/H_2 molar ratios demonstrate that Cu(0) acts as an efficient catalyst for hydrogenation of the C=C bond of mesityl oxide rather than the C=O bond of acetone. The result of decreasing the acetone conversion with increasing acetone/H_2 molar ratio is in agreement with the results reported in the literature for different catalysts [3].

4.2.3.4. Effect of Pd loading

Addition of 0.1 and 0.3 wt% of Pd to the Zn-Cr-Cu (1:1:1) had little effect on the catalyst performance, slightly increasing acetone conversion and MIBK selectivity (Table 4.11). The acetone conversion without palladium loading was 48.9%. This value increased to 50.7% and 52.8% with adding 0.1 and 0.3 wt% Pd respectively. MIBK and DIBK selectivities also increased slightly along with some decrease in IP selectivity. This enhancement of the catalyst activity and product selectivity may be due to the synergetic effect of Pd and Cu which can be explained in terms of hydrogen spillover as well as a better performance stability [11] (Section 1.6.2.5). With Pd, catalyst deactivation was not observed during 10 h of continuous operation (Figure 4.8). The catalyst reached steady state in 1-2 h and after that performed with constant activity and selectivity.

Table 4.11 Effect of Pd loading on the catalytic performance of Zn-Cr-Cu (1:1:1)[a].

Pd loading (%)	Conversion (%)	Selectivity (%)						
		MIBK	DIBK	C_3	IP	MO	Mesitylene	Others
0	48.9	46.4	25.6	0.8	11.3	0	0	16.0
0.1	50.7	47.3	28.8	1.3	6.8	0	0	15.7
0.3	52.8	48.5	28.2	0.8	5.9	0	0	16.6

[a] Reaction conditions: 300°C, 0.2 g catalyst of 45-180, acetone/H_2 = 37:63 (mol/mol), 20 mL/min H_2 flow rate, 0.2 g catalyst of 45-180 μm particle size, 10 h time on stream.

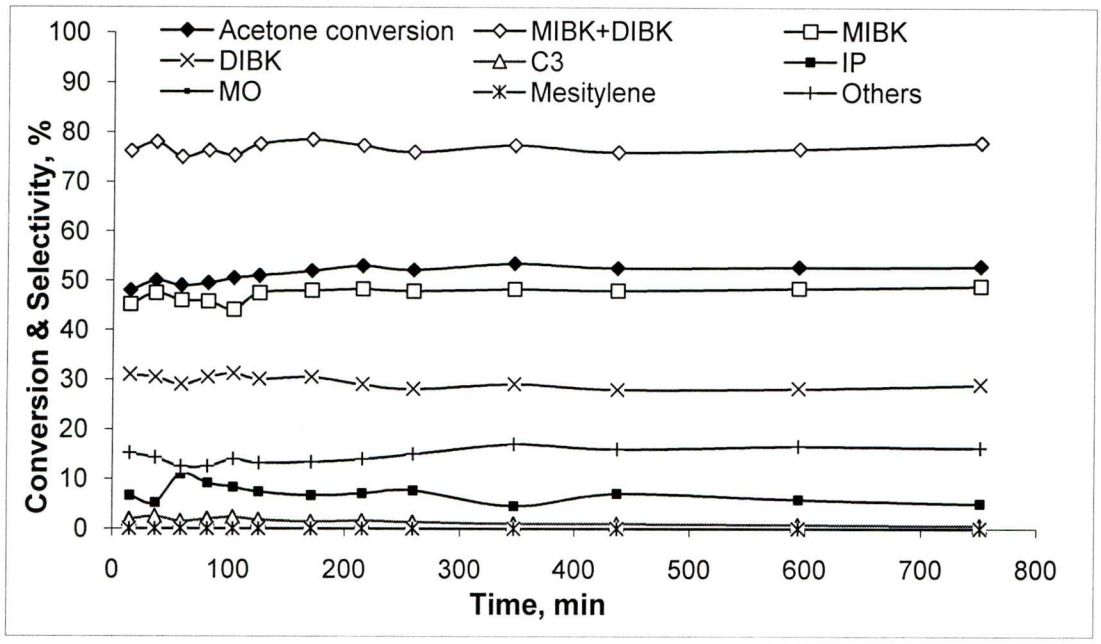

Figure 4.8 Acetone conversion and product selectivities vs. time on stream (0.2 g 0.3%Pd/Zn-Cr-Cu (1:1:1), 20 mL/min H_2 flow, acetone/H_2 = 37:63 mol/mol, 300°C).

4.3. Catalyst reproducibility and re-use

In this section, the results of our study into the reproducibility and re-use of Pd/Zn-Cr catalysts for one-step synthesis of MIBK from acetone and hydrogen in both liquid and gas phases are presented and discussed.

4.3.1. Catalyst reproducibility in the gas-phase process

The study of catalyst reproducibility was carried out for the whole range of Pd/Zn-Cr catalysts in the continuous gas-phase process using the same reaction conditions that were used in the previous experiments. For these tests, different catalyst samples were prepared by the procedures described in Section 2.3. Table 4.12 represents some results of the testing of catalyst reproducibility in the gas phase process over Pd/Zn-Cr oxides. These new results are very close to those reported in Section 4.2.1 (Tables 4.1 and 4.2), which demonstrates their reliability.

Table 4.12 Catalyst reproducibility in the gas-phase synthesis of MIBK.[a]

Entry	Catalyst	H_2 flow (mL/min)	Conversion (%)	Selectivity[b] (%)					
				MIBK	DIBK	C_3	IP	MO	Others
1	0.3%Pd/Zn-Cr (1:1)	10	40.4	69.2	20.2	1.0	2.1	0.4	6.6
2	0.3%Pd/Zn-Cr (1:1)[b]	20	33.6	69.3	16.6	1.1	4.1	0.3	8.6
3	0.1%Pd/Zn-Cr (1:1)	20	19.5	73.5	12.5	3.2	4.0	0.5	6.3
4	1.0%Pd/Zn-Cr (1:1)	20	18.2	70.7	13.8	2.5	4.5	0.7	7.8
5	0.3%Pd/Zn-Cr (1:1)	30	29.2	71.5	15.6	1.1	4.1	0.4	7.3
6	0.3%Pd/Zn-Cr (10:1)	10	34.9	69.8	19.2	1.0	4.7	0.1	5.2
7	0.3%Pd/Zn-Cr (20:1)	10	38.5	54.8	27.9	0.7	4.2	0	12.4

[a] Reaction conditions: 300°C, acetone/H_2 = 37:63 (mol/mol), 0.2 g catalyst of 45-180 μm particle size, 3 h time on stream.

[b] Reaction time, 2 h.

4.3.2. Catalyst reproducibility and re-use in the liquid-phase process

Table 4.13 shows some results on catalyst reproducibility in the liquid-phase process over newly prepared Pd/Zn-Cr catalysts. Like for the gas-phase reaction

(Section 4.2.1), these new results are very close to those reported in Section 4.2.2 (Tables 4.5 and 4.6), which demonstrates the reliability of our results for the liquid-phase reaction.

Catalyst re-use was attempted in the case of 0.3%Pd/Zn-Cr (1:1) in liquid-phase reactions using different catalyst pre-treatments (Table 4.13). In one attempt, the catalyst isolated after the first run (entry 4) was heated at 150°C in vacuum for 1 h prior to re-use (entry 5). Another attempt included the same heat treatment followed by heating under a hydrogen flow at 250°C for 1 h (entry 6). Both attempts gave similar results: acetone conversion was regained at its initial level, albeit with a reduced MIBK selectivity and an increased amount of IP. This indicates that the post-reaction catalyst partly lost its acidity while maintaining high hydrogenation activity.

Table 4.13 Catalyst reproducibility and re-use in the liquid-phase synthesis of MIBK.[a]

Entry	Catalyst	Conversion (%)	Selectivity (%)					
			MIBK	DIBK	C_3	IP	MO	Others
1	0.3%Pd/Zn-Cr(1:30)	54.3	65.2	11.1	1.3	5.5	0.8	16.1
2	0.3%Pd/Zn-Cr(1:10)	42.5	73.1	10.1	2.3	8.2	0.9	5.4
3	0.1%Pd/Zn-Cr(1:1)	32.5	74.3	12.2	0.8	4.2	1.4	7.1
4	0.3%Pd/Zn-Cr(1:1)	38.3	78.4	11.9	1.9	4.7	0.8	2.3
5	0.3%Pd/Zn-Cr(1:1)[b]	38.3	59.6	4.4	3.1	30.9	1.7	1.3
6	0.3%Pd/Zn-Cr(1:1)[c]	39.4	60.5	3.4	3.2	31.4	1.3	0.2
7	1%Pd/Zn-Cr(1:1)	34.5	56.3	8.2	0.8	28.3	3.3	3.1
8	0.3%Pd/Zn-Cr(10:1)	34.1	56.2	3.0	2.5	33.5	3.1	1.7
9	0.3%Pd/Zn-Cr(20:1)	24.9	37.9	0.9	0.9	55.6	3.3	1.4

[a] Reactions in 45-mL autoclave, 180°C, 7.5 bar initial H_2 pressure (RT), 2.0 g acetone, 0.20 g catalyst powder of 45-180 μm particle size, 800 rpm stirring speed, 2 h.

[b] Reuse of entry 4 run; prior to reuse, the catalyst was separated and heated at 150°C under vacuum for 1 h.

[c] Reuse of entry 4 run; prior to reuse, the catalyst was first treated as in (b) then heated in H_2 flow at 250°C for 1 h.

4.4. Discussion of catalyst performance on one-step synthesis of MIBK

This study has shown that palladium metal supported on Zn-Cr mixed oxide and palladium-free Zn-Cr-Cu oxide are efficient heterogeneous bifunctional catalysts that contain acid and metal functionalities and are therefore capable of carrying out all three reaction steps in the one-step synthesis of MIBK from acetone and H_2 in gas and liquid phases without separating the intermediate DAA and MO. The synergy of palladium or copper and catalyst acidity was a requirement for MIBK to be produced in the one-step process. This is evident from the fact that mesityl oxide was the main product in the absence of palladium sites, whereas with palladium present MIBK became the major reaction product. A significant increase in acetone conversion was observed with Pd/Zn-Cr catalyst, which is an indication that the bifunctional catalyst shifts the equilibrium controlled condensation reaction towards the production of MIBK *via* the irreversible hydrogenation of mesityl oxide.

The optimisation of catalyst composition has led to the preferred catalyst formulation comprising 0.3% Pd on the amorphous Zn-Cr (1:1) oxide for both gas and liquid phase processes. Both the continuous gas-phase process and the batch liquid-phase process produced MIBK with a selectivity of 70-78% and 90% total MIBK + DIBK selectivity at 38-40% acetone conversion, on a par with the best results reported to date.

Metal functionality, palladium or copper, in supported catalysts were more selective towards hydrogenating the C=C bond in MO rather than the C=O group in

acetone which led to high selectivities of MIBK and DIBK and much lower IP and C_3 gases selectivity. This selective hydrogenation step appears to be the rate-limiting step in MIBK synthesis over Pd/Zn-Cr oxide in the gas-phase process, and probably in the liquid-phase process as well.

This study has shown that the Pd/Zn-Cr catalyst, as a heterogeneous multifunctional catalytic system, has a higher stability towards catalyst deactivation compared to the Zn-Cr-Cu oxide. The latter shows slight deactivation probably caused by sintering of copper particles as well as by site blocking by heavy condensation byproducts.

4.5. Conclusion

- Pd metal supported on Zn^{II}-Cr^{III} mixed oxide was found to be an efficient bifunctional catalyst for one-step synthesis of MIBK from acetone and H_2 in the gas and liquid phase. The reaction involves acid-catalysed condensation of acetone to mesityl oxide followed by its hydrogenation to MIBK.
- For both the continuous gas-phase process and the batch liquid-phase process, the preferred catalyst formulation comprises 0.3 wt% Pd on the amorphous Zn-Cr (1:1) oxide (S_{BET} = 132 m^2/g) possessing Lewis acid sites (1.2 mmol/g density) with an enthalpy of NH_3 adsorption of -155 kJ/mol.
- Both processes produce MIBK with a selectivity of 70-78% and 90% MIBK + DIBK total selectivity at 38-40% acetone conversion.
- Evidence is provided that hydrogenation of mesityl oxide to MIBK is the rate-limiting step in both process.

References

[1] E.F. Kozhevnikova, I.V. Kozhevnikov, J. Catal. 238 (2006) 286.

[2] P.Y. Chen, S.J. Chu, C.C. Chen, N.S. Chang, W.C. Lin, T.K. Chuang, US Patent 5059724 (1991).

[3] V. Chikán, Á. Molnár, K. Baláznik, J. Catal. 184 (1999) 134.

[4] Y. Higashio, T. Nakayama, Catal. Today 28 (1996) 127.

[5] S. Narayanan, R. Unnikrishnan, Appl. Catal. A 145 (1996) 231.

[6] S.-M. Yang, Y.M. Wu, Appl. Catal. A 192 (2000) 211.

[7] Y.Z. Chen, C.M. Hwang, C.W. Liaw, Appl. Catal. A 169 (1998) 207.

[8] Y.Z. Chen, B.J. Liaw, H.R. Tan, K.L. Shen, Appl. Catal. A 205 (2001) 61.

[9] A.A. Nikolopoulos, B.W.L. Jang, J.J. Spivey, Appl. Catal. A. 296 (2005) 128.

[10] M. Fujiwara, H. Ando, M. Tanaka, Y. Souma, Bull. Chem. Soc. Jpn. 67 (1994) 546.

[11] I. Melian-Cabrera, M.L. Granados, J.L.G. Fierro, Catal. Lett. 79 (2002) 165.

[12] Y. Ogino, M. Oba, H. Uchida, Bull. Chem. Soc. Jpn. 33 (1960) 358.

[13] C.Y. Shiau, S. Chen, J.C. Tsai, S.I. Lin, Appl. Catal. A 198 (2000) 95.

[14] I.V. Kozhevnikov, J. Mol. Catal. A. 262 (2007) 86.

Chapter 5. One-step synthesis of p-cymene from α-pinene over Zn-Cr oxide in gas phase

5.1. Introduction

Described in this chapter is a substantially improved synthesis of p-cymene by one-step transformation of α-pinene in the gas phase using Zn-Cr mixed oxide as a new, noble-metal-free, bifunctional catalyst. The Zn-Cr oxide has been used previously as a catalyst for various reactions, for example, synthesis of methanol from synthesis gas, fluorination of hydrocarbons with HF, dehydrogenation of alcohols and hydrogenation of carboxylic acids ([1] and references therein). Recently, we have reported Pd/Zn-Cr as an efficient bifunctional catalyst for the one-step synthesis of methyl isobutyl ketone [1,2], which is described in Chapter 4. To our knowledge, Zn-Cr oxide has not been used as a catalyst for any terpene conversion so far.

5.2. α-Pinene conversion to p-cymene: Results and Discussion

α-Pinene, like many other terpenes, is a highly reactive compound. It undergoes thermal rearrangement in the gas phase between 300 – 400°C without any catalyst to give a complex mixture of cyclic and acyclic monoterpene isomers $C_{10}H_{16}$ [3]. Catalysts cause great effect on the reaction products [4, 5]. Figure 5.1 (A) shows the products for the thermal rearrangement of α-pinene at 350°C in the gas phase, which was carried out by passing an N_2 flow containing 2% α-pinene through the empty

reactor. Limonene was the main product (40% selectivity at 93% α-pinene conversion), with only traces of p-cymene being formed (Table 5.1). In striking contrast, Figure 5.1 (B) displays the products for the catalysed reaction over Zn-Cr (1:1) oxide under the same conditions at an optimum contact time of 1.7 s. In this case, p-cymene formed in 78% selectivity at 100% α-pinene conversion, with no limonene found among reaction products.

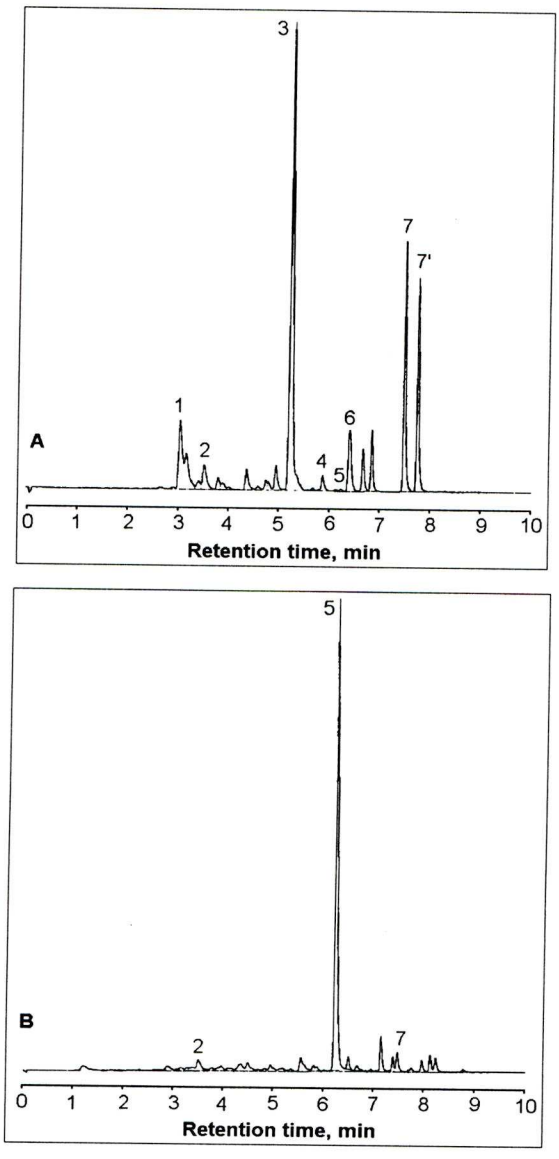

Figure 5.1 GC traces for products of (A) thermal and (B) catalytic (0.3 g Zn-Cr (1:1), 1.7 s contact time) conversion of α-pinene in the gas phase (350°C, 2 vol.% α-pinene in N_2, 7.5 mL/min flow rate; α-pinene (1), camphene (2), limonene (3), γ-terpinene (4), p-cymene (5), terpinolene (6), alloocimene (7, 7')).

5.2.1. Effect of catalyst acidity

The enhancing effect of catalyst acidity on catalyst activity can be seen from the results at 300°C which showed α-pinene conversions below 100% (Table 5.1). The more acidic Zn-Cr (1:10) oxide gave a higher α-pinene conversion (89%) than the less acidic Zn-Cr (1:1) oxide (57%). As expected for a consecutive reaction, the first oxide gave higher p-cymene selectivity than the second one at the expense of camphene and limonene. The two catalyst exhibited close turnover frequencies (TOF) which is probably due to non-differential conditions of these experiments, levelling the catalyst activities.

Table 5.1 Effect of catalyst acidity on dehydroisomerisation of α-pinene: Zn-Cr (1:10) vs. Zn-Cr (1:1)[a]

Catalyst	Conversion (%)	TOF[b] (h^{-1})	Selectivity (%)			
			p-Cymene	Camphene	Limonene	Others
Zn-Cr (1:10)	89	0.63	35	26	10	29
Zn-Cr (1:1)	57	0.61	20	33	23	24

[a] 300°C, 0.2 g catalyst, 2 vol.% α-pinene in N_2, 10 mL/min flow rate, 0.83 s contact time, 2 h time on stream.

[b] Turnover frequency calculated using the acid site densities from Table 3.10 in Chapter 3.

5.2.2. Catalyst stability

Zn-Cr catalysts exhibited excellent performance stability regardless of their Zn/Cr ratio. The best catalyst, Zn-Cr (1:1), showed no deactivation during at least 30 h of continuous operation (Figure 5.2). The catalyst reached steady state in about 1 h and after that performed with constant activity and selectivity. It should be pointed out that

hydrogen was not supplied to the reactor to prevent coke formation. Indeed, some coke was found in post reaction catalysts. Its amount grew with the time on stream: from 0.5% after 4 h to 4% after 60 h at 350°C for Zn-Cr (1:1). This, however, did not affect catalyst performance due to a relatively weak sensitivity of oxide catalysts to deactivation by coke compared to supported metals. In contrast, the Pd/SiO_2 catalyst used by Hölderich et al. [5] suffers from deactivation by coke, and to maintain stable performance of this catalyst (up to 4 h on stream) hydrogen supply to the gas feed ([α-pinene]/[H_2] = 4 mol/mol) is required to prevent deactivation. It should be noted that in our case addition of H_2 to the gas flow (N_2:H_2 = 2:1) reduced the yield of p-cymene from 78% to 69% (Table 5.2 in Section 5.2.3).

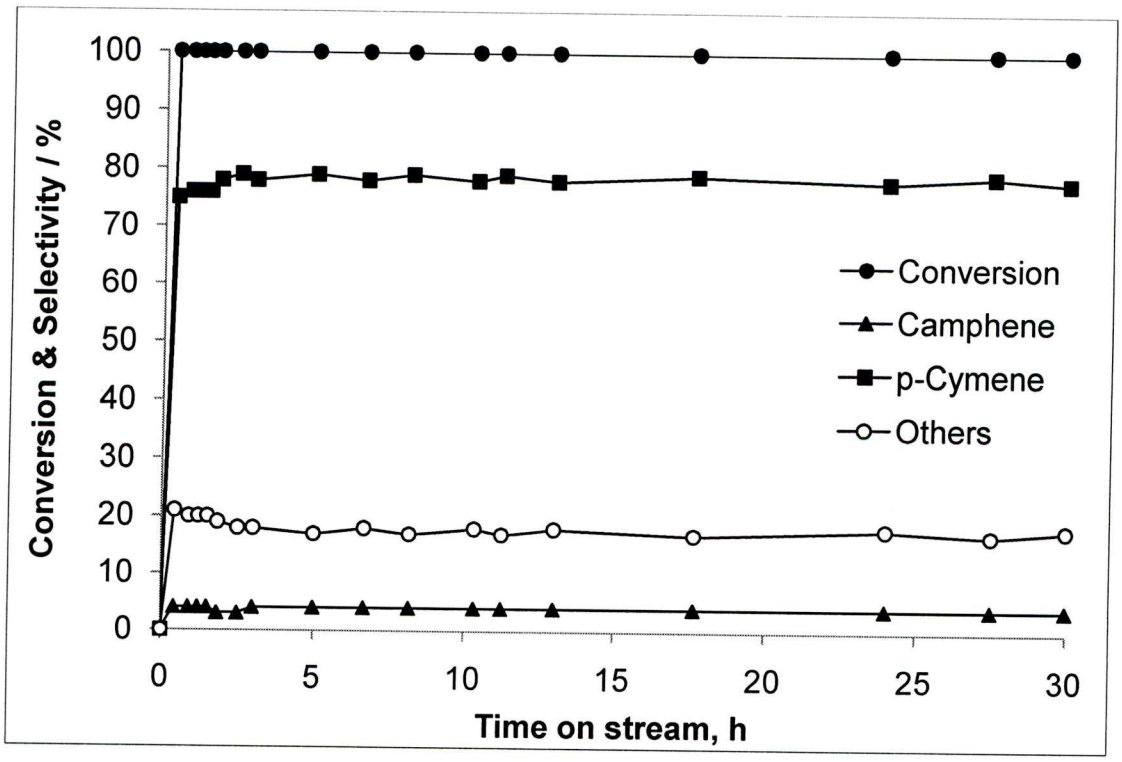

Figure 5.2 α-Pinene conversion and product selectivity vs. time on stream (350°C, 0.3 g Zn-Cr (1:1), 2 vol.% α-pinene in N_2, 7.5 mL/min flow rate, 1.7 s contact time).

5.2.3. Effect of Zn/Cr atomic ratio

The results of experiments that were carried out with varying the Zn/Cr atomic ratio from 1:30 – 20:1 for the direct conversion of α-pinene to p-cymene over Zn-Cr oxides are detailed in Table 5.2. In general, variation of the Zn/Cr atomic ratio from 1:30 – 20:1 under optimal conditions (350°C, 1.7 s contact time) had practically no effect on α-pinene conversion but affected reaction selectivity (Table 5.2). All the catalysts exhibited 100% α-pinene conversion, hence their activity could not be differentiated. The catalyst activity is not the issue for α-pinene dehydroisomerisation, since even without catalyst the thermal conversion of α-pinene was as high as 93%. It is the selectivity to p-cymene that matters. As can be seen from Table 5.2, the Zn/Cr atomic ratio affected the p-cymene selectivity, but this effect was moderate one (61-78%) despite the wide range of Zn/Cr ratio variation. The Zn-Cr (1:1) oxide possessing an intermediate acid strength and acid site density, as well as an intermediate surface area, exhibited the highest p-cymene selectivity of 78% at 100% α-pinene conversion. The Cr-rich amorphous oxides, Zn-Cr (1:10) and Zn-Cr (1:30), possessing stronger acidities, exhibited lower p-cymene selectivities. This can be explained by enhancing acid-catalysed isomerisation of monoterpene intermediates in the case of those oxides. On the other hand, the Zn-rich crystalline oxides, Zn-Cr (10:1) and Zn-Cr (20:1), were less efficient probably because of their low surface area and low acidity. The fact that the wide variation in catalyst acidity (both acid strength and acid site density) across the whole Zn/Cr ratio range studied caused only a relatively small effect on the catalyst performance suggests that the acid-catalysed isomerisation of α-pinene is fast, and the whole process is limited by dehydrogenation of p-cymene precursor(s). This implies that dehydrogenating ability of Zn-Cr oxides should be more important for the p-cymene selectivity than their acid properties.

Table 5.2 Effect of catalyst composition[a]

Catalyst	Conversion (%)	Selectivity (%)			
		p-Cymene	Camphene	Limonene	Others
No catalyst	93	<1	3	40	57
Zn-Cr (1:30)	100	61	5	0	34
Zn-Cr (1:10)	100	63	5	0	32
Zn-Cr (1:1)	100	78	4	0	18
Zn-Cr (1:1) [b]	100	69	4	0	27
Zn-Cr (10:1)	100	74	4	0	22
Zn-Cr (20:1)	100	62	6	1	31

[a] 350°C, 0.3 g catalyst, 2 vol.% α-pinene in N_2, 7.5 mL/min flow rate, 1.7 s contact time, 2 h time on stream.

[b] $N_2 + H_2$ (2:1) gas mixture instead of N_2, 13 mL/min flow rate.

The p-cymene yield of 78% obtained with Zn-Cr (1:1) oxide exceeds the one obtained by Hölderich et al. (67%) [5]. It should be noted, however, that increasing α-pinene concentration in the gas feed from 2 to 10 vol.% reduced the selectivity to p-cymene from 78% to 70%. The higher selectivity of Zn-Cr oxide compared to the Pd/SiO_2 catalyst can be explained as follows. First, the Zn-Cr oxide possesses Lewis acid sites rather than Brønsted acid sides, which appears to restrict favourably monoterpene isomerisation. Second, due to the lack of metal sites in the catalyst Zn-Cr oxide does not cause C-C bond breaking which would yield light by-products.

5.2.4. Effect of reaction temperature

Figure 5.3 shows the effect of reaction temperature on the catalytic performance of Zn-Cr (1:1) catalyst in p-cymene synthesis. Increasing the reaction temperature from 300°C to 380°C caused significant effect on the α-pinene conversion. The highest α-

pinene conversion of 100% was reached at 350°C and above. The selectivity to p-cymene also increased from 20% to 67% with increasing reaction temperature from 300°C to 350°C and then decreased with further increase in the reaction temperature. Camphene and limonene were found to be the main products at 300°C, with 33% and 23% selectivity respectively and then decreased in selectivity as the temperature increased. This indicates that camphene and limonene are the primary products, formed in α-pinene isomerisation, followed by dehydrogenation to form p-cymene.

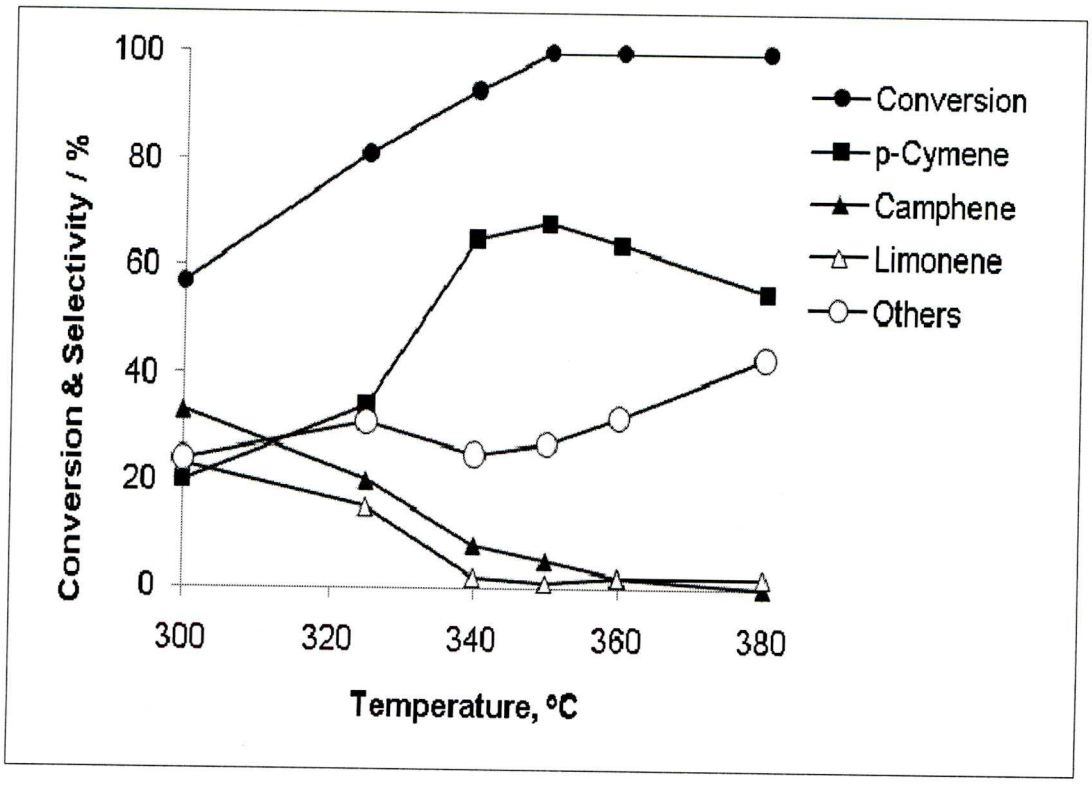

Figure 5.3 Effect of temperature on α-pinene conversion (0.2 g Zn-Cr (1:1), 2 vol.% α-pinene in N_2, 10 mL/min flow rate, 0.83 s contact time, 2 h time on stream).

5.2.5. Effect of contact time

Figure 5.4 represents the effect of contact time on the performance of Zn-Cr (1:1) catalyst in p-cymene synthesis. In general, increasing the contact time from 0.4 to

1.7 s (by reducing the flow rate and increasing the catalyst load) improved the p-cymene selectivity from 61% to 78%. The conversion of α-pinene increased significantly from 96% to 100% when the catalyst contact time was increased from 0.4 s to 0.8 s (Figure 5.4) with a simultaneous decrease in camphene and limonene selectivity from 8% and 3% to 4% and 0% respectively.

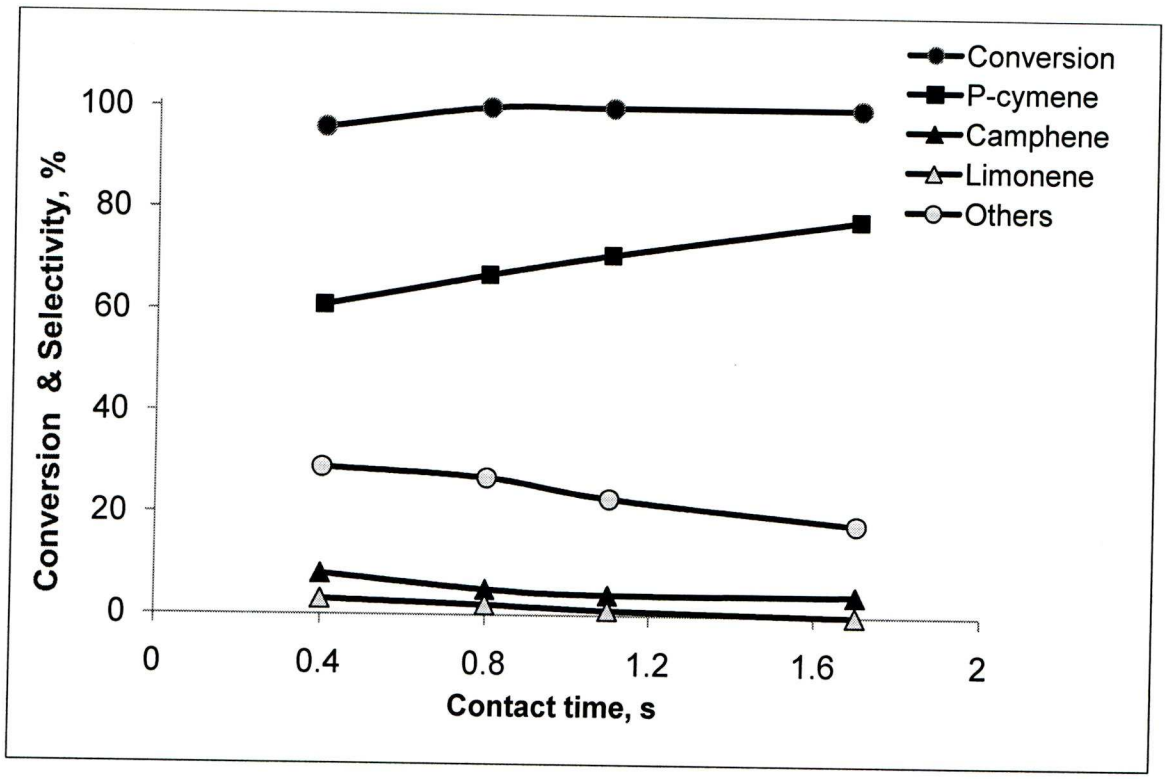

Figure 5.4 Effect of contact time on the catalytic performance of Zn-Cr(1:1) oxide in α-pinene conversion to p-cymene at 350°C, 2 vol.% α-pinene in N_2, 2 h time on stream.

5.2.6. Effect of Pd loading

Table 5.3 shows the effect of Pd loading on the catalytic performance of Pd/Zn-Cr catalysts. Increasing the Pd loading from 0.3% to 1% caused a decrease in p-cymene selectivity, with no effect on the α-pinene conversion. The highest p-cymene selectivity of 78% was obtained with no palladium loaded on the catalyst (entry 1) at the optimum

reaction temperature of 350°C. When 0.3% palladium was introduced to the catalyst support, a slight decrease in the p-cymene selectivity was observed (entry 2).

Loading of 1% palladium caused a further decrease in p-cymene selectivity (entry 3). As the palladium loading increased the yield of monoterpene isomers was increased and light by-products were produced by C-C bond breaking.

Table 5.3 Effect of palladium loading on the catalytic performance of Zn-Cr(1:1) oxide[a]

Entry	Catalyst	Conversion (%)	Selectivity (%)			
			p-Cymene	Camphene	Limonene	Others
1	Zn-Cr (1:1)	100	78	4	0	18
2	0.3%Pd/Zn-Cr (1:1)	100	68	4	0	28
3	1%Pd/Zn-Cr (1:1)	100	62	7	0	31

[a] Reaction conditions: 350°C, 0.3 g catalyst of 45-180 μm particle size, 2 vol.% α-pinene in N_2, 7.5 mL/min flow rate, 1.7 s contact time, 2 h time on stream.

5.3. Reaction mechanism

Zn(II) and Cr(III) oxides are both known as hydrogenation and dehydrogenation catalysts [6], hence both Zn(II) and Cr(III) oxo species can act as dehydrogenating sites in the Zn-Cr mixed oxides. It may be thought that in our system the dehydrogenating ability of Zn(II) and Cr(III) oxo species is similar. This is supported by the moderate effect of the Zn/Cr ratio on p-cymene selectivity (Table 5.2).

Therefore, the dehydroisomerisation of α-pinene to p-cymene can be viewed proceeding via the mechanism of bifunctional catalysis proposed by Hölderich et al. [5]. It involves fast α-pinene isomerisation to p-menthadienic (limonene and its isomers) and camphenic compounds on acid sites of the catalyst followed by rate-limiting

dehydrogenation of p-menthadienic precursor(s) on Zn(II) and Cr(III) oxo species to form p-cymene (Scheme 1). The effects of temperature (Figure 5.3) and contact time (Figure 5.4) on reaction selectivity indicate that camphene is a relatively stable intermediate in this reaction, as also suggested previously for the reaction with Pd/SiO_2 [5].

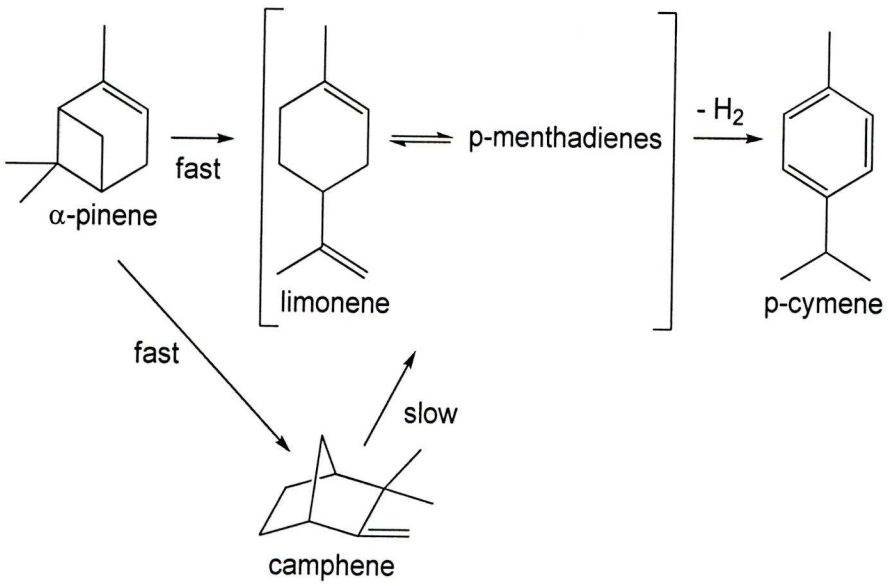

Scheme 1. Proposed mechanism for the catalytic conversion of α-pinene to p-cymene.

5.4. Conclusion

In conclusion, Zn-Cr mixed oxide possessing acid and dehydrogenation catalytic functions is a new, efficient, noble-metal-free catalyst for the one-step dehydroisomerisation of α-pinene to p-cymene. It provides high p-cymene yield (78% at 100% α-pinene conversion) and exhibits stable performance without hydrogen supply. This reaction is a good example of the use of heterogeneous multifunctional catalysis for the green conversion of renewable feedstock into value-added chemicals. Besides the useful H_2 co-product, monoterpene $C_{10}H_{16}$ isomers are the only by-products in this process, which could be utilised as a bio-derived transportation fuel.

References

[1] E.F. Kozhevnikova, I.V. Kozhevnikov, J. Catal. 238 (2006) 286.

[2] F. Al-Wadaani, E.F. Kozhevnikova, I.V. Kozhevnikov, J. Catal. 257 (2008) 199.

[3] A. Stolle, B. Ondruschka, W. Bonrath, Eur. J. Org. Chem. (2007) 2310.

[4] A. Corma, S. Iborra, A. Velty, Chem. Rev. 107 (2007) 2411.

[5] D.M. Roberge, D. Buhl, J.P.M. Niederer, W.F. Hölderich, Appl. Catal. A 215 (2001) 111.

[6] K. Weissermel, H.-J. Arpe, Industrial Organic Chemistry, 3rd ed., VCH, Weinheim, 1997.

Chapter 6. Conclusions

Methyl isobutyl ketone (MIBK) is produced on an industrial scale and is widely used as a solvent for paint and protective coatings [1]. Traditionally MIBK is manufactured *via* a three-step process involving base-catalysed aldol condensation of acetone to diacetone alcohol (DAA), acid-catalysed dehydration of DAA to mesityl oxide (MO) and metal-catalysed hydrogenation of MO to MIBK [2]. The first two steps, the aldol condensation and the dehydration, are catalysed by a liquid alkali such as NaOH and an acid such as H_3PO_4, respectively. Active hydrogenation metals such as Pd, or Ni supported on a high surface area support, are employed for the hydrogenation of the MO. To save the time, energy and financial costs associated with the separation of the reaction intermediates, DAA and MO, multifunctional heterogeneous catalysts that are able to perform all three reactions in a one-pot, cascade reaction have been investigated. These catalysts possess both acid and/or base functions in addition to metal sites for the selective hydrogenation of MO.

p-Cymene is another important chemical produced on an industrial scale and used, amongst others, for the synthesis of p-cresol, which is further transformed to the widely used antioxidant 2,6-di-tert-butyl-p-cresol [3]. Currently, p-cymene is produced in a mixture with o- and m-isomers by the alkylation of toluene with propene, followed by isomer separation. Given the projected shortage of petroleum-based feedstock, a more attractive route to p-cymene can be the transformation of cyclic monoterpenes – naturally occurring renewable feedstock [4, 5].

In this study, an in-depth investigation of multifunctional catalysts based on Zn-Cr and Zn-Cr-Cu mixed oxides and their Pd doped derivatives was carried out, focusing on catalyst optimisation with respect to the Zn/Cr/Cu ratio and Pd loading complemented by a thorough characterisation of catalyst texture, acid properties (type, density and strength of acid sites) and Pd dispersion. These catalysts were used for the direct synthesis of MIBK from acetone and hydrogen and p-cymene from α-pinene. These catalysts possess multiple chemical functionalities and environmentally and economically can be attractive for a variety of chemical reactions.

A series of Zn-Cr and a Zn/Cr/Cu mixed oxides with a Zn/Cr and a Zn/Cr/Cu atomic ratio of 1:30-20:1 and 1:1:0.1-1:1:2 respectively, were prepared by co-precipitation of Zn^{II}, Cr^{III} and Cu^{II} hydroxides. Zn-Cr oxides were then doped with Pd using an impregnation method. The catalysts were characterised by various techniques. TGA was used to determine the thermal stability of the catalysts and the water content. The BET method was used for the determination of the surface area and the porosity. XRD studies were carried out to determine the catalyst composition. ICP spectroscopy was used to measure the zinc, chromium and copper composition within the Zn-Cr and Zn-Cr-Cu oxide catalysts, as well as to determine the palladium content supported on Zn-Cr oxides. H_2 adsorption was used for measuring Pd dispersion in Pd/Zn-Cr catalysts. The number and strength of acid sites in the bulk Zn-Cr oxides was measured by differential scanning calorimetry of ammonia adsorption in a gas-solid system and by microcalorimetry of pyridine adsorption in a liquid-solid system. The nature (Brønsted or Lewis) of acid sites was determined by FTIR of adsorbed pyridine. The main characterisation results can be summarised as follows:

- For the Zn-Cr mixed oxide series, the Zn-rich oxides (Zn/Cr = 10:1 – 20:1) were crystalline materials, exhibiting the XRD pattern of ZnO crystalline phase. In contrast, Cr-rich oxides (Zn/Cr = 1:1 – 1:30) were amorphous materials. The amorphous Cr-rich oxides had larger surface areas and greater pore volumes, but smaller average pore diameters than the crystalline Zn-rich oxides. The surface area of the Cr-rich oxides increased substantially with increasing the Cr content. The Cr-rich amorphous oxides had a more regular pore structure. In contrast, the Zn-rich crystalline oxides had a much broader pore size distribution. Palladium loading did not change the catalyst texture, but slightly decreased the surface area and pore volume, as expected. The TGA analysis of Zn-Cr oxides and Pd/Zn-Cr catalysts showed a monotonous loss of water in the temperature range from 30°C to 600°C. The amount of water depended on the Zn/Cr ratio: ~9 wt% for the amorphous oxides (Zn/Cr = 1:30 – 1:1) and 2.0 – 2.8 wt% for the crystalline ones (Zn/Cr = 10:1 – 20:1). The acid strength of Zn-Cr oxides in terms of the heat of adsorption of NH_3 or pyridine increased monotonously with increasing Cr content. The entire series of Zn-Cr oxides was found to possess Lewis acid sites. Only one oxide, Zn-Cr (1:30), with the largest Cr content, had Brønsted acid sites strong enough to protonate pyridine. Palladium dispersion in Pd/Zn-Cr catalysts (0.1 – 1 wt% Pd), decreased with increasing Pd loading from 0.1 to 1.0 wt% on Zn-Cr (1:1) oxide. At a constant Pd loading of 0.3 wt%, the dispersion decreased with the decrease in the Cr content in Zn-Cr oxides.
- For the Zn-Cr-Cu mixed oxide series, the oxides pre-treated under nitrogen, exhibited only the characteristic XRD peaks attributable to the CuO crystalline phase, while under hydrogen pretreatment, the XRD showed the characteristic peaks attributable to Cu(0). This was due to the fact that copper was reduced from Cu(II) to Cu(0) under hydrogen at 300°C. The catalyst surface area depended on the Cu content,

increasing substantially with a decrease in the Cu content, whereas the pore diameter increased slightly with increasing the Cu content. The pre-treatment of catalysts under H_2 reduced the surface area to a small extent and this can be attributed to the sintering of microcrystalline metallic copper. The introduction of palladium into the oxides did not change the catalyst texture, but, as expected, decreased the surface area and the pore volume to a small extent.

Pd/Zn-Cr and Pd-free Zn-Cr-Cu oxide were found to be efficient bifunctional catalysts for the one-step synthesis of MIBK from acetone and H_2 in both gas-phase and liquid-phase processes. When Zn-Cr oxides were used in this process in the absence of Pd and/or Cu, it went with a low acetone conversion, and mesityl oxide (the product of the acid-catalysed condensation of acetone) was the major product, whereas the selectivity to MIBK was very low. This shows that the Zn-Cr oxide itself mainly acts as an acid catalyst, possessing a weak hydrogenation activity. In the presence of Pd and/or Cu, acetone conversion and MIBK selectivity increased dramatically, indicating that the thermodynamically favourable hydrogenation of MO to MIBK on Pd sites drives the process forward. Hence co-operation between the hydrogenation and the acid/base functions is essential to drive the one-step reaction forward towards the desired product MIBK.

In the gas-phase MIBK synthesis, the Pd/Zn-Cr catalyst reached a steady state in ca. 1 h and showed constant activity and selectivity for at least 10 h on stream. For both the continuous gas-phase process (300°C, ambient pressure) and the batch liquid-phase process (180°C, 7.5 bar H_2 pressure), the preferred catalyst formulation comprised 0.3 wt% Pd on the amorphous Zn-Cr (1:1) oxide (S_{BET} = 132 m^2/g) possessing Lewis acid sites (1.2 mmol/g density), with an enthalpy of NH_3 adsorption of

-155 kJ/mol. Both processes produced MIBK with a selectivity of 70-78% and 90% MIBK + DIBK total selectivity at 38-40% acetone conversion, on a par with the best results reported to date. Evidence was obtained that the hydrogenation of the C=C bond in MO is the rate-limiting step in the gas-phase MIBK synthesis over Pd/Zn-Cr oxide.

The hydroisomerisation of α-pinene to p-cymene was carried out over Zn-Cr mixed oxides in the gas-phase. These oxides, which possess both acid and dehydrogenation functions, were found to be efficient, noble-metal-free catalyst for the one-step dehydroisomerisation of α-pinene to p-cymene. This reaction is a good example of the use of heterogeneous multifunctional catalysis for the conversion of renewable feedstock (α-pinene) into value-added chemicals. It involves acid-catalysed α-pinene isomerisation, followed by the dehydrogenation of p-cymene precursor(s). The reaction was carried out over a fixed catalyst bed in the gas phase at 350°C. Amongst Zn-Cr oxides studied (Zn/Cr = 20:1–1:30), the preferred catalyst is Zn-Cr (1:1) oxide which produces p-cymene with a 78% yield at 100% α-pinene conversion. This catalyst shows stable performance for over 30 h without co-feeding hydrogen to the reactor. The new catalyst is superior to the Pd/SiO_2 catalyst, previously developed by Holdrich et al., in both p-cymene yield (78% compared to 67%) and its stability.

References

[1] W.F. Hoelderich, Stud. Surf. Sci. Catal. 41 (1988) 83.

[2] K. Weissermel, H.-J. Arpe, Industrial Organic Chemistry, 4th ed., Wiley-VCH, 2003.

[3] K. Weissermel, H.-J. Arpe, Industrial Organic Chemistry, 3rd ed., VCH, Weinheim, 1997.

[4] A. Corma, S. Iborra, A. Velty, Chem. Rev. 107 (2007) 2411.

[5] D.M. Roberge, D. Buhl, J.P.M. Niederer, W.F. Hölderich, Appl. Catal. A 215 (2001) 111.

Appendix

Appendix (I)

The value of the molar extinction coefficients (ε), obtained by plotting the absorbance of UV light against pyridine concentration (Figure 1), was $1.818 \cdot 10^3$ $Lmol^{-1}cm^{-1}$ at wave length (λ) = 250 nm.

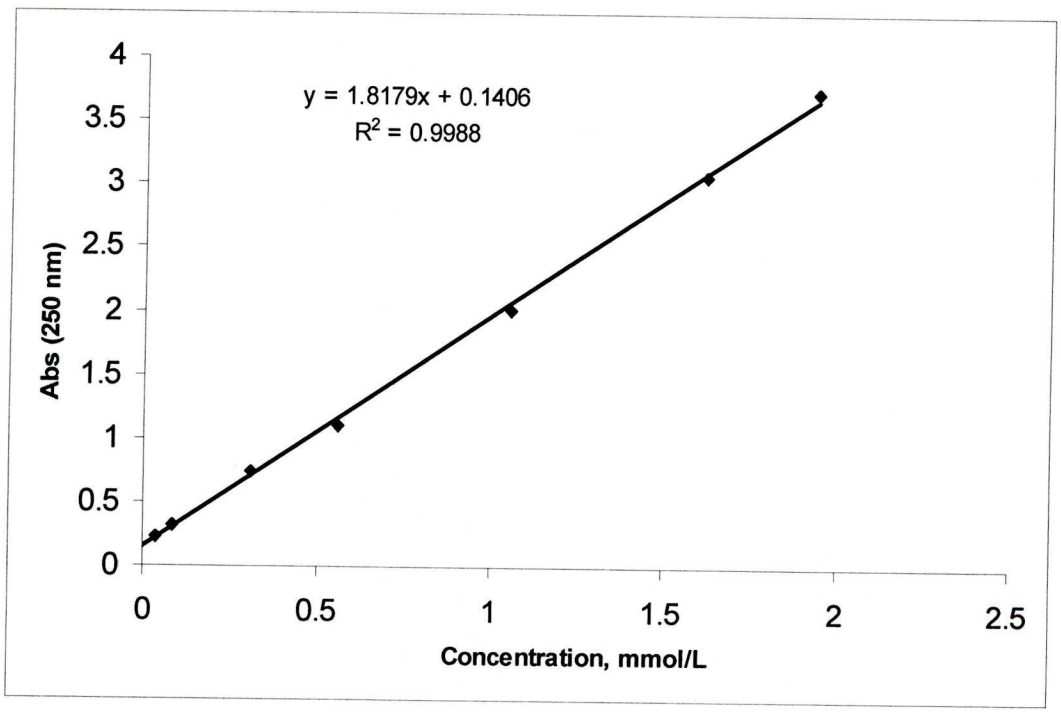

Figure 1 Calibration for pyridine in cyclohexane solution.

Appendix (II)

The calibration plots (equation (2.4) in Chapter 2) for the compounds involved in the conversion of acetone to MIBK are shown in Figures 2-7.

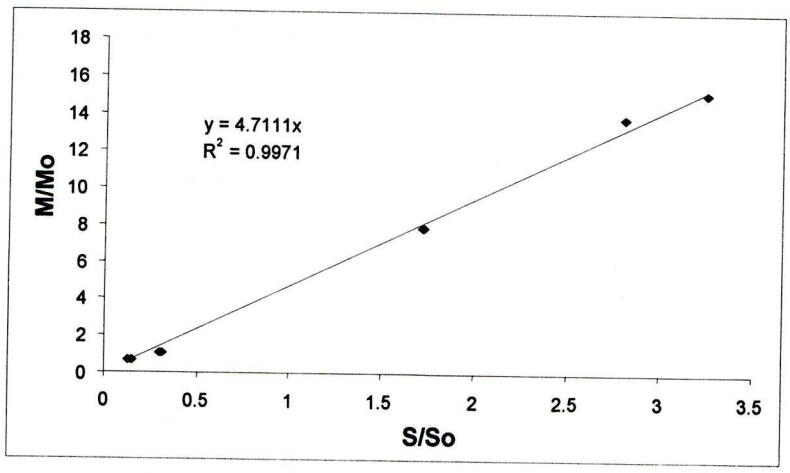

Figure 2 Calibration for acetone with decane as a standard.

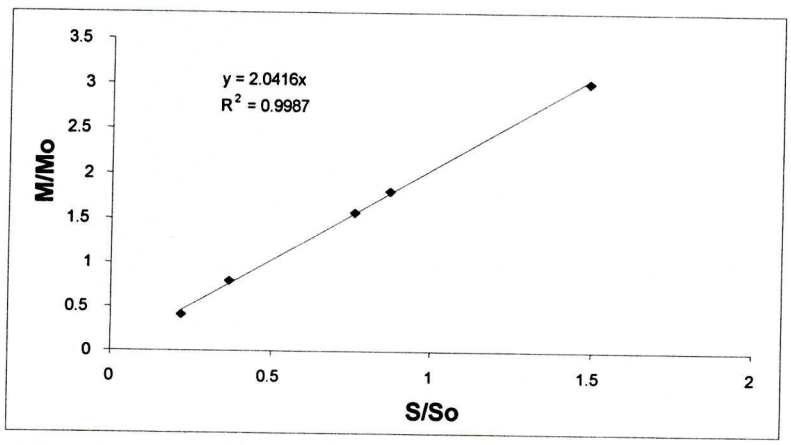

Figure 3 Calibration for MIBK with decane as a standard.

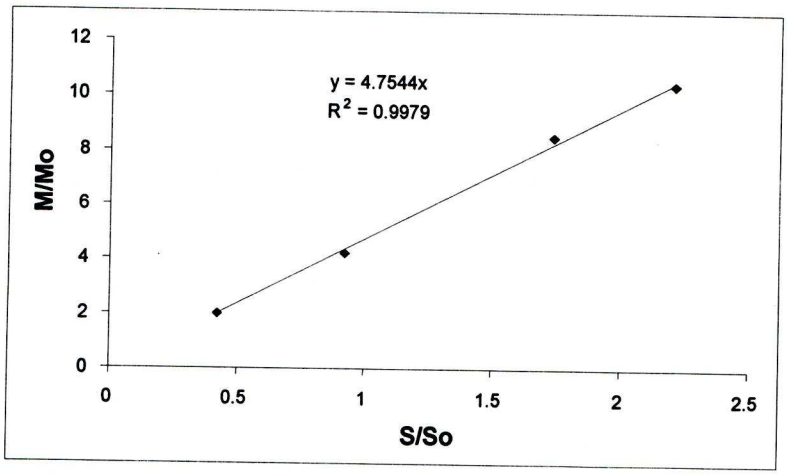

Figure 4 Calibration for IP with decane as a standard.

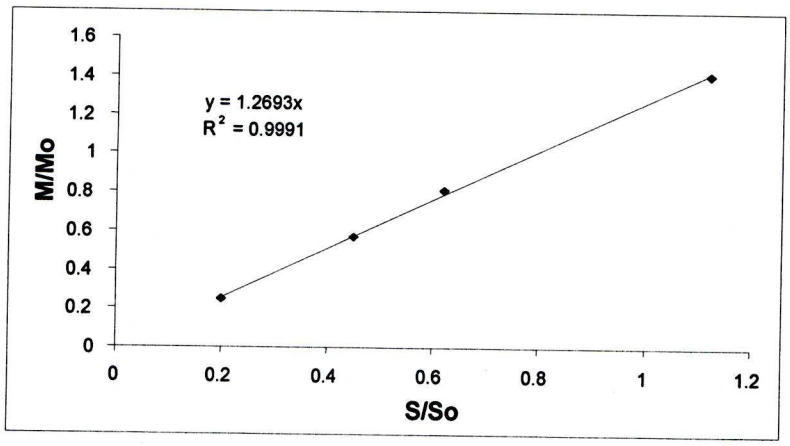

Figure 5 Calibration for DIBK with decane as a standard.

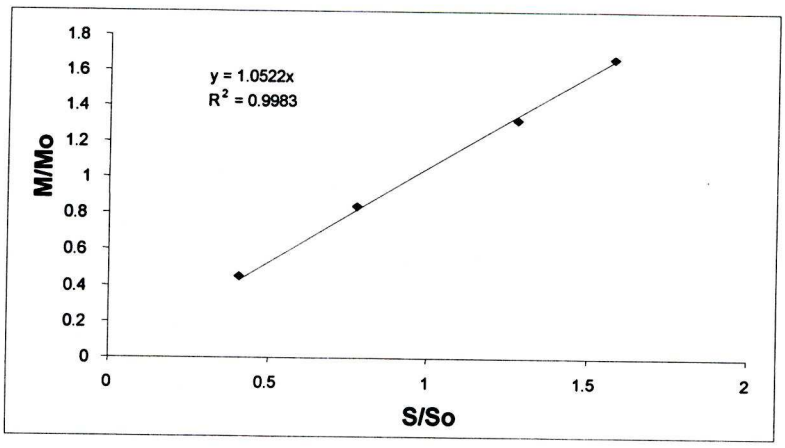

Figure 6 Calibration for MS with decane as a standard.

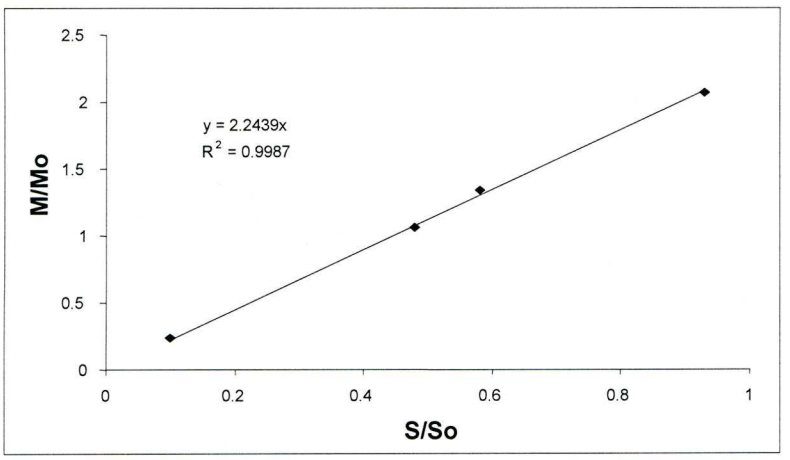

Figure 7 Calibration for MO with decane as a standard.

Appendix (III)

Figures 8 shows a typical heat and mass profiles for the pulse NH_3 adsorption.

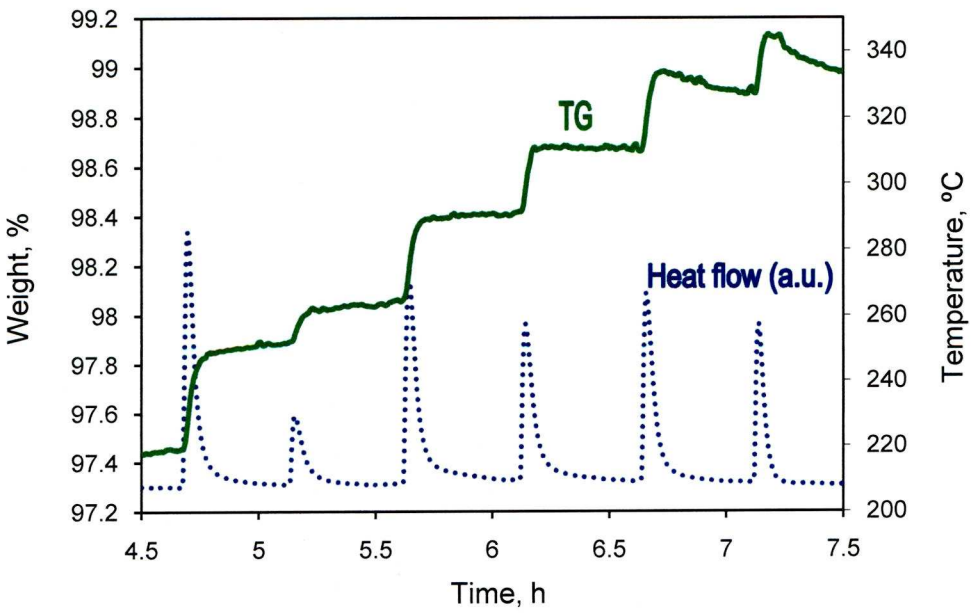

Figure 8 TG-DSC signals occurring during pulse adsorption of ammonia at 100°C on bulk Zn-Cr (1:30) oxide (helium as the carrier gas).

Appendix (IV)

The mass spectra obtained for MIBK, DIBK and MO products identified by GC/MS are shown in Figures 9-11 which give primary mass/charge ratios of 100, 142, and 120 respectively.

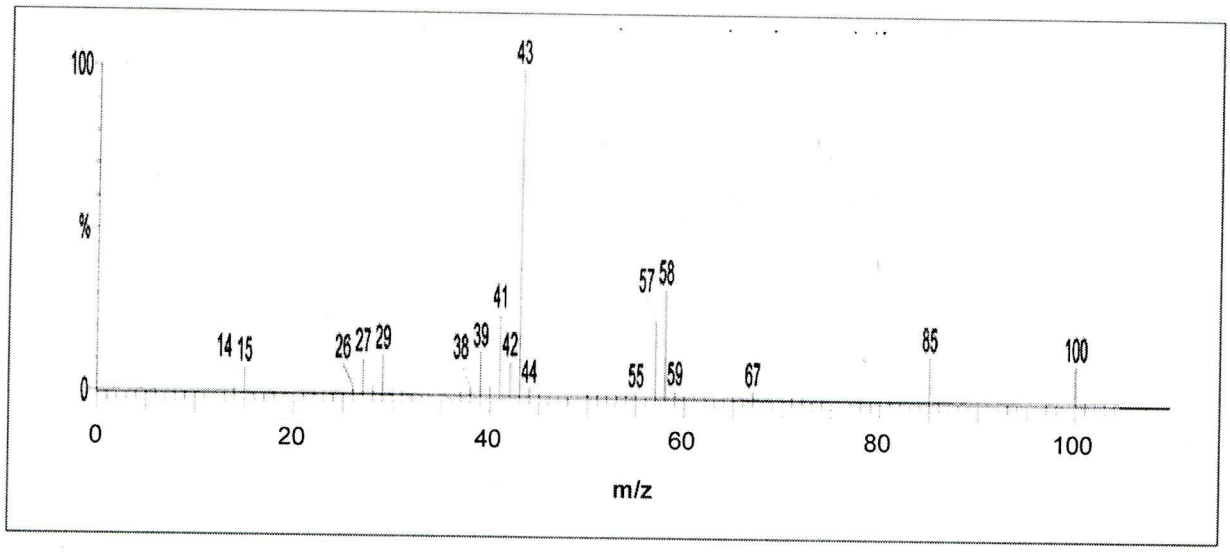

Figure 9 Mass spectrum of methyl isobutyl ketone (MIBK). Relative molecular mass-100.

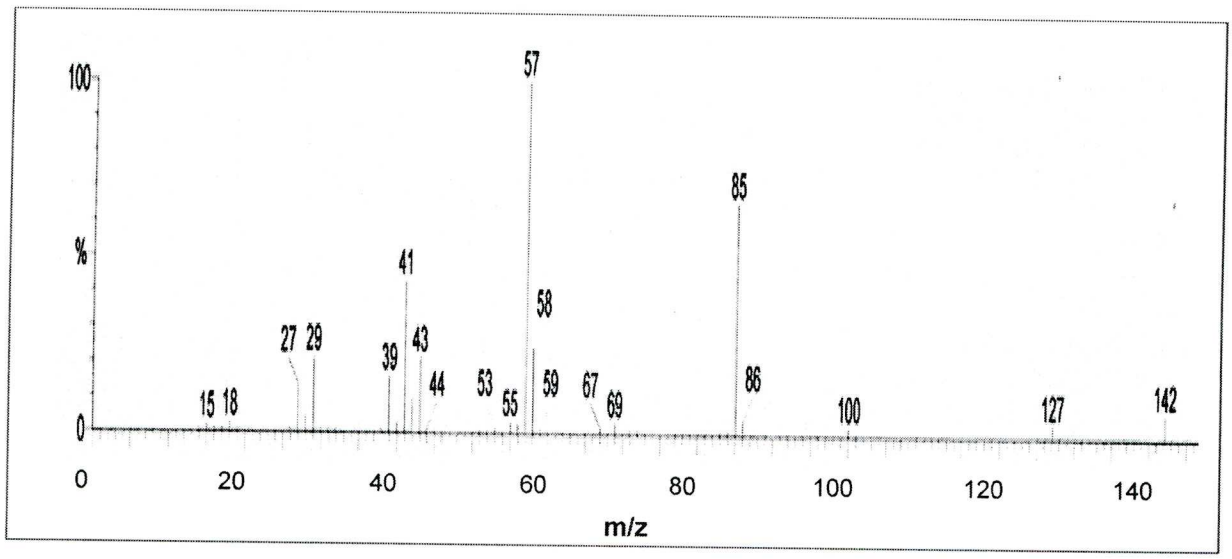

Figure 10 Mass spectrum of diisobutyl ketone . Relative molecular mass-142.

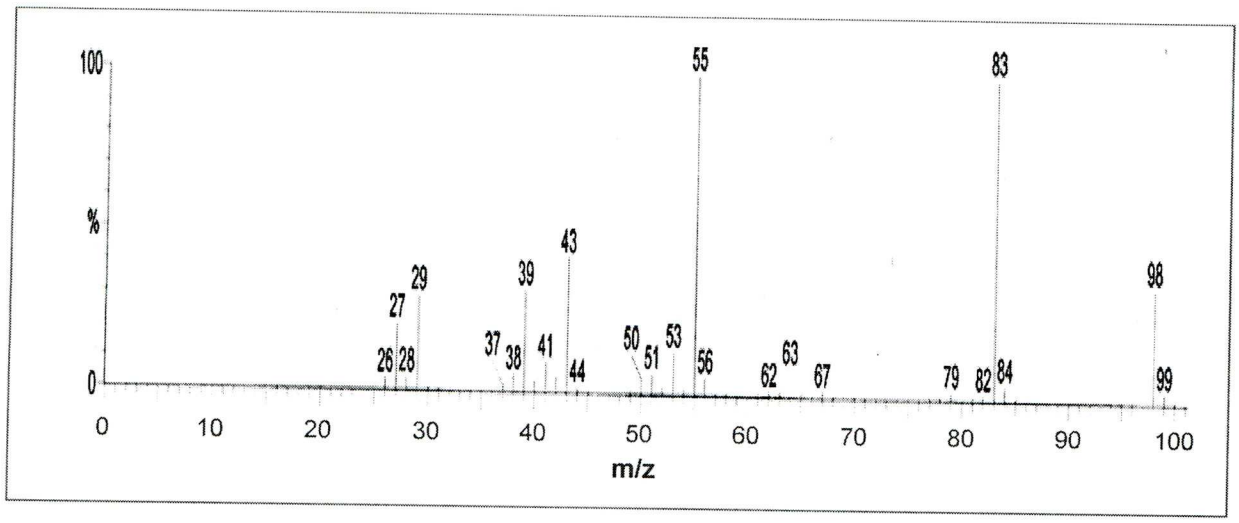

Figure 11 Mass spectrum of mesityl oxide. Relative molecular mass-98.

Appendix (V)

Figure 12 shows a GC trace for the gas phase conversion of acetone to MIBK over 0.3% Pd/Zn-Cr (1:30).

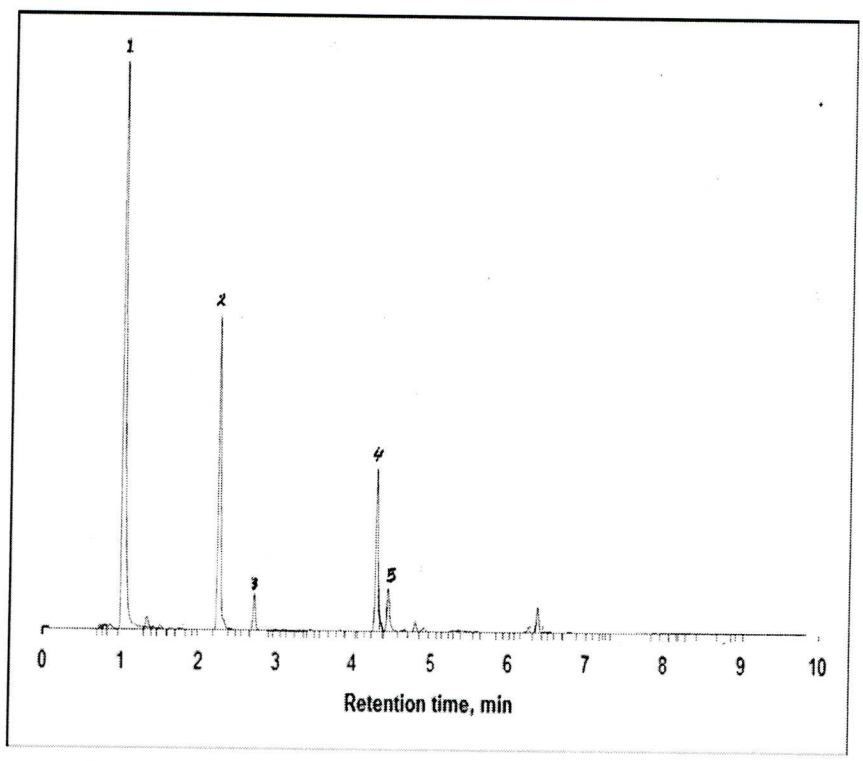

Figure 12 GC trace for products of catalytic conversion of acetone to MIBK in the gas phase (0.2 g 0.3% Pd/Zn-Cr (1:30), 0.3 s contact time, 300°C, 37 vol. % acetone, 10 mL/min H_2 flow rate; acetone (1), MIBK (2), mesityl oxide (3), DIBK (4), mesitylene (5)).

Appendix (VI)

The mass spectra obtained for camphene, limonene and p-cymene products identified by GC/MS are shown in Figures 13-15 which give primary mass/charge ratios of 136, 136, and 134 respectively.

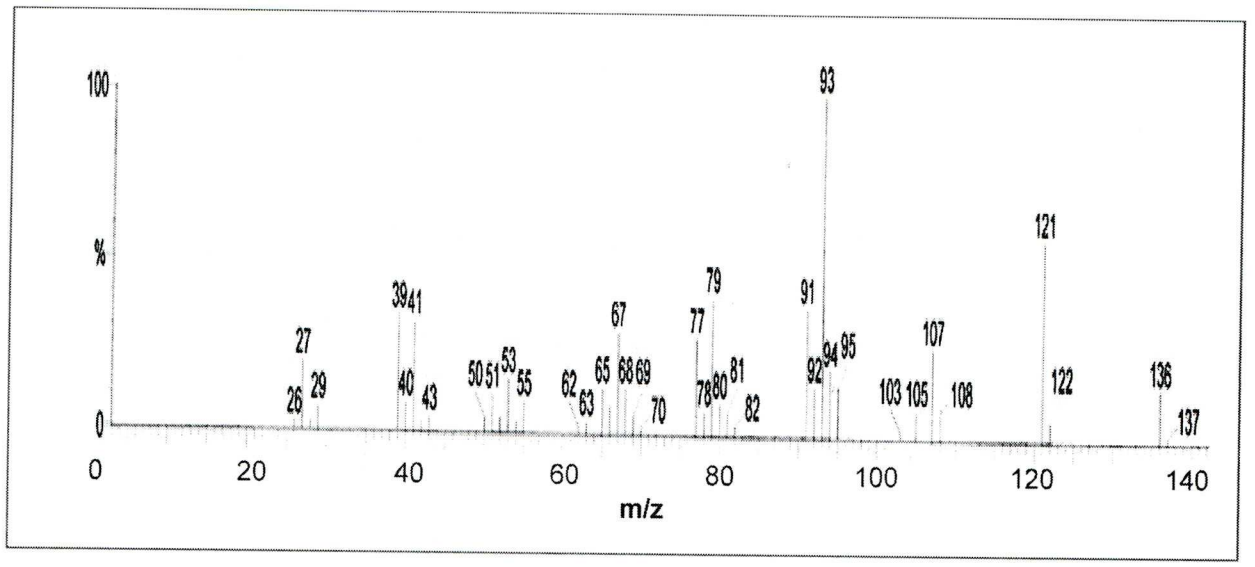

Figure 13 Mass spectrum of camphene. Relative molecular mass-136.

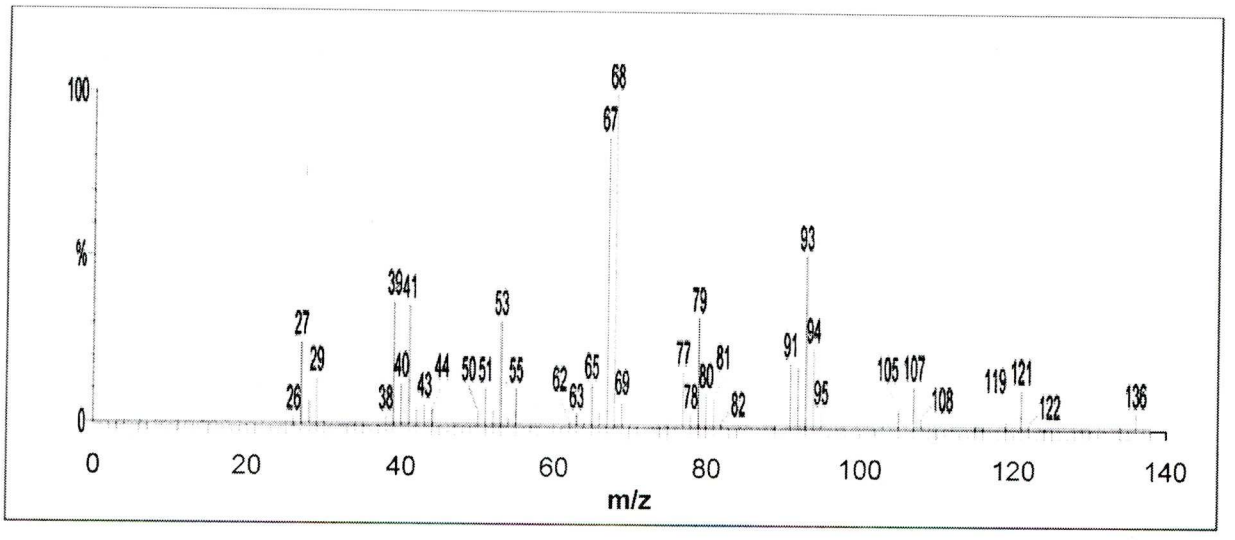

Figure 14 Mass spectrum of limonene. Relative molecular mass-136.

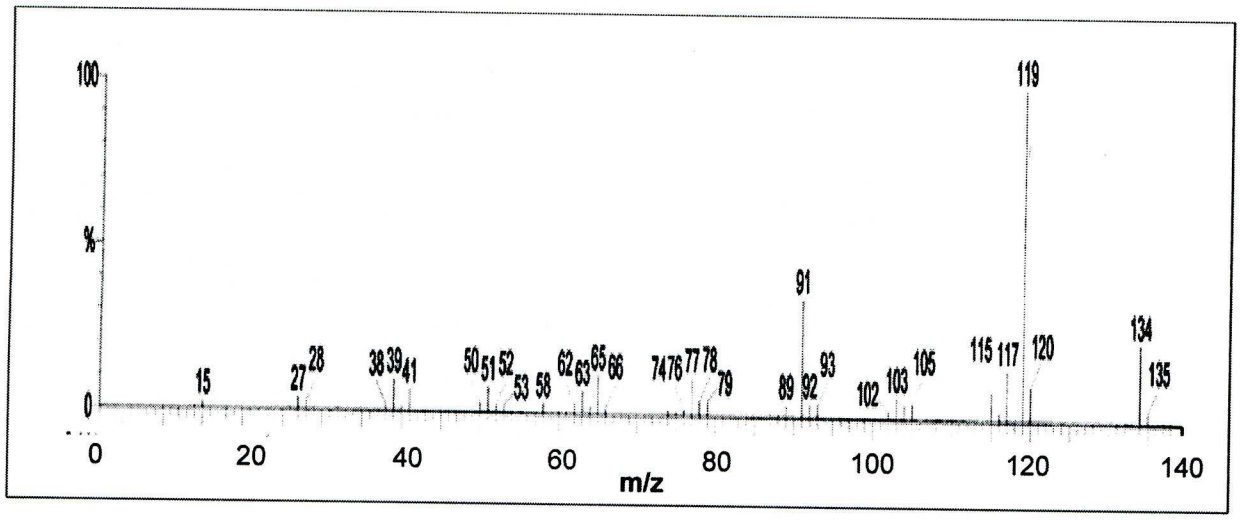

Figure 15 Mass spectrum of p-cymene. Relative molecular mass-134.